CELSR1 SUPPRESSES *WNT5A*-MEDIATED CHEMOATTRACTION TO PREVENT INCORRECT ROSTRAL MIGRATION OF FACIAL BRANCHIOMOTOR NEURONS

A Dissertation Presented to

the Faculty of the Graduate School

at the University of Missouri

In Partial Fulfillment

of the Requirements for the Degree

Doctor of Philosophy

By

DEVYNN S. HUMMEL

Dr. Anand Chandrasekhar, Dissertation Advisor

May 2022

The undersigned, appointed by the dean of the Graduate School, have examined the dissertation entitled

CELSR1 SUPPRESSES *WNT5A*-MEDIATED CHEMOATTRACTION TO PREVENT INCORRECT ROSTRAL MIGRATION OF FACIAL BRANCHIOMOTOR NEURONS

presented by Devynn Hummel,

a candidate for the degree of Doctor of Philosophy,

and hereby certify that, in their opinion, it is worthy of acceptance.

_____

Professor Anand Chandrasekhar

_____

Professor Elizabeth Bryda

_____

Professor Dawn Cornelison

_____

Professor Bing Zhang

ACKNOWLEDGMENTS

First and foremost, I would like to thank ***my parents, Scott and Jill Hummel***, for always encouraging me to pursuit my dreams. You have always reassured me that I am capable of anything I set my mind to. You remind me to appreciate the opportunities that I've been presented with. Through love and guidance, you have always encouraged me to work hard and persevere while also making time for the simple pleasures in life. If it weren't for the qualities that you have instilled upon me from such a young age, none of this would have otherwise been possible. Thank you mom and dad. I love you

I would like to thank ***my advisor, Dr. Anand Chandrasekhar,*** for teaching me the importance of scientific rigor. You've always encouraged me. You've taught me to ask the right questions and to anticipate outcomes. Most importantly, you have taught me to accept the inevitability of failed efforts, and to address problems levelheadedly. Thank you Anand

I would like to thank ***my mentor, Dr. Derrick Glasco*** for providing me technical training and words of encouragement. Thank you Derrick

I would like to thank ***my better half, Lauren Million.*** Your love provides me a safe haven from the daily hustle n' bustle. No matter what the day holds, I know that as long as I have you by my side, everything will turn out just fine. You encourage me in so many ways and your positive attitude is most inspiring. Thank you for taking this journey with me. I love you

I would like to thank ***my committee members, Dr. D Cornelison, Dr. Elizabeth Bryda, and Dr. Bing Zhang*** who have provided me with various resources, excellent scientific suggestions, as well as professional guidance. Thank you

I would like to thank ***Post-doctoral Fellow, Dr. Robert Arpke,*** member of the Cornelison lab, for his technical assistance but more importantly, his friendship. Thank you Robert

Last but certainly not least, I would like to thank current ***undergraduate students, Alex Becks, Gana Aleti, and Christina Chung, graduate student, Vimal Arora,*** as well as ***past graduate students, Emilia Asante and Suman Gurung*** for making the lab a fun and productive environment to do research. Thank you

TABLE OF CONTENTS

LIST OF FIGURES

LIST OF TABLES

ABSTRACT

As the nervous system develops, neurons often migrate from where they originate to their functional locations prior to them contributing to the circuits that drive cognitive and motor function. Within the vertebrate hindbrain, facial branchiomotor (FBM) neurons migrate caudally from rhombomere 4 (r4) to r6 and assemble into the circuits that drive facial and jaw movements. While several components of the Wnt/PCP (Planar Cell Polarity) pathway have been investigated based on their necessary role in initiating FBM neuron migration, much less is known regarding the mechanisms that determine directionality. However, our lab discovered that in mice lacking the Wnt/PCP component *Celsr1*, many FBM neurons inappropriately migrate rostrally. Tissue-specific knockouts indicate that *Celsr1* is functioning non-cell autonomously within the ventricular zone rostral to r4 in order to prevent rostral migration. Intriguingly, *Celsr1* and potential chemoattractant *Wnt5a* are expressed in overlapping domains within the rostral hindbrain. Based on these findings, we hypothesize that under normal conditions, *Celsr1* suppresses *Wnt5a* activity rostral to r4 to block the inappropriate rostral migration of FBM neurons.

Therefore, if WNT5A functions as the primary chemoattractive cue lending to the rostral migration observed among *Celsr1* mutants, then rostral migration should be suppressed in *Celsr1; Wnt5a* double knockouts. Indeed, FBM neurons in *Celsr1; Wnt5a* double knockout embryos never migrate rostrally. Furthermore, if WNT5A acts as the source of chemoattraction in the rostral hindbrain of *Celsr1* knockouts, then rostral migration should observed in wildtype hindbrains with

WNT5A-coated beads placed in r3. We found that FBM neurons migrated rostrally toward WNT5A beads in >80% of wildtype explants, demonstrating that excess WNT5A can allow for FBM neurons to overcome the endogenous effects of *Celsr1*. Importantly, rostral migration towards beads is significantly reduced in *Dvl2* mutants, suggesting that the *Wnt5a*-mediated chemoattraction of FBM neurons is dependent on *Wnt5a-Dvl2* signaling. Lastly, our model predicts that rostral migration of FBM neurons should be enhanced in *Celsr1* mutants overexpressing *Wnt5a* in r3. As expected, when a *Wnt5a* gain-of-function allele is used to overexpress *Wnt5a* in r3 of *Celsr1* mutants, the proportion of rostrally migrating FBM neurons is substantially greater than in control mutants, further supporting the chemoattractive model. These results reveal a novel role for a Wnt/PCP component regulating neuronal migration through suppressing chemoattraction (Chapter 3).

In other studies, we used transgenic zebrafish that express various calcium indicators in order to characterize calcium dynamics and neural activity, as calcium has been shown to allow for neuron migration as well as circuit establishment spanning multiple neuronal contexts. Here we show that FBM neurons exhibit fluctuations in intracellular calcium (Ca_i) among both cell bodies and neurite processes during their caudal migration. We also found that beginning at 60 hpf (hours post fertilization), synchronized patterns of neuronal activity extend to most hindbrain neurons, as well as caudal-most midbrain neurons (Chapter 4).

In separate studies, we used a transgenic line expressing nitroreductase in BM neurons to evaluate the ability of BM neurons to regenerate following metronidazole-mediated ablation. Surprisingly, BM neurons were not regenerated even after 1 week of recovery. Moreover, treatments shown to stimulate the regenerative response in other contexts failed to elicit BM neuron regeneration. These results suggest that different neuronal populations in zebrafish vary in their regenerative potential (Chapter 5).

CHAPTER 1: Introduction

1.1 Cell Migration During Early Development

Migration is the means by which cells move from one location to another. Many cells must migrate from where they are specified to new locations before performing a concerted function as part of a tissue/organ system. How cells acquire the competency to migrate has been extensively studied in the context of the immune system as well as other mature tissues. Not surprisingly, appropriate cell migration is also critical for normal development (Horwitz and Webb, 2003). The earliest form of migration occurs during gastrulation, where cells migrate and differentiate in order to form the multi-layer body plan comprised of the endoderm, mesoderm, and ectoderm (Keller and Shook, 2008; Tam and Behringer et al., 1997). Cells residing within each layer then participate in an extensive and cooperative migratory event referred to as convergence and extension. During convergence and extension cells of the mesoderm and ectoderm specifically migrate and further differentiate to form somites and the neural tube respectively (Solnica-Krezel, 2005). Subsequently, pluripotent neural crest cells delaminate from neural tube in order to migrate towards more distal locations (Mayor and Theveneau, 2013). As neural crest cells initiate migration, they simultaneously begin expressing various transcription factors and therefore differentiate into various precursor cells. These precursors also migrate and eventually give rise to a vast array of tissues including smooth muscle, bone, and various neurons (Christiansen et al., 2000; Le Douarin and Dupin, 2003; Weston et al., 1970).

Importantly, several sub-cellular processes must occur before any cell has the capacity to migrate. For example, the concerted collapse and reformation of actin and microtubule filaments during cytoskeletal rearrangement allows cells to take on dynamic morphologies that support movement in a particular direction. While mechanisms of cytoskeletal rearrangement appear to be somewhat universal among migratory cell types, mechanisms of chemoattraction and cell-cell adhesion seem to vastly differ and therefore confer specificity among migrating cells. This is particularly true in the case of neuron migration.

1.2 An Overview of Neuron Migration

During development of the nervous systems, many neurons will migrate extensively in order to reach their appropriate location among corresponding inputs and outputs. More specifically, proper neuronal position is achieved by means of either radial or tangential neuron migration and is generally recognized as a critical step during the formation of complex circuits. As neurons initiate migration, filopodia and lamellipodia projections perceive and respond to various attractive and repulsive cues, which provide spatial and temporal information to ultimately determining a neurons final destination. These cues typically include different cell adhesion molecules and/or secreted molecules which are perceived extracellularly. As neurons interpret attractive signals, actin and microtubule filaments associate the plasma membrane resulting in extension of one or more leading processes. Conversely, repulsive signals lead to retraction of said processes (Lambert de Rouvroit and Goffinet, 2001; Tsai and Gleeson, 2005).

Importantly, the analysis of several neuronal cell types has led to a much more thorough understanding of how neuron migration is achieved.

1.3 Neuron Migration Within the Cerebral Cortex

Neuron migration has been most prominently studied within the context of the cerebral cortex where first, neurons of the subplate as well as Retzius (CR) neurons migrate to an area below the cortical plate and pia, respectively. Subsequently, glia cells undergo somal translocation away from the pial surface, towards the ventricular zone, leaving behind an axon which gives rise to individual cortical columns (Miyata et al., 2001; Noctor et al., 2001).These radially-oriented glia cells i.e radial glia (RG), then transdifferentiate into projection neurons and various neuronal precursors. After extensive proliferation, projection neurons as well as other cell types destined for more superficial layers of the cortex associate RG cells allowing them to traverse cortical layers before differentiating into other neurons (Anton et al., 1999; Hatten, 1999; Hatten, 2002; Nadarajah and Parnavelas, 2002). Simultaneously, cortical interneurons as well as Corridor cells, born within the subpallium layer, migrate from ganglionic eminences perpendicular to RG cells in order to reach their proper position among cortical columns (Silva et al., 2019). Once glia-guided migration is complete, RG cells transform into astrocytes which support the formation of synaptic connections (Hatten, 1999).

Based on the step wise order of migration within the cerebral and cerebellar cortex, the earliest born neurons are generally found deep within the cortical plate, whereas neurons born later are found within more superficial layers of the brain.

This gives rise to an “inside-out” arrangement of neurons which is thought to be critical for normal brain function. (Hatten, 1999; Honda et al., 2003; Pearlman et al., 1998).

1.3.1 Mechanisms of Radial Neuron Migration

Radial migration or migration along the pial-ventricular axis is the most commonly utilized mode of migration among all migratory neurons. Appropriately, radial neuron migration is also most extensively investigated form of neuron migration and therefore, several studies have led to keen insights into how these interactions are maintained. For example, the Reelin pathway has been shown to regulate several aspects of radial migration and is the most well understood and commonly studied genetic mechanism proven to regulate neuron migration. Reelin signal transduction has particularly been shown to allow for glia guided radial migration within the cortex. Here, receptors of Reelin including the Very Low Density Lipoprotein Receptor (VLDLR) and Apolipoprotein E receptor-2 (ApoER2) bind REELIN, and activate LIM-Kinase 1 (LIMK1; Hirota and Nakajima, 2017). LIMK1 prompts the phosphorylation of n-cofilin which is expressed within the lead processes of migrating neuron and promotes the degradation and reformation of actin filaments during cytoskeletal rearrangement (Chai et al., 2009).

Reelin signal transduction also results in the phosphorylation of Disabled1 (Dab1) which activates the GTP exchange factor C3G, and GTPase, RAP1. RAP1 then promotes cell adhesion through the activation of various N-cadherins that act to stabilize the leading process of radially migrating neurons (Chai et al.,

2009; Franco et al., 2011). N-cadherins as well as Netrins are also required for proper polarization of filopodial projections (Ju et al. 2013; Stanco et al. 2009; Gartner et al., 2012). Importantly, while N-cadherins are generally viewed as attractive cues, Netrins are capable of acting as either attractive or repulsive cues during neuron migration (Park et al., 2003). The last step of glia-guided radial migration within the cortex termed terminal translocation, is also dependent on DAB1 phosphorylation leading to RAP1 activation, however, results in stimulation of the cell adhesion molecule *Integrin α5β1* (Sekine et al., 2012).

In comparison to earlier stages of glia guided radial migration within the cortex, terminal translocation relies on both N-cadherins as well as *Integrin α5β1.* (Sekine et al., 2012; Chai et al., 2009; Franco et al., 2011). Various other integrins including *Itga3*, *Itga5*, *Itgb1* are also involved in glia-guided radial migration (Anton et al. 1999**;** Belvindrah et al. 2007). Upon reaching more superficial layers of the cortex, neurons must disassociate radial glia by attenuating N-cadherin-mediated cell adhesion present between neurons and radial glial scaffolds. This largely dependent upon Slit/Robo signaling which results in β-CATENIN phosphorylation, and deactivation of N-cadherin (Rhee et al., 2007). Therefore, SLIT1/2 as well as are generally viewed as repulsive cues (Zheng et al. 2012) This is in contrast to SEMA-3A which binds NEUROPILIN-1 to allow for chemo attraction (Chen et al. 2008).

Once glia-guided migration is complete within the cortex, neurons have been shown to disperse by means of EPHRIN-A5-mediated repulsion (Villar-

Cerviño et al. 2013). Acknowledging that radial migration is the far more commonly utilized mode of migration among all migratory neurons, tangential migration on the other hand appears to be a more specialized or specific means of achieving proper position within the nervous system (Marin and Rubenstein, 2003).

1.3.2 Mechanisms of Tangential Neuron Migration

In contrast to radial migration, tangential migration occurs in the plane of the rostro-caudal and/or medial-lateral axis and is achieved independent of radial glia. Instead, tangentially migrating olfactory interneurons for example will utilize adjacent astrocytes as a substrate allowing for their migration (Chazal et al., 2000), while the tangential migration of cranial motor neurons has been shown to rely on adjacent or leading neurons in a process referred to as collective cell migration. Here, “pioneer neurons” of similar identity to that of surrounding neurons first initiate migration leaving behind a trailing axon. This axon, like RG cells of the cortex, provides a cellular scaffold which signals to follower neuron to initiate their migration (Wanner & Prince, 2013; Rebman et al., 2016). Analogous relationships

Figure 1. Radial and Tangential Migration within the Cortex

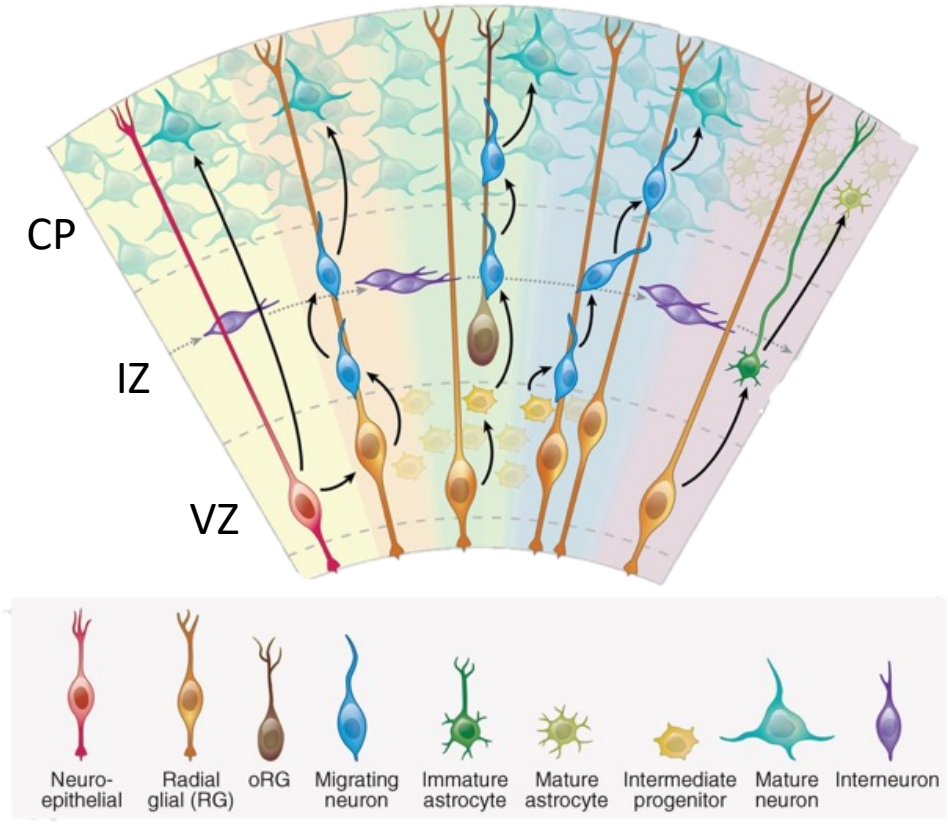

Adopted from: Poduri et al., 2013

Figure 1. Radial and Tangential Migration within the Cortex

A visual representation of neuron migration within the cerebral cortex. Note that many neurons as well as neuronal precursors will associate radial glia axons in order to ascend cortical layers. However, neurons that undergo somal translocation do not require radial glia for migration. Also, note the tangential migration of cortical interneurons which occurs perpendicular to radial glia allows for proper position among cortical columns which also occurs independent of radial glia.

exist within the context of the cerebral and visual cortex as well as in the spinal cord (Morante-Oria et al., 2003; Deng and Elberger, 2001; Nural et al, 2007). Therefore, as compared to radial migration that requires glia functioning as cellular scaffolds, tangentially migrating neurons are thought to utilize more diverse substrates perhaps suggestive of more context dependent mechanisms of regulation. Another marked difference between radially and tangentially migrating neurons is that typically, tangentially migrating neurons will extend multiple projections or elaborate branches as compared to radially migrating neurons that will extend one or very few projections (Valiente and Marin, 2010). Much of what we know regarding tangential neuron migration comes from studies examining the migration of cortical interneurons as they migrate from the medial ganglionic eminence (MGE) and subsequently position themselves among cortical columns. Neurons will also tangentially migrate from the lateral ganglionic eminence (LGE) in order to give rise to the olfactory bulb (Kriegstein and Noctor, 2004, Marin and Rubenstein, 2001).

Like radial neuron migration, the tangential migration of interneurons from the MGE has also been shown to depend upon Reelin signaling functioning upstream of N-cadherin mediated cell adhesion (Morante-Oria et al., 2003, Jossin and Cooper 2011). Reelin signaling is also required for the tangential migration of midbrain dopaminergic (mDA) neurons as well as somatic motor neurons within the spinal cord (Prakash et al., 2009; Bodea et al., 2014). Cell adhesion, made possible through *Integrin α3β1* (like *integrin α5β1* in the case of radial migration) is also necessary for proper interneuron migration (Stanco et al. 2009; Schmid et

al., 2004). Likewise, *Netrin1* is required for both radial and tangential neuron migration (Stanco et al. 2009). During the tangential migration of interneurons from the MGE, NETRIN-1 binds its receptor UNC5H3 which triggers repulsion away from the external granule layer (Alcantara et al., 2000). Similarly, tangentially migrating striatal neurons are also repelled away from the subventricular zone upon perception of NETRIN-1 as they migrate from the MGE (Marin and Rubenstein, 2003).

While Robo signaling is required for interneurons to be repelled away from the striatum, SLIT, the primary ligand to ROBO appears to be dispensable in this regard (Andrews et al., 2007; Marín et al. 2003). Interestingly, migrating interneurons are repelled away from the striatum by means of SEMA-3A and SEMA-3F. This repulsion is accomplished through SEMA binding its receptors, NEUROPILIN-1 (NPN1) and NPN2, another marked difference between radial migration within the cortex and tangential migration from ganglionic eminences (Marin et al., 2001). Through binding their PLEXIN coreceptors, SEMA-3A and SEMA-3F also allow for proper “sorting” of cortical and striatal interneurons (Marin and Rubenstein, 2001). Furthermore, EPHRIN-A3 functioning as a repulsive cue has been shown to prevent the inappropriate migration of tangentially migrating interneurons into the striatum through binding its receptor, EPH-A4 (Rudolph et al., 2010). While the molecules contributing to these processes are largely conserved between model systems and humans, in many cases it is unclear how defects in these pathways can result in neurological disorder. Therefore, we must

continue to investigate the mechanisms essential to neuron migration, in particular those affected in neurological disorders.

1.3.3 Neuron Migration Disorders

As a function of the many pathways involved, as well as the numerous neuronal cell types in existence, deficiencies in neuron migration manifests as a vast spectrum of developmental disorders characterized by uncontrolled motor output and/or severe cognitive disability. The critical role for neuron migration is evident among those affected by neuronal migration disorders (NMDs), a class of disorders that embody a daunting number of human syndromes of varying severity. For example, Lissencephaly (LIS) 1 is a gene named after the human condition, that upon mutation results in a smooth cerebral surface due to a lack of neuron migration (Copp and Harding, 1999). Appropriately, the word lissencephaly literally means smooth-brain. Lissencephaly (the condition) along with Paraventricular Heterotopia, polymicrogyria, Aicardi syndrome, and cortical dysplasia are all considered NMDs and result in the malformation of multiple brain regions (Copp and Harding, 1999; Gleeson and Walsh, 2000; Guerrini and Parrini, 2010; Pearlman et al., 1998). As previously described, several studies have also lead to a well-supported role for the Reelin pathway during cortical neuron migration. Appropriately, human mutations in *Reelin* have been shown to result in epilepsy, schizophrenia, and autism (Ishii et al., 2016). Fortunately, many neuronal cell types have emerged as models for investigation into how a mispositioning of neurons can ultimately result in abnormal circuit output and/or reduced fitness.

Acknowledging that breathing and feeding are critical to human health and survival, the underlying circuits responsible for these behaviors have also been the focus of extensive investigation. The branchiomotor neurons originating in the vertebrate hindbrain are of extreme clinical significance being that these neurons innervate the muscles that drive respiratory and feeding behaviors. Based on their stereotyped migration, the facial branchiomotor (FBM) neurons have specifically proved to be an efficient model for studies into how deficient migration can ultimately result in reduced or abnormal behavior (Asante et al., 2021; Allen et al., 2017; McArthur and Fetcho, 2017).

Facial Branchiomotor Neuron Migration and the Developing Hindbrain

Native to the vertebrate hindbrain, FBM neurons are specified and migrate from hindbrain segment, rhombomere 4 (r4) to more caudal rhombomeres. In both zebrafish and mice, FBM neurons specifically exit cranial nerve VII to innervate the abductor and hyoid muscles of the jaw derived from the 1st and 2nd pharyngeal (branchial) arches (Chandrasekhar, 2004; Guthrie, 2007). FBM neuron migration in mice largely occurs from embryonic stage E10.5-E13.5 and results in translocation as far as r6, while in zebrafish, migration largely occurs from 18-36 hours post fertilization (hpf) and results in migration as far as r7 (Chandrasekhar, 2004; Guthrie, 2007). Once FBM neurons migrate from r4 and pass medial to the nucleus abducens (nVI) in r5, they begin to migrate laterally (Song et al., 2006). FBM neurons then undergo a radial, glia and Reelin dependent migration to form 2 mature motor nuclei within r6 or r7 (Goffinet, 1984; Ohshima et al., 2002;

Figure 1.2 The Mouse and Zebrafish Cranial Motor Neuron Circuit

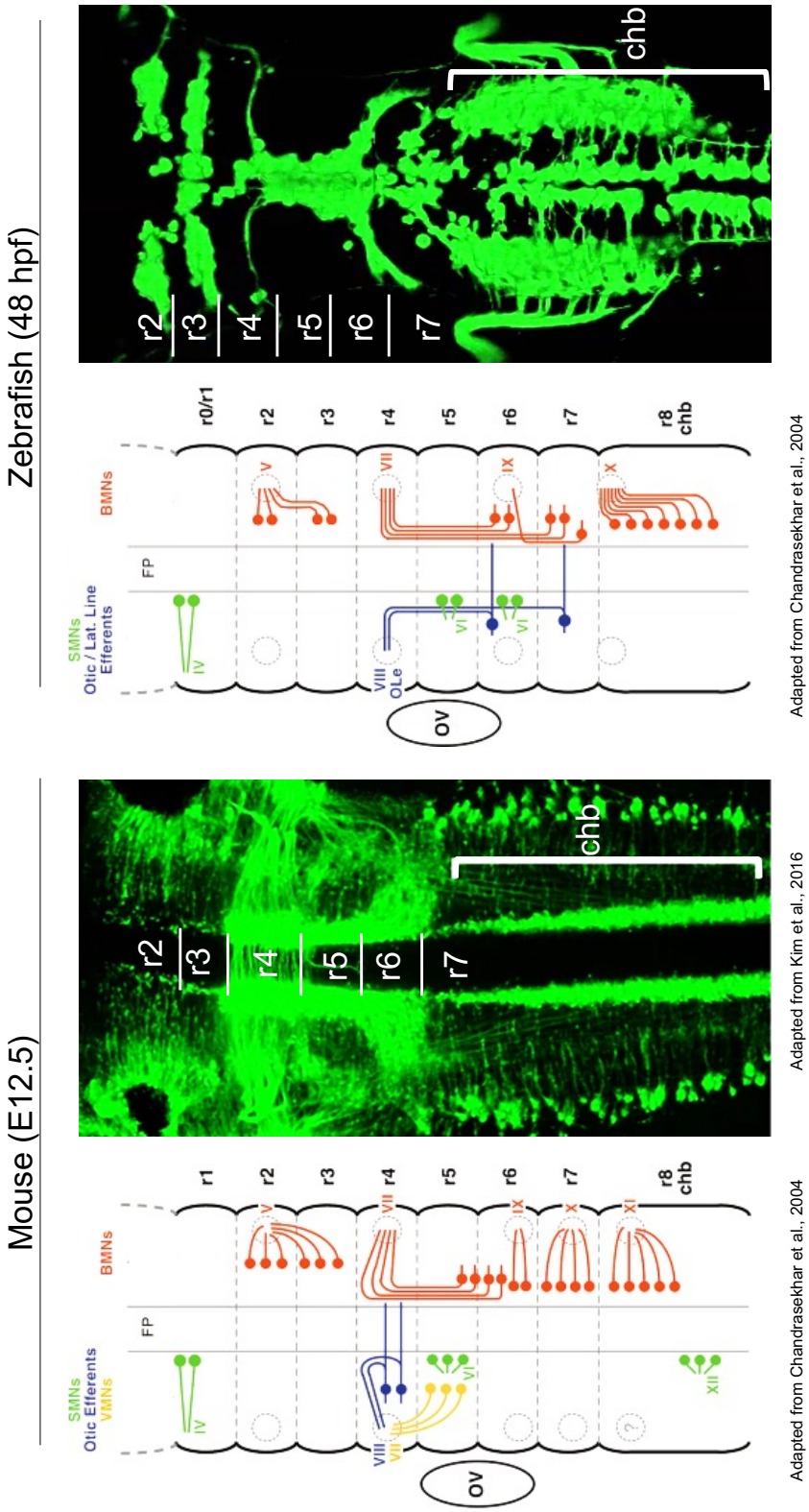

Figure 1.2 The Mouse and Zebrafish Cranial Motor Neuron Circuit

Organization of cranial motor neurons in both zebrafish and mice. Rhombomeres are denoted by horizontal dashed lines in schematics and horizontal solid white lines in florescent images. Florescent images are transgenic animals expressing GFP in cranial motor neurons under the regulation of the Islet1 promoter (Islet1:GFP). In schematics, branchiomotor neurons are shown in red, the somatomotor neurons (SMNs) in green, the otic and lateral line efferent (VIII, OLe) neurons in blue, and the visceromotor neurons (VMNs) in yellow. For clarity, neuron populations are depicted on only one side of the hindbrain. FP marks the floor plate region. The nerve exit points of the BMN, VMN, and otic efferent axons are shown as grey circles. These exit points appear to be more ventral in zebrafish, although their depicted locations are estimates. OV, otic vesicle.

Chandrasekhar, 2004). Interestingly, studies in zebrafish show that FBM neuron migration depends upon a single “pioneer” neuron defined as the first FBM neuron to initiate migration. As a pioneer neuron begins to migrate, it leaves behind a trailing axon. “Follower” neurons of similar identity then associate the trailing axon allowing for their tangential migration to more caudal locations (Wanner & Prince 2013). Subsequently, FBM neurons associate medial longitudinal fasciculus (MLF) neurons in order to complete their caudal migration (Wanner & Prince 2013; Rebman et al., 2016).

Importantly, various genes widely recognized as core components of the Wnt/Planar Cell Polarity (PCP) pathway have been investigated based on their critical role in *initiating* FBM neuron migration (Chandrasekhar, 2004; Guthrie, 2007). Several other genes are similarly required for FBM neuron migration, and upon mutation, result in either partial or complete migration block. This is in contrast to PCP component *Celsr1*, which upon mutation results in abnormal rostral migration (Glasco et al., 2012; Qu et al., 2010).

1.4.1 *Celsr1* Mediates Directionality Among Migrating FBM Neurons

In animals deficient for atypical cadherin and PCP component *Celsr1,* some FBM neurons inappropriately migrate rostrally into r3 and r2 instead of caudally (Qu et al., 2010*)*. Interestingly, *Celsr1* is expressed during FBM neuron migration (E10.5-E12.5) within the ventricular zone, directly adjacent and lateral to the floor plate, spanning the entire rostro-caudal extent of the hindbrain (Qu et al., 2010). Previously, various Cre lines specific to individual hindbrain domains were used in

combination with a floxed *Celsr1* allele to allow for the tissue-specific knockout of *Celsr1* among differing hindbrain domains. These experiments indicate that *Celsr1* does not within FBM neurons but instead functions non-cell autonomously within the ventricular zone rostral to r4 in order to prevent inappropriate rostral migration (Glasco et al., 2016).

Furthermore, in order to determine the origin of both rostrally and caudally migrating neurons in *Celsr1* mutants, lipophilic dyes were used to label both rostrally and caudally migrating neurons. The dye would travel through the axons of injected cells to where neurons had migrated from and out of the hindbrain through cranial nerve exit points lateral to each neuron's original starting position. In all samples tested, the rostral streams of migrating neurons always occupied more rostral positions of r4 suggesting that the rostral migration of FBM neurons in *Celsr1* mutants is not due to a random loss of polarity, but is instead due to a change in local guidance cues (Glasco et al., 2016). Intriguingly, *Wnt5a,* a putative chemoattractant, is expressed in a domain that overlaps with the domain of *Celsr1* expression and has been proposed to regulate the caudal migration of FBM neurons (Vivancos et al., 2009). Since *Celsr1* does not function within FBM neurons during migration and is instead required within and rostral to r4, *Celsr1* must function non-cell autonomously to regulate FBM neuron migration (Qu et al., 2010 & Glasco et al., 2016). Also, acknowledging that Wnt ligand binds FRIZZLED receptors extracellularly, Wnt ligands are also thought to function non-cell autonomously. Importantly, WNT5A and CELSR1 have not been shown to directly associate one another in any context.

1.5 The Canonical and Non-canonical Wnt Signaling Pathway

During canonical Wnt signaling, Wnt ligands are secreted via retrograde transport. WNT molecules are lipid modified glycoproteins typically 350–400 amino acids in length (Cadigan and Nusse, 1997). The palmitoylation as well as glycosylation of WNT molecules through the addition of a lipid and carbohydrate modification, respectively, in part allows for export/secretion. Prior to export, Wnt trafficking proteins WNTLESS and PORCUPINE must associate WNT (Yu et al., 2014; Kurayoshi et al., 2007). Therefore, modulation of WNTLESS and PORCUPINE activity represents an indirect means of regulating Wnt signaling (Yu et al., 2014). Once secreted, WNT molecules are perceived by the G-protein coupled receptor (GPCR) FRIZZLED and at times the coreceptor LRP*5/6* which together associate DISHEVELLED (*DVL*). Interestingly, knockout of *Dvl2* has been shown to rescue the *Celsr1* mutant phenotype where FBM neurons migrate rostrally instead of caudally (Glasco et al.,2012). The palmitoylation of Wnt is also required for associating *Frizzled* receptors (Janda et al., 2012; Hosseini et al., 2019). Cytoplasmic DVL then recruits AXIN1 and the kinases CK1 and GSK3 to the membrane, which prevents both ß-CATENIN phosphorylation and degradation. As a result, ß-catenin molecules accumulate in the cytoplasm and subsequently translocate into the nucleus, where they activate TCF/LEF transcription sites.

In contrast to the canonical Wnt pathway, non-canonical Wnt signaling is achieved independent of ß-catenin and results in activation of ROCK and JNK

through the small GTPases RhoA and Rac1 ultimately leading to cytoskeletal rearrangement and transcriptional activation (Palomer et al 2019). Furthermore, non-canonical Wnt signaling also results in PKC/PLC activation, and therefore regulates intracellular calcium concentrations. Interestingly, FRIZZLED3 has been shown to mediating ß-CATENIN phosphorylation and is also capable of stimulating PKC activation (Umbhauer et al., 2000; Sheldahl et al., 1999). Likewise, *Wnt5a* is considered a "non-canonical" Wnt (Sinha et al., 2012; Vivancos et al., 2009; Cheng et al., 2008) yet has been shown to result in ß-CATENIN activation and is therefore capable of mediating both canonical and non-canonical Wnt signaling pathways (Topol et al., 2003; Dissanayake et al., 2007; Mikels and Nusse 2006; Okamoto et al., 2014)

While WNT5A has been investigated as a potential chemoattractant allowing for FBM neuron migration, *Wnt5a* mutants animals exhibit relatively normal migration therefore, the role for either canonical or non-canonical Wnt signaling remains uncertain (Vivancos et al., 2009). Nevertheless, WNT5A has well demonstrated roles in the nervous system and has been shown to function as a chemoattractant during commissural axon outgrowth (Lyuksyutova et al., 2003; Onishi et al., 2013). *Wnt5a* has also been shown to function as a chemorepellent for corticospinal as well as callosal neuron axon outgrowth (Hutchins et al., 2011). Furthermore *Wnt5a* also mediates the migration of macrophages during inflammation and regulates the migration and metastasis of cancer cells (Ka Toh and Ka Toh, 2006; Hasan et al., 2017; Kim et al., 2020). Importantly, several genes

required for Wnt signaling, are also considered core components of the PCP pathway, and therefore, the two pathways overlap significantly.

1.6 Mechanisms of Planar Cell Polarity (PCP)

During PCP signaling, mutually antagonistic interaction between core PCP components FRIZZLED and VAN GOGH result in their asymmetric localization (Davey et al., 2016), through mechanisms that are not entirely clear (Benzing et al., 2007). Nevertheless, the intracellular PCP components, DISHEVELLED and DIEGO are thought to promote the asymmetric localization of FRIZZLED and VAN GOGH-LIKE 2 (VANGL2; Feng et al., 2012). Importantly, CELSR molecules on neighboring cells participate in homophylic interactions and simultaneously bind core PCP components FRIZZLED and VANGL2 in order to further assist in their asymmetric localization *(*Stahley et al., 2021; Bastock et al., 2003; Chen et al., 2008; Devenport and Fuchs, 2008; Strutt, 2008; Struhl et al., 2012*).* Appropriately, knockout of either *Frizzled3* or *Vangl2* results in a complete FBM neuron migration block (Vivancos et al., 2009; Glasco et al., 2012). Based on the critical role for *Vangl2* during FBM neuron migration, we know that Wnt signaling, in the absence of PCP, is not sufficient for FBM neuron migration. During FBM neuron migration, VANGL2 has been shown to lend to filopodia retraction, whereas FRIZZLED3A instead acts to stabilize extending projections suggestive of an attractive role for Wnt signaling (Davey et al., 2016). *Frizzled*3 as well as *Celsr*2/3 compound mutants also exhibit extensive migration defects within the cerebral cortex by adulthood (Qu et al., 2014). Deletion of *Celsr*2/3 also prevents FBM neuron migration (Qu et al., 2010). Furthermore, while *Celsr1* mutants are characterized

by a partial reverse of FBM neuron migration, *Celsr1* mutant mice also exhibit microcephaly by adulthood, reminiscent of the human condition (Ravnir et al., 2009; Boucherie et al., 2018).

Interestingly, while PCP achieved through *Frizzled* and *Vangl2* has been shown to give rise to the rostral-caudal axis spanning various cell types, the Fat and Dachsous mechanism of polarity instead gives rise to the medial-lateral axis (Brzoʹska et al., 2016; Zakaria et al., 2014). Specifically, PCP component *Celsr1* is required for rostro caudal patterning of the kidneys and skin (Brzoʹska et al., 2016; Ravnir et al., 2009). Furthermore, it's been shown that *Celsr1* is downregulated in hepatocellular carcinomas and mantle cell lymphoma (Del Giudice et al. 2012; Ammerpohl et al. 2012), however, is upregulated in B lymphocytes of chronic lymphocytic leukemia patients, and thus it is unclear how *Celsr1* may be contribute to cancer and metastases (Kaucka et al. 2013).

1.7 Outline of Thesis

Prior to this work, others have demonstrated that *Celsr1* functions to mediate directionality among migrating FBM neurons, as in *Celsr1* mutants, a portion of FBM neurons inappropriately migrate rostrally instead of caudally (Glasco et al. 2012; Qu et al., 2010). In addition, WNT5A has been investigated as a potential chemoattractant functioning to regulate FBM neuron migration, however, based on the subtle phenotype observed among *Wnt5a* mutants, this role remains uncertain. Also, *Celsr1* and *Wnt5a* expression domains overlap within the context of the rostral hindbrain. Based on these data, we examined a possible

role for *Celsr1* functioning as a suppressor of *Wnt5a*-mediated chemoattraction. We propose that the suppression of *Wnt5a* via *Celsr1* ensures the exclusively caudal migration of FBM neurons. We also examine a role for *Dvl2* regulating the *Wnt5a*-mediated chemoattraction of FBM neurons (Chapter 3).

Also, since calcium-mediated signaling has been shown to regulate neuronal migration and circuit formation, in separate experiments, we use transgenic zebrafish that express genetically-encoded calcium indicators, GCaMP6s or GCaMP6f, to characterize calcium dynamics and neural activity among FBM neurons as well as other hindbrain neurons (Chapter 4). We also tested whether the branchiomotor neurons would regenerate following chemo-genetically induced ablation (Chapter 5).

Figure 1.3 A potential Mechanism for the Wnt/PCP Pathway During FBM Neuron Migration

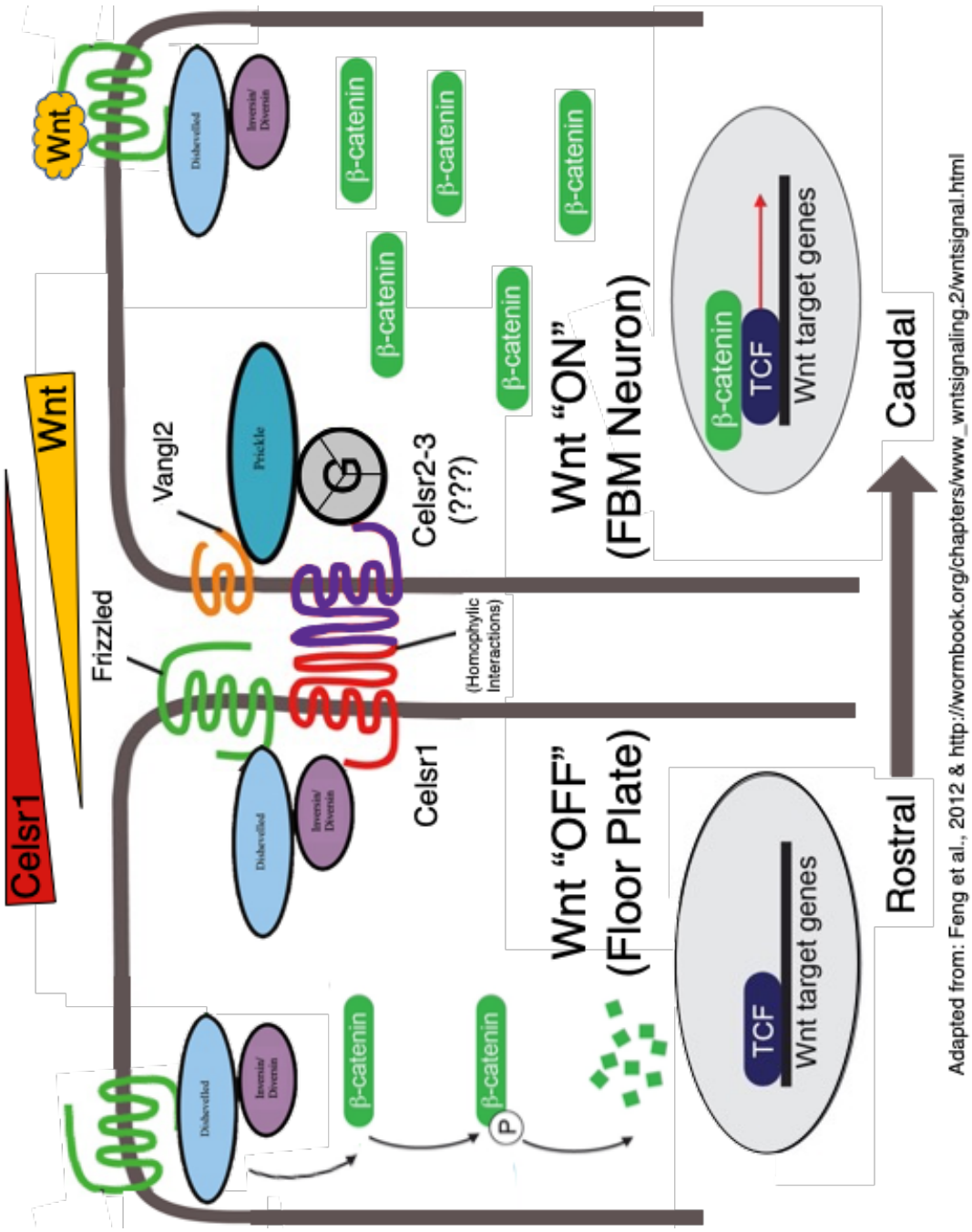

Figure 1.3 A potential Mechanism for the Wnt/PCP Pathway During FBM Neuron Migration

As previously described, both Wnt and PCP signaling pathways are required for (normal) FBM neuron migration. Several lines of evidence support the interactions depicted. Most notably, recent work has shown that *Celsr1* physically interacts with *Frizzled* and *Vangl*2 (in mouse epidermal cells; Stahley et al., 2021). We also know that *Celsr1* does not function within FBM neurons to prevent their rostral migration and instead functions within the surrounding environment (Qu et al., 2010; Glasco et al., 2016). Furthermore, Davey et al., 2016 reports that VANGL2 is enriched at the anterior (rostral) side floor plate cells of the hindbrain (Davey et al., 2016). Lastly, Vivancos et al., 2009, suggests that WNT5A is capable of acting as a chemoattractant and is broadly expressed caudal to rhombomere 4. --- Schematics from Feng et al., 2012 & "http://wormbook.org/chapters/www_wntsignaling.2/wntsignal.html" were adpted and merged.

CHAPTER 2: MATERIALS AND METHODS

2.1. Adult Mice

2.1.1. Colony maintenance

Mice used in these studies were maintained using standard protocols approved by the Animal Care and Use Committee at the University of Missouri. The mouse colony was housed in the Vivarium of the Bond Life Sciences Center where a 12- hour day/night cycle, 72 – 73 °C temperature, and a humidity of 30 – 70% was maintained. Mice were kept in conventional housing with at least one source of housing enrichment. For social enrichment, they were housed in groups with the exception of designated breeder males which were used for timed matings.

2.1.2. ID tagging

All mice were ID tagged at weaning age (P21) for the purpose of tracking and genotyping. Each mouse was restrained by hand, and a small ear tag (National Band & Tag, catalog number 1005-1, laser etched) was applied using an ear tag applicator (National Band & Tag, catalog number 1005s1). Ear tags were soaked in 70% ethanol immediately before use to prevent infection. Moreover, ear tags were applied midway down the pinna in order to avoid puncturing cartilaginous tissue.

2.1.3. Tissue collection and genomic DNA isolation from tail snips

For genotyping purposes, DNA was purified from tail clips of mice at postnatal day 21 (P21). Each mouse was restrained by hand, and 0.5 cm of the tail was removed using a clean razor blade. To stop the bleeding, pressure and Kwik Stop® Styptic Powder with Benzocaine (Fisher, catalog number NC9482281) was applied to the wound. Tail clips were always collected at P21 and mice were immediately weaned. Genomic DNA purification was subsequently carried out using the DNeasy® Blood & Tissue Kit (QIAGEN, catalog number 69504) according to the manufacturer's instructions.

2.1.4. Timed matings

For timed matings, male studs were housed individually for breeding. Up to two female mice were introduced to male breeders in the late afternoon and were left overnight to allow for mating. Each morning thereafter, females were examined for copulation plugs as an indication of successful mating (Papaioannou and Behringer, 2005). Each plugged female was transferred from the male's cage back into her original cage and embryo collection was planned according to the developmental stage desired. Noon on the day plugs were found, embryos were considered to be E0.5 (Nagy, 2003). Potentially pregnant females were weighed for several days prior to dissections in order to ensure pregnancy. Females were euthanized for embryo collection only if they had exhibited at least 20% weight gain from the plug date.

2.1.5. Euthanasia

Adult mice were euthanized by asphyxiation in 100% CO_2. A cervical dislocation was then performed to ensure death. For female mice used for embryo collections, two minutes were sufficient since the freshest embryonic tissue is required. Mice euthanized for other reasons (e.g. age, colony size reduction) were left in the CO_2 chamber for 5-10 minutes before cervical dislocation. All procedures performed on live mice were approved by the University of Missouri Animal Care and Use Committee.

2.2. Embryos

2.2.1. Dissection and staging

Pregnant females were euthanized via CO_2 asphyxiation and cervical dislocation as previously described. The mouse was laid on its back and its abdomen was soaked with 70% ethanol spray to minimize contamination. The uterus containing the embryos was then removed using standard technique (Nagy, 2003), and was subsequently placed in a 100 mm x 15 mm petri dish containing ice-cold PBS. After rinsing the intact uterus, it was then transferred to a new dish containing fresh PBS for dissection. The method of removing embryos from the uterus was different based upon the age(s) required. For E10.5 and younger, the uterine swellings were cut individually and the muscular layer was then removed using forceps (Nagy, 2003). For E11.5 and older, a single incision was made down the muscular layer using surgical scissors to remove the constricting uterus. Dissections using scissors at early ages will result in destruction of embryonic

tissues. Embryos were then removed (Nagy, 2003), and transferred to a dish containing fresh PBS for staging and hindbrain dissection. The approximate age of each clutch was already known based on the day of copulation, however, was confirmed using the Thieler method of staging (Nagy, 2003).

2.2.2. Fixation and storage

The time between sacrificing of the mother and fixation of embryos should be minimized to ensure consistent results. Embryo tissue fixation (in 4% paraformaldehyde in PBS) varies depending upon the age of embryos. Embryos younger than E9.5 should be fixed for a maximum of 5 hours, however older embryos should be fixed overnight.

2.2.3. Tissue collection and genomic DNA isolation

For embryos requiring genotyping, a small amount of tissue was collected during dissection for genomic DNA isolation. To minimize contamination between samples, clean forceps were used and wiped down with 70% ethanol between samples. A small amount of tissue – the size of an E12.5 handplate – was collected into a 1.5-mL microcentrifuge tube containing 500ml of PBS. After all dissections were complete, the PBS was removed, replaced with 100 µL of lysis buffer, and incubated at 55 °C for two hours with occasional mixing. DNA was precipitated by adding 1 µL of glycogen (Roche, catalog number 10901393001) plus 200 µL of 100% ethanol per sample, gently mixed, then stored at -20 °C overnight. The following day, DNA was pelleted at 14,000 rpm for 5 minutes, washed in 250 µL of

70% ethanol, air dried at 37 °C, and resuspended in 35 µL of QIAGEN buffer EB (available in QIAGEN PCR purification kits). If a smaller tissue sample was recovered, these samples should be suspended in only 15 ml of EB.

Lysis buffer for genomic DNA isolation of hand plates (97.7 mL)

Component	Amount	[Stock]	[Final]
Tris-HCl, pH 8.0	5 mL	1 M	50 mM
EDTA	1 mL	0.5 M	5 mM
NaCl	10 mL	1 M	100 mM
SDS	2.5 mL	20%	0.5%
ddH2O	to 4L	-	-

Mix each of the components in a sterile 100-mL bottle and store at room temperature. Proteinase K (Sigma P4850, >800 U/mL) is added fresh to each aliquot during use. To make a 1-mL working aliquot, combine 977 µL of the stock lysis buffer and 23 µL of proteinase K into a 1.5-mL tube. The working concentration of proteinase K for digestion is >18.4 U/mL.

2.3. Mouse Lines & Genotyping

2.3.1. *Celsr1* KO mutant mouse line

Celsr1 KO mice, were revived from frozen sperm. In *Celsr1* KO mice, exons 26 through 29 of the *Celsr1* gene are deleted and correspond to transmembrane domains 5 through 7 (Ravni et al., 2009). Importantly, homozygous *Celsr1* KO mice are smaller, have defects in hair follicle orientation, as well as a kinked or

curly tail (Ravni et al., 2009). Mice will also spin, perhaps depending on the severity of improper hair follicle orientation. While ~20% of mutants die in utero, many survive to adulthood (Ravni et al., 2009).

Genotyping of the *Celsr1* KO allele was performed by PCR amplifying the region between introns 25 and 29 of *Celsr1*, however, this at times proved problematic during amplification of the WT allele which would result in a band 3504 bp. This is as compared to the mutant allele which would result in a 596 bp band. To simplify the genotyping procedure, a third primer was designed, specific to the deleted introns, and therefore would only anneal in WT samples. This also allowed for the use of GoTaq Green Master Mix (Promega M7123) and significantly shorted the time in the thermocycler. PCR conditions are as follows (25 µL reaction):

Component	[Stock]	[Final]	µL/reaction
nuclease-free water	--	--	7.75
GoTaq Green Master Mix (Promega M7123)	2X	1X	12.5
reverse primer (common) 5'-GGGAAAGAGACTGTTGGTGAGCAGAAGCC	10 µM	0.5 µM	1.25
forward primer (WT Allele) 5'-GGACAAAGCTTGGTCCCTGCTCCG	10 µM	0.5 µM	1.25
forward primer (mutant allele) 5'-GCGCCTCTGTTGACTTCTGACTGGG	10 µM	0.5 µM	1.25
genomic DNA (purified via QIAGEN DNeasy Kit)	--	--	1

Thermocycler conditions: 94 °C, 2 min; [(94 °C, 30 sec), (64 °C, 1 min), (72 °C, 45 sec)] x 40 cycles; 72 °C, 5 min; hold at 4 °C.

The resulting product was analyzed by running 10ml on a 2% agarose gel.

2.3.2. *Wnt5a* KO mutant mouse line

The *Wnt5a* KO allele (*B6;129S7-Wnt5a*^{tm1Amc}) were purchased from Jackson Laboratory (Bar Harbor, ME). Animals homozygous for the *Wnt5a* KO allele die at birth due to respiratory failure (Yamaguchi et al., 1999). The genotyping assay outlined below results in a 400-bp band characteristic of the KO allele while the WT allele is characterized by a 484-bp band. PCR conditions are as follows (25 µL reaction):

Component	[Stock]	[Final]	µL/reaction
nuclease-free water	--	--	7.75
GoTaq Green Master Mix (Promega M7123)	2X	1X	12.5
reverse primer (common) 5'- CATCTCAACAAGGGCCTCAT-3'	10 µM	0.5 µM	1.25
forward primer (WT Allele) 5'- GAGGAGAAGCGCAGTCAA TC-3'	10 µM	0.5 µM	1.25
forward primer (mutant allele) 5'- GCCAGAGGCCACTTGTGTAG-3'	10 µM	0.5 µM	1.25
genomic DNA (purified via QIAGEN DNeasy Kit)	--	--	1

Thermocycler conditions: 94 °C, 3 min; [(94 °C, 30 sec), (50 °C, 30 sec), (72 °C, 1 min)] x 35 cycles; 72 °C, 10 min; hold at 4 °C.

The resulting product was analyzed by running the entire reaction on a 2% agarose gel.

2.3.3. *Dishevelled2* KO mutant mouse line

*Dvl*2 knockout mice (129s;*Dvl2*^{tm1Awb}) were purchased from Jackson Laboratory (Bar Harbor, ME). Importantly, It was previously shown that 50% of *Dvl2* homozygous mutants die due to cardiac defects before or immediately after birth (Hamblet et al., 2002). Based upon the genotyping assay outlined, the WT allele is characterized by a 263-bp band, whereas the mutant allele produces a 209-bp band. Heterozygous mice show both 263 bp and 209 bp bands. PCR conditions are as follows (25 µL reaction):

Component	[Stock]	[Final]	µL/reaction
nuclease-free water	--	--	7.75
GoTaq Green Master Mix (Promega M7123)	2X	1X	12.5
forward primer (common) 5'- GCCAGAGGCCACTTGTGTAG-3'	10 µM	0.5 µM	1.25
reverse primer (WT Allele) 5'- CCACCTCCAAATGCTATGCT-3'	10 µM	0.5 µM	1.25
reverse primer (mutant allele) 5'- GAATCGGTGACACTGCTGAA-3'	10 µM	0.5 µM	1.25
genomic DNA (purified via QIAGEN DNeasy Kit)	--	--	1

Thermocycler conditions: 95 °C, 5 min; [(95 °C, 45 sec), (55 °C, 1 min), (72 °C, 1 min)] x 35 cycles; 72 °C, 2 min; hold at 4 °C.

The resulting PCR product was analyzed by running 10ml on a 2% agarose gel.

2.3.4. *Krox20*-Cre mouse line

Krox20-Cre mice (Egr2$^{tm2(cre)Pch}$), were revived from frozen sperm. Importantly, *Krox20*-Cre mice were generated by replacing, a portion of exons 1 and exon 2 with nls-Cre. This places Cre under the control of the *Krox20* regulatory elements, however, generates a *Krox20* null allele (Voiculescu et al., 2000). Therefore, it is important to use and maintain heterozygous animals since loss of *Krox20* function prevents the formation of r3 and r5 and is lethal (Schneider-Meunoury et al., 1993). The *Krox20* allele is characterized by a 500-bp band while the WT is characterized by a 659-bp band. PCR conditions are as follows (25 µL reaction):

Component	[Stock]	[Final]	µL/reaction
nuclease-free water	--	--	7.75
GoTaq Green Master Mix (Promega M7123)	2X	1X	12.5
reverse primer (common) 5'- CTTTACACAGCATCGCCAAG-3'	10 µM	0.5 µM	1.25
forward primer (WT Allele) 5'- TTGACCAGATGAACGGAGTG-3'	10 µM	0.5 µM	1.25
forward primer (Krox allele) 5'- ATCAGGACATAGCGTTGGCT-3'	10 µM	0.5 µM	1.25

genomic DNA (purified via QIAGEN DNeasy Kit)	--	--	1

Thermocycler conditions: 95 °C, 5 min; [(95 °C, 45 sec), (53 °C, 1 min), (72 °C, 1 min)] x 35 cycles; 72 °C, 2 min; hold at 4 °C.

The resulting PCR product was analyzed by running the entire reaction on a 1% agarose gel.

2.3.5. *Wnt5a* GOF mouse line

*Wnt5a*GOF mice, carrying the conditional *Wnt5a*GOF allele, were generated by inserting a floxed *Wnt5a* expression construct into the ROSA26 locus (Cha et al., 2014), Crossing to a Cre-driver results in the excision of the flox-stop-flox allowing for *Wnt5a* overexpression in a Cre-dependent manner. Presence of the *Wnt5a*^{GOF} transgene is characterized by a 192-bp band along with a 500-bp band. WT animals exhibit a 330-bp band. PCR conditions are as follows (25 µL reaction):

Component	[Stock]	[Final]	µL/reaction
nuclease-free water	--	--	5.75
GoTaq Green Master Mix (Promega M7123)	2X	1X	12.5
reverse primer (GOF forward) 5'- CACACAGGCATAGAGTGTCTGCT-3'	10 µM	0.5 µM	1.25
forward primer (GOF reverse) 5'- AGAACTTGGAAGACATGGCACCT-3'	10 µM	0.5 µM	1.25

forward primer (ROSA10) 5'- CTCTGCTGCCTCCTGGCTTCT-3'	10 µM	0.5 µM	1.25
forward primer (ROSA11) 5'- CGAGGCGGATCACAAGCAATA -3'	10 µM	0.5 µM	1.25
forward primer (ROSA reverse) 5'- GCGAAGAGTTTGTCCTCAACC-3'	10 µM	0.5 µM	1.25
genomic DNA (purified via QIAGEN DNeasy Kit)	--	--	1

Thermocycler conditions: 94 °C, 3 min; [(94 °C, 30 sec), (53 °C, 30 sec), (72 °C, 30 sec)] x 35 cycles; 72 °C, 10 min; hold at 4 °C.

The resulting PCR product was analyzed by running 20ml on a 2% agarose gel.

2.3.6. SE1::GFP mouse line

The SE1::GFP (*Tg(Isl1-EGFP)2Slp*) transgenic mouse line was revived from frozen sperm. The original genotyping protocol was modified in order to reduce the possibility of false positives (which was often an issue when carrying out gel electrophoresis for this allele). In doing so the number of cycles during PCR was reduced from 35 to 30. Presence of the GFP transgene is characterized by a 383-bp band (Shirasaki et al., 2006). All other PCR conditions are as follows (25 µL reaction):

Component	[Stock]	[Final]	µL/reaction
nuclease-free water	--	--	7.75
GoTaq Green Master Mix (Promega M7123)	2X	1X	12.5

reverse primer (forward) 5'- CGCACCATCTTCTTCAAGGACGAC	10 µM	0.5 µM	1.25
forward primer (revearse) 5'- AACTCCAGCAGGACCATGTGATCG	10 µM	0.5 µM	1.25
genomic DNA (purified via QIAGEN DNeasy Kit)	--	--	1

Thermocycler conditions: 94 °C, 3 min; [(94 °C, 30 sec), (60 °C, 30 sec), (72 °C, 1 min)] x 30 cycles; 72 °C, 10 min; hold at 4 °C.

The resulting PCR product was analyzed by running 5ml on a 1% agarose gel.

2.4. In Situ Probe Synthesis

2.4.1. Synthesis of labeled RNA

To generate DNA for synthesis of in situ hybridization probes, plasmid DNAs encoding various genes of interest (cds sequences) were linearized just downstream of the gene to allow for transcription termination. Subsequently, linearized plasmid DNA was then purified using a PCR purification kit (QIAGEN, catalog number 28104). Probe synthesis was carried out using a Digoxigenin or fluorescein RNA labeling kit (Roche, catalog number 11175025910 or 11685619910) as follows:

Component	[Stock]	[Final]	µL/reaction
nuclease-free water	--	--	31.8
Transcription buffer	10X	1X	5

dig (or flu) labeled NTP mix	10X	1X	5
RNAse inhibitor	20 U/µL	0.8 U/µL	2
Linearized template DNA	1 µg/µL	0.02 µg/µL	1.2
RNA polymerase (T7, SP6, T3)	10 µM	0.5 µM	2.5

The reaction mixture was then incubated for 2 hours at 37 °C. However, since the SP6 polymerase is a weak promoter, reactions using this enzyme were incubated for 3 hours. To precipitate the labelled RNA probe, 1 µL of 20 µg/µL glycogen (Roche, catalog number 10901393001), 5 µL of 0.2 M EDTA, 6.3 µL of 4 M LiCl, and 190 µL of 100% ethanol were added, and the sample was allowed to precipitate overnight at -20 °C. The following day, the RNA was pelleted at 15,000 rpm at 4 °C for 10 minutes, washed with 250 µL of 70% ethanol, and resuspended in 30 µL of nuclease-free water. Probes were stored at -20 °C for short term or -80 °C for several years. Before storage and use, transcript quality was assessed via RNA gel electrophoresis.

2.4.2. RNA gel electrophoresis

RNA probes were assessed on a denaturing gel to minimize secondary structure formation and allow for accurate size determination. In a 500-mL conical flask, 1 g of agarose was dissolved in 84.8 mL of dH2O. Inside a fume hood on a hot plate, 5.2 mL of 37% formaldehyde (Fisher, catalog number BP531) was added, followed by 10 mL of 10X MOPS and mixed by swirling gently. The gel was

cast immediately, and after solidifying, the chamber was flooded with 1X MOPS running buffer. Each lane was loaded with 1-2 µL of RNA probe, 1 µL of 0.1% ethidium bromide (Fisher, catalog number BP1302), and 17 µL of 2X RNA loading buffer (supplied with labelling kit). Distinct bands on the gel indicate a high-quality synthesis (Figure 2.3), whereas a smear indicates a lower quality synthesis or degradation. Multiple bands due to residual template DNA is normal and will still produce good in situ results.

2.5. Expression Analysis

2.5.1. Whole mount in situ hybridization

Mouse hindbrain tissue can be effectively processed for whole mount in situ hybridization provided unique requirements for each age and tissue type are taken into consideration. E8.5 – 9.5 embryos can be processed whole as long as the E9.5 embryos have holes poked in brain ventricles and should only be fixed in PFA for a maximum of 4-5 hours. E10.5 embryos are best processed with the trunks removed and small holes poked, however, some trapping in the brain ventricles is unavoidable. For E11.5 and older, thorough dissection of the hindbrain away from the pial membrane and surrounding tissues is essential for high quality staining. For embryos E11.5 – 12.5, the removal of the pial membrane can be performed before or after staining. E10.5 embryos and older were fixed in PFA-DEPC overnight at 4 °C. The next day, embryos were subjected to 10-minute washes in 25%, 50%, 75% and 100% methanol diluted in PBS-DEPC. After the wash in 100% methanol, the methanol was replaced and the tissue stored at -20 °C. Strong

staining can be achieved with embryos stored in methanol for eight months or less, and up to two years in some cases. All reagents up to and including the post-hybridization washes at 70 °C should be DEPC treated to avoid RNA degradation. A clean workspace is necessary to further minimize the possibility of RNAse contamination. Samples should be constantly rocking during the procedure for best reagent penetration. Also, 20-mL scintillation vials with a minimum of 5 mL of solution should be used, with the exception of the hybridization step and antibody steps.

To begin the *in situ* hybridization procedure, embryos were bleached in 5:1 methanol:30% hydrogen peroxide at room temperature for 30 minutes. Next, they were rehydrated via 10-minute washes in 66% and 33% methanol in PBT, followed by two five-minute washes in PBT. To permeabilize the tissues, embryos were treated with 20 µg/mL proteinase K in PBT for one minute per embryonic day of development; for example, an E12.5 hindbrain is treated for 12.5 minutes. After two five-minute PBT washes, the embryos were re-fixed in 4% PFA/0.25% glutaraldehyde for 20 minutes, followed by two more five-minute PBT washes. After transferring the embryos to 2-mL screwcap tubes, samples were washed with pre-warmed hybridization buffer at 69 °C for 5 minutes, and then incubated with new buffer for at least two hours at 69 °C, however, longer is preferred. To hybridize the probe, samples were incubated in diluted probe (diluted to either 1:250 for less sensitive probes or 1:500 for more sensitive probes) in pre-warmed hybridization buffer overnight with gentle rocking.

The next day, the probe solution was removed and stored at -20 °C. Diluted probes can be reused up to three times. Embryos were then transferred to new 20-mL scintillation vials and incubated twice for 45 minutes each with 2X SSC/0.1% CHAPS, then 0.2X SSC/0.1 CHAPS for 30 minutes (all 4 washes should still be kept at 69 °C). Next, samples were brought to room temperature with two five-minute washes in TBST. To remove any remaining non-hybridized probe, embryos were incubated in 50 µg/mL RNAse A in TBST for 30 minutes at 37 °C, followed by two five-minute washes in TBST at room temperature. For the blocking step, samples were incubated in 3 mL of 20% heat-inactivated goat serum in TBST for at least one hour at 4 °C, however, longer incubations, up to 4 hours long appeared to result in far less background. The secondary antibody, anti-digoxygenin or anti-fluorescein conjugated to alkaline phosphatase (Roche, catalog number 11093274910 or 1426338) was then added directly to the vial at 1:1500 and was incubated overnight at 4 °C.

The next day, unbound antibody was washed away with at least six washes in TBST at 4 °C, followed by an overnight wash in a larger volume at 4 °C. On the final day, embryos were washed three times for 30 minutes each with TBST at 4 °C. To create optimal conditions for the alkaline phosphatase enzyme, samples were washed twice for 15 minutes in AP buffer, and were then transferred to 12-well tissue culture plates (Falcon 353043). To initiate the color reaction, samples were incubated in the dark at 37 °C with the substrates NBT (2.34 µg/mL) and

BCIP (1.75 µg/mL) diluted in AP buffer. A typical color reaction takes three to four hours, though some probes can take several days at room temperature. Probes proven to require longer incubations can be accelerated by incubation at 37°C and NBT/BCIP solutions can be replaced as needed, as they will come out of solution during longer incubations. Once the color reaction was satisfactory, samples were washed twice in PBS for 5 minutes, followed by an overnight fixation in 4% PFA.

To prepare for imaging after fixation, embryos were washed twice in PBS for 5 minutes, followed by 25%, 50%, then 70% glycerol for a minimum of 10 minutes for each, however, slowly transitioning to glycerol reduces shrinkage of the samples. Samples were then mounted on slides in 70% glycerol and imaged. Samples stored in glycerol are good for many years if kept at 4 °C.

2.5.2. Two-color whole mount in situ hybridization

Two-color staining, though difficult, can be achieved. The initial steps are identical to the single-color technique (2.5.1), except that both probes should be added at the hybridization step. One probe must contain the digoxygenin hapten and the other must contain the fluorescein hapten. The initial color reaction must be done with the NBT/BCIP substrates, but can be used to detect either the digoxygenin or fluorescein probe. For two-color staining, the NBT/BCIP color reaction was stopped by washing with 0.1% Tween, followed by 0.1 M glycine-HCl (pH 2.2) for 30 minutes at room temperature in order to deactivate alkaline phosphatase. It is vital to not fix in PFA at this step. After transferring the embryos

to new scintillation vials, they were washed twice with TBST at room temperature. Thereafter, the blocking step, antibody incubation, and post-antibody washes were performed as in the single-color in situ protocol (2.5.1).

To prepare samples for the second color reaction, samples were moved to 12-well culture plates and washed rapidly, at least three times with Tris-HCl (pH 8.2). The Fast Red substrate was then prepared according to the manufacturer's instructions (Sigma, catalog number F4648), using 1 mL per well. Subsequently, embryos were incubated in the dark at room temperature for as long as necessary, usually several days. The Fast Red substrate should be replaced up to four times per day, as it will rapidly come out of solution. Also AP activity with FastRed substrate persists much slower as compared to AP activity with NBT/BCIP. Once the desired color intensity was obtained, the samples were then rinsed twice in PBS for five minutes, followed by an overnight fixation in 4% PFA at 4 °C. The embryos were brought to 70% glycerol as before and were subsequently imaged. This is more instructions than a method section

2.6. Hindbrain explant and bead migration assay

2.6.1. Hindbrain Dissection and Culture

Timed matings were set up between mice expressing GFP in branchiomotor neurons (SE1::GFP). Embryos collected at E11.5. were first screened for the presence of the GFP transgene. Embryos were kept in ice-cold L-15 media (Gibco, 21083-027, stored at 4°C). Based on the number of GFP-expressing embryos, a

6 well plate containing 8.0 µm polycarbonate membrane inserts (Corning costar, 3428) was prepared by placing 200 µL laminin (Sigma, L2020, prepared at 0.003 µg/µl in 1X-PBS-DEPC) on each filter. The 6-well plate was then placed in a 37°C, 5% CO2 incubator for an hour to allow for sufficient coating (Heraeus, Hera Cell 150). Neurobasal mix was prepared and warmed to 37°C.

GFP-expressing embryos were dissected in cold L-15 media. To determine genotype, hand plates were taken from embryos at the same time that the hindbrain was removed, however, genotyping was performed only after the scoring of the chemoattraction/rostral migration phenotype ensuring blinding. After all hindbrains were dissected, the 6 well plate was removed from the incubator. Inserts were processed one at a time by removing the insert from the plate, blotting it on a clean KimWipe to remove excess laminin, and was then placed in a separate sterile 6-well plate. A Hindbrain explant was placed on each insert and positioned so that it was as flat as possible. Excess L-15 transferred while placing the explant was removed by dabbing on a clean kimwipe. After the explants were plated and excess media removed, 340 µL of fresh Neurobasal mix was added to the underside of each membrane filter. Once all hindbrain explants were placed on to filters, 6-well plates contain explants were then place into the 37°C, 5% CO2 incubator for 30 minutes to allow hindbrains to adhere to the filter. After 30 minutes had elapsed, protein coated or PBS treated beads were placed immediately rostral to FBM neurons using forceps and a stereomicroscope equipped with epifluorescence. Because beads dry out very quickly, it was important to keep

them in a covered dish containing 1X-PBS between explants. Also, as beads dry out, 0.5ml of PBS should be added to beads as needed. Once beads were positioned, plates were again place into the 37°C, 5% CO2 incubator for another 30 minutes to allow beads to settle into position before imaging. Explants were viable for ~48 hours under these conditions.

2.6.2. Preparing *Wnt5a*-soaked beads

Affi-gel blue gel (Bio-Rad, 153-7301, stored at 4°C) are composed of agarose beads cross-linked to a blue dye that allows for the specific binding of proteins. To allow for efficient protein binding, the beads were soaked in WNT5A protein or 1X-PBS-DEPC for 24 hours before use. To prepare the beads, 200 µL of beads were centrifuged at 5000 rpm (Eppendorf microfuge, 5424) in 1.5 mL tubes at room temperature for 2 minutes, the supernatant was discarded, and the beads were washed in 1X-PBS-DEPC two times. Clean beads were stored in 400 µL 1X-PBS-DEPC at 4°C for up to one week. 25 µL of clean beads were then placed in a 35mm petri dish, and the 1X-PBS-DEPC was carefully removed. Five µL of WNT5A protein (R&D, 645-WN, stored at -80°C), or 1X-PBS-DEPC was then pipetted onto the beads. The petri dish was then sealed, placed inside of a larger dish containing 1X-PBS-DEPC, and then stored at 4°C overnight.

2.6.3. Imaging explants and scoring migration phenotype

After the beads were placed on explants, they were incubated at 37°C for another 30 minutes to allow the tissue to adhere to the filter. Explants were first

imaged at this time, designated as time zero. Explants were then incubated (37°C, 5% CO2 incubator, Heraeus, Hera Cell 150) and imaged 24 hr and 48 hr later. In early experiments, images were acquired under brightfield illumination (Olympus SZX12 stereomicroscope) to observe the health of the tissue and the bead placement. Images were also acquired under GFP fluorescence to observe the migration of the FBM neurons. The distribution of FBM neurons at the three time points was scored by comparing the images to the zero time point image. Importantly, this was done before genotyping, allowing one to assess chemoattraction in a blinded fashion. In most cases, FBM neurons migrated up to and surrounding the most caudally placed beads into r3. Chemoattraction resulting in rostral migration surpassing 1 bead diameter was considered “strong” migration, while chemoattraction resulting in rostral migration extending less than one bead diameter was considered “weak” migration.

2.7. Other Protocols and Methods

2.7.1. Common use solutions

1X PBS (4 L)

Component	Amount	[Stock]	[Final]
NaCl (M.W. 58.44)	32g	100%	136.89mM
KCl (M.W. 74.56)	0.8g	100%	2.68mM
Na2HPO4 • 7 H2O (M.W. 268.07)	640 mL	0.1M	16mM

NaH2PO4 • H2O (M.W. 137.99)	160 mL	0.1M	4mM
ddH2O	to 4L	-	-

Add enough ddH2O to dissolve solids, then bring up to 4 L with ddH2O in a 4-L beaker. Aliquot into 4 x 1 L and 8 x 500 mL bottles and autoclave.

4% PFA-PBS (1 L)

Component	Amount	[Stock]	[Final]
Paraformaldehyde	41.67g	96%	4%
1X PBS-DEPC	to 1L	-	-

In a fume hood, add the solid paraformaldehyde and approximately 800 mL of 1X PBS to a 2-L conical flask. Cover the opening of the flask with plastic wrap and stir with medium heat for 20 minutes or up to an hour to dissolve. Add 6 to 8 drops of 10 N NaOH to clear the solution. Filter the solution though a funnel fitted with filter paper into a 1-L graduated cylinder, then bring up to 1 L with 1X PBS-DEPC. Aliquot into 15- or 50-mL tubes and store at -20 °C.

10X TBE (1L)

Component	Amount	[Stock]	[Final]
Tris base (M.W. 121.14)	108 g	100%	0.88 M

Boric acid (M.W. 61.83)	55 g	100%	0.88 M
EDTA, pH 8.0	40 mL	0.5 M	0.2 M
ddH2O	to 1L	-	-

This reagent does not need to be autoclaved. Dilute to 0.5X – 1X concentration for use in electrophoresis.

10X MOPS Buffer (1L)

Component	Amount	[Stock]	[Final]
MOPS (M.W. 209.26)	46.3 g	100%	0.2 M
EDTA • 2 H2O (M.W. 372.24)	3.72 g	100%	0.01 M
ddH2O	to 1 L	-	-

Adjust to pH 7.0 before bringing to final volume of 1 L. Autoclave for 20 minutes.

Heat Inactivation of serum

Heat-inactivated serum is desirable for some protocols and applications. To prepare for heat inactivation, thaw unopened serum at 4 °C. Bring a waterbath to 56 °C. Then, bring the unopened container of serum to 56 °C, swirling every five minutes to assure even heating. Once thawed, incubate the serum for precisely 30 minutes. Immediately after incubation, place the serum on ice, separate into aliquots, and store at -20 °C. Multiple freeze-thaw of serum should be avoided.

Treatment of solutions with diethyl pyrocarbonate (DEPC)

DEPC treatment of solutions is desirable in applications where RNAse contamination and degradation of RNA is of concern (e.g. in situ hybridization). To inactivate RNAse, DEPC can be added directly to a previously autoclaved or freshly made solution. Add 1 mL of 100% DEPC (Sigma, catalog number D-5758) per 1 L of solution (0.1% final concentration). Shake vigorously, incubate overnight in a fume hood with loosened caps, then autoclave the following day.

2.7.2. Reagents for whole mount in situ hybridization

To eliminate RNAse contamination during in situ hybridization, use diethyl pyrocarbonate (DEPC)-treated reagents for all steps up to and including the hybridization of the riboprobe. After hybridization, either DEPC-treated or untreated solutions may be used.

PBT (50 mL)

Component	Amount	[Stock]	[Final]
Triton X-100 (in PBS-DEPC)	500 µL	10%	0.1%
PBS-DEPC	45.5 mL	-	-

Do not autoclave. Make fresh during in situ hybridization procedure.

Proteinase K Solution (5 mL)

Component	Amount	[Stock]	[Final]
Proteinase K (Sigma P4850)	4 µL	800 U/mL	0.64 U/mL
PBS-DEPC	4.996 mL	-	-

Do not autoclave. Make fresh during in situ hybridization procedure.

PFA/Glutaraldehyde Solution (5 mL)

Component	Amount	[Stock]	[Final]
Glutaraldehyde (EMD GX015305)	50 µL	25%	0.25%
PFA-DEPC	4.95 mL	-	-

Do not autoclave. Make fresh during in situ hybridization procedure.

20X SSC (1 L)

Component	Amount	[Stock]	[Final]
NaCl (M.W. 58.44)	175.3 g	100%	2.99 mM
sodium citrate	88.2 g	100%	290 mM
ddH2O	to 1 L	-	-

Dissolve solids in approximately 800 mL of ddH2O. Adjust to pH 7.0 with 10 N NaOH, then bring to final volume. Autoclave for 20 minutes.

Hybridization Buffer (50 mL)

Component	Amount	[Stock]	[Final]
Formamide (Fisher BP228)	25 mL	100%	50%
SSC-DEPC	12.5 mL	20X	5X
EDTA-DEPC, pH 8.0	500 µL	0.5 M	5 mM
Triton X-100	500 µL	10%	0.1%
CHAPS (Sigma C3023)	500 µL	10%	0.1%
Heparin (Sigma H3393)	50 µL	50 mg/mL	100 µg/mL
Yeast tRNA (Roche 10109223001)	50 mg	-	-
Blocking reagent (Roche 1096176)	1 g	-	-
ddH2O-DEPC	to 50 mL	-	-

Prepare this buffer in a 50-mL tube, inverting frequently during preparation. Incubate in 55 °C water bath to help dissolve. Seal the cap with laboratory film and store at -20 °C.

2X SSC/0.1% CHAPS Post-Hybridization Wash (50 mL)

Component	Amount	[Stock]	[Final]
SSC-DEPC	5 mL	20X	2X
CHAPS (Sigma C3023)	50 mg	100%	0.1%
ddH2O-DEPC	45 mL	-	-

Do not autoclave. Prepare this solution at the end of day 1 of the in situ hybridization procedure, and incubate overnight in the hybridization oven.

0.2X SSC/0.1% CHAPS Post-Hybridization Wash (50 mL)

Component	Amount	[Stock]	[Final]
SSC-DEPC	500 mL	20X	0.2X
CHAPS (Sigma C3023)	50 mg	100%	0.1%
ddH2O-DEPC	49.5 mL	-	-

Do not autoclave. Prepare this solution at the end of day 1 of the in situ hybridization procedure, and incubate overnight in the hybridization oven.

RNAse A Solution (10 mL)

Component	Amount	[Stock]	[Final]
Ribonuclease A (Sigma R4642)	50 µL	30 mg/mL	50 µg/mL
TBST	9.950 mL	-	-

Do not autoclave. Make fresh during in situ hybridization procedure.

TBST (100 mL)

Component	Amount	[Stock]	[Final]
Tris-HCl, pH 7.5	5 mL	1 M	50 mM
NaCl	15 mL	1 M	150 mM
KCl	1 mL	1 M	1 mM
Triton X-100 (Fisher BP151)	1 mL	100%	1%
ddH2O	78 mL	-	-

Do not autoclave. Make fresh during in situ hybridization procedure.

20% Goat Serum in TBST (10 mL)

Component	Amount	[Stock]	[Final]
Heat inactivated goat serum (Invitrogen 16210, not filtered, heat inactivated at 56 °C)	2 mL	100%	20%

TBST	8 mL	-	-

Do not autoclave. Make fresh during in situ hybridization procedure and store on ice until use.

Alkaline Phosphatase (AP) Buffer (50 mL)

Component	Amount	[Stock]	[Final]
Tris-HCl, pH 9.5	5 mL	1 M	100 mM
NaCl	5 mL	1 M	100 mM
MgCl2	2.5 mL	1 M	50 mM
Tween-20 (Sigma P9416)	50 µL	100%	0.1%
ddH2O	37.45 mL	-	-

Do not autoclave. Make fresh during in situ hybridization procedure.

NBT/BCIP Color Reaction Solution (~5 mL)

Component	Amount	[Stock]	[Final]
NBT (Roche 1383213001)	16.88 µL	100 mg/mL	2.34 µg/mL
BCIP (Roche 1383221001)	17.5 µL	50 mg/mL	1.75 µg/mL

AP buffer	5 mL	-	-

Do not autoclave. Make fresh during in situ hybridization procedure.

2.7.3. Reagents for hindbrain explants

Neurobasal Mix (4 mL)

Component	Amount	[Stock]	[Final]
Neurobasal media (4° C) (Invitrogen 12348-017)	3.44 mL	1x	0.85x
GDNF in Neurobasal media (4° C) (R&D 212GD)	400 µL	0.001%	0.00085%
Antibiotic Antimycotic (AA) (-20° C) (Sigma A5955)	40 µL	100x	1x
GlutaMAX (Room Temperature) (Invitrogen 35050-079)	40 µL	100x	1x
B-27 (-20° C) (Invitrogen 17504-044)	80 µL	50x	1x

GDNF stock was reconstituted at 10 mg/mL in sterile 1XPBS containing 0.1% BSA and stored in 5 µL aliquots at -20°C until diluted 1:1000 in neurobasal media. The dilution could be stored at 4°C for up to one month.

Chapter 3: *Celsr1* Suppresses *Wnt5a*-Mediated Chemoattraction to Prevent Incorrect Rostral Migration of Facial Branchiomotor Neurons

3.1 INTRODUCTION

During vertebrate brain development, many types of differentiating neurons will migrate considerable distances in order to establish the complex circuits required for cognitive and motor function. Within the hindbrain, facial branchiomotor (FBM) neurons, which innervate the facial and jaw muscles, typically migrate caudally from rhombomere 4 (r4) to form a motor nucleus in r6 (nVII; Chandrasekhar, 2004; Guthrie, 2007; Song, 2007), however, in mice lacking the atypical cadherin and PCP component *Celsr1* (Curtin et al., 2003), some FBM neurons inappropriately migrate rostrally into r3 and r2 instead of caudally (Qu et al., 2010). As a PCP gene, *Celsr1* is involved in polarizing various tissues during development (Wansleeben et al., 2011, Chen et al., 2008, Ravni et al., 2009, Brzoska et al., 2016, Qu et al.,2014). During PCP signaling, CELSR molecules on neighboring cells participate in homophilic interactions and simultaneously bind mutually antagonistic PCP components FRIZZLED and VANGL2 to allow for their asymmetrical localization *(*Shafer et al., 2011; Kelly et al., 2016; Montcouquiol et al., 2006 Stahley et al., 2021; Bastock et al., 2003; Struhl et al., 2012*). Celsr1* may also function to regulate assembly of the FRIZZLED-DISHEVELLED complex required for canonical Wnt signal transduction (Nishimura et al., 2012, Chen et al., 2008).

To determine where *Celsr1* is functioning within the hindbrain to prevent inappropriate rostral migration of FBM neurons, several tissue-specific conditional *Celsr1* knockouts were previously generated using a floxed *Celsr1* allele in combination with various Cre drivers. Interestingly, the deletion of *Celsr1* exclusively in FBM neurons *did not* result in rostral migration as seen in *Celsr1* knockout embryos, suggesting that *Celsr1* is functioning non-cell autonomously to prevent rostral migration (Qu et al., 2010). Furthermore, inactivation of *Celsr1* in floorplate cells using a *Sonic Hedgehog (Shh) -Cre* did not result in any rostral migration. Deletion of *Celsr1* exclusively in rhombomere 4 (r4-Cre) generated a weak rostral migration phenotype. Importantly, inactivation of *Celsr1* in r3 and r5 (*Krox-Cre*) or in the ventricular zone of all rhombomeres (*Nkx6.2-Cre*) both resulted in extensive rostral migration, and frequently resembled the *Celsr1* knockout phenotype. These data strongly suggest that *Celsr1* functions within the ventricular zone, rostral to r4 to suppress the inappropriate rostral migration of FBM neurons (Glasco et al., 2016). Furthermore, anterograde dye-labeling experiments suggested that the rostral migration of FBM neurons in *Celsr1* mutants is not due to a loss of polarity, but is instead due to the loss of a local guidance cue (Glasco et al., 2016).

Importantly, the suposed chemoattractant, *Wnt5a*, is expressed rostral to r4, directly adjacent to the floorplate/midline. However, caudal to r4, *Wnt5a* is expressed in a broad fashion with areas of greater expression found more laterally (Fig.3.1). It is unclear whether *Celsr1* and *Wnt5a* are co-expressed. Interestingly, *Wnt5a* has been shown to regulate the migration of several non-neuronal cell types

(Ka Toh and Ka Toh, 2007; Hasan et al., 2017; Kim et al., 2020), as well as the axon out-growth/pathfinding of commissural neurons (Lyuksyutova et al., 2003; Onishi et al., 2013). Based on the expression of *Wnt5a* within the hindbrain and its known chemotactic roles, others have embedded beads treated with WNT5A protein into the hindbrains of mouse embryos cultured *ex vivo* in order to provoke the ectopic migration of FBM neurons (Vivancos et al., 2009). While this would suggest that *Wnt5a* is indeed capable of acting as a chemoattractive cue, *Wnt5a* knockout animals exhibit relatively normal caudal migration, and thus the role for *Wnt5a* during the caudal migration of FBM neurons remains uncertain (Vivancos et al., 2009).

Instead, we propose that the rostral migration of FBM neurons in *Celsr1* mutants could be dependent on *Wnt5a*-mediated chemoattraction i.e. *Celsr1* acts to suppress *Wnt5a* in r3 of the hindbrain to prevent the inappropriate rostral migration of FBM neurons (Fig. 3.1). To investigate *Wnt5a* as the sole source of chemoattraction acting to entice the rostral migration of FBM neurons in *Celsr1* mutants, we evaluated the extent of rostral migration in *Celsr1*; *Wnt5a* double mutants as well as *Celsr1* mutants with increased *Wnt5a* expression in hindbrain segment r3 (*Celsr1*$^{KO/KO}$; *Wnt5a*^{GOF}).

Furthermore, the downstream regulator of Wnt signalling, *Dishevelled2* (*Dvl2*), is expressed throughout the hinbrain and in contrast to *Celsr1* mutants, *Celsr1*; *Dvl2* double mutants **do not** exhibit inappropriate rostral migration (Glasco et al., 2012). Based on this, we asked whether *Dvl2* function is required for the

Wnt5a-mediated chemoattraction of FBM neurons. To examine a possible role for *Dvl2* regulating *Wnt5a*-mediated chemoattraction, we evaluated the apparent chemoatttraction of FBM neurons in response to agarose beads treated with WNT5A protein, in a *Dvl2*-deficient background.

3.2 RESULTS

3.2.1 Celsr1 is Expressed in a Complementary Domain with respect to FBM Neurons and Wnt5a

To provide further insight into how *Celsr1* is functioning to regulate FBM neuron migration, its expression was examined relative to migrating FBM neurons and the area of *Wnt5a* expression. Importantly, it appears that *Celsr1* is expressed within the peri-ventricular zone from E10.5-E12.5, adjacent and lateral to the floor plate, spanning the entire rostro-caudal extent of the hindbrain. At E11.5, *Celsr1* is expressed within the ventricular zone, spanning all rostro-caudal levels of the hindbrain, however, only in an area immediately dorsal to the floor plate (Qu et al., 2010; Fig. 3.1).

Importantly, *Celsr1* is not expressed (Fig. 3.1) nor does it function within FBM neurons, suggesting that *Celsr1* is functioning non-cell autonomously (Qu et al., 2010). *Wnt5a* also exhibits a restricted expression pattern at E11.5, with a rostro-medial domain extending up to the r3-r4 boundary, and a more broad expression domain evident from the r4-r5 boundary. Therefore, *Celsr1* and *Wnt5a* expression domains overlap within r3 and r2 (Fig. 3.1C-E). Importantly, even though the rostral *Wnt5a* domain extends up to and abuts the rostral most FBM

neurons in r4 (Fig. 3.1), these neurons never migrate into r3 of wildtype embryos (Qu et al., 2010). Also, *Wnt5a* expression does not appear to be affected in *Celsr1* mutants (Glasco et al., 2016).

3.2.2 Rostral Migration Phenotype is Rescued in Celsr1; Wnt5a Double Mutants

We propose that the putative chemoattraction of FBM neurons near the r3-r4 boundary (and therefore, the rostral source of *Wnt5a*) is normally suppressed by *Celsr1* (Glasco et al., 2016) (Fig. 3.1). However, in *Celsr1* knockouts, this suppression is relieved, resulting in FBM neurons migrating into r3 and r2 (Fig. 3.1). Furthermore, if *Wnt5a* is functioning as the primary chemotactic cue acting to entice the inappropriate rostral migration observed in *Celsr1* mutants, and *Celsr1* normally acts to suppress *Wnt5a* in the WT hindbrain preventing chemoattraction, then knockout of *Wnt5a* in addition to *Celsr1* should result in rescue of the rostral migration phenotype. Our model predicts that the rostral migration seen in *Celsr1* single mutants would not occur in *Celsr1*; *Wnt5a* double mutants because the rostral source of *Wnt5a* has been removed (Fig. 3.1).

But first, to examine how individual genetic backgrounds combined with *Celsr1* and *Wnt5a* mutation lends to penetrance and expressivity of the rostral migration phenotype, a thorough analysis of both *Celsr1* and *Wnt5a* single mutants was performed. Here, embryos were processed via in situ hybridization using digoxygenin-labelled Tbx20 probe. Because in *Celsr1* mutants, left and right hemispheres often exhibit varying amounts of rostral migration, we speculate that the two sides/populations are to some extent regulated independently of one

Figure 3.1 *Celsr1* and *Wnt5a* Expression Domains Overlap within the Rostral Hindbrain

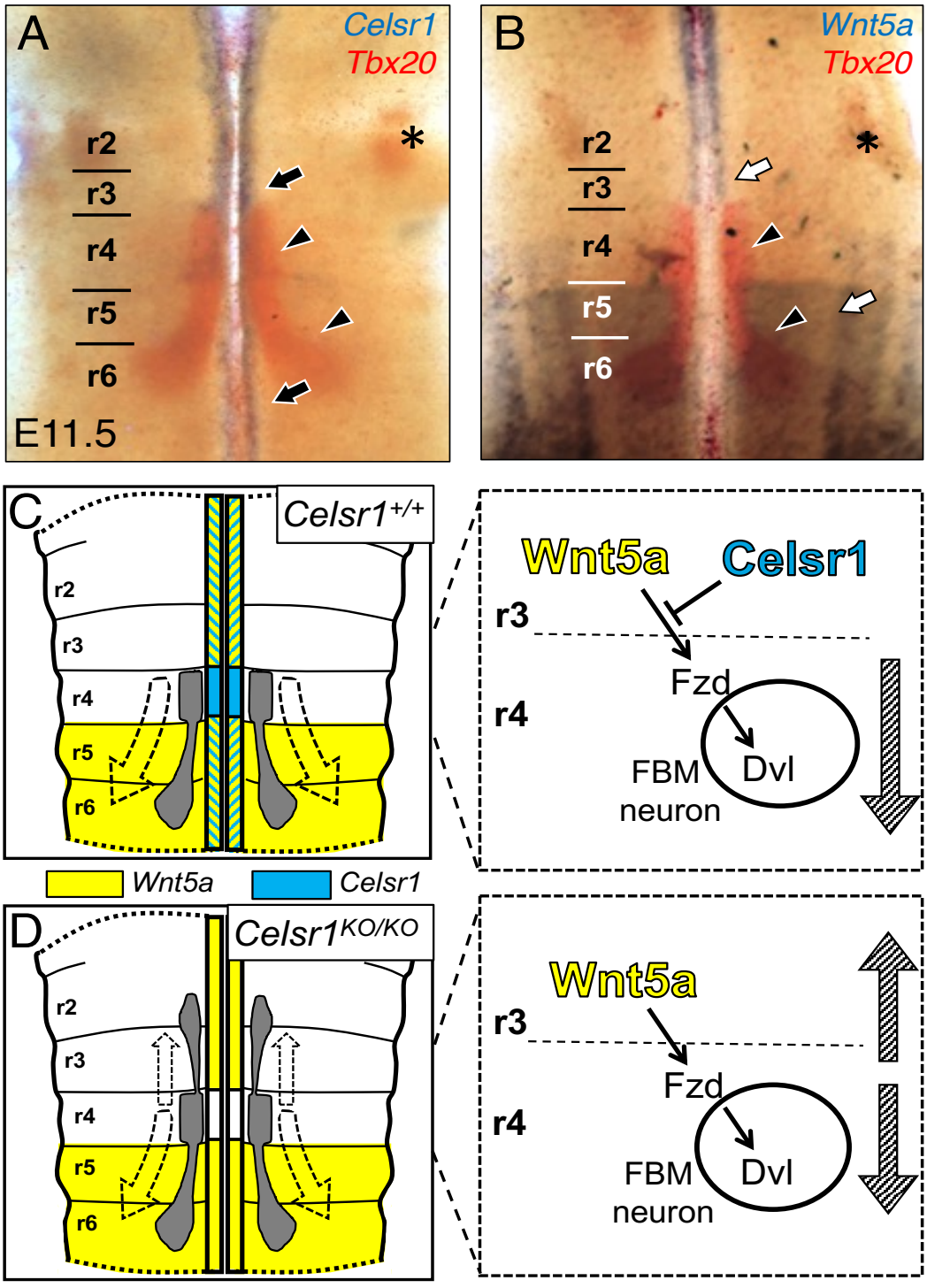

Figure 3.1 *Celsr1* and *Wnt5a* Expression Domains Overlap within the Rostral Hindbrain

(A, B) Dorsal views of hindbrains processed for two-color in situ hybridization. Transcription factor, *Tbx20* (red) is expressed within and marks FBM neurons (arrowheads in A, B) as well as the trigeminal motor neurons in r2 (asterisks). (A) *Celsr1* is expressed medially along the entire rostrocaudal extent of the hindbrain (black arrows). (B) *Wnt5a* expression (white arrows) is absent in r4, extends medially up to the r3/r4 boundary and is evident in a broad domain in the caudal hindbrain from the r4/r5 boundary. (C) Schematic of *Celsr1* and *Wnt5a* expression patterns in a wildtype hindbrain and working model for regulating FBM directionality. Broken line arrows denote the birth of FBM neurons in r4, caudal migration into r5 and r6, and subsequent dorsolateral migration within r6. In r3, *Celsr1* suppresses *Wnt5a* function and prevents the rostral migration of FBM neurons into r3, resulting exclusively in caudal migration (hatched “down” arrow). (D) In a *Celsr1* knockout (KO), loss of *Celsr1* expression (function) relieves suppression of *Wnt5a* function, leading to rostral migration of some FBM neurons (“up” arrows) toward the WNT5A chemoattractant in the rostral hindbrain. A large number of FBM neurons migrates caudally as in wildtype (“down” arrows). Scale bar (in B) for A-B, 400 μm.

another. For this reason, each side was scored separately. Consistent with previous observations, no rostral migration was observed among *Wnt5a* KO/KO embryos (Vivancos et al., 2009), however, in *Celsr1* KO/KO animals, extensive rostral migration was evident. This was true for 86% (43/50) of all *Celsr1* mutant hemispheres scored, while only 7% (2/28) of *Celsr1* +/KO exhibited any amount of rostral migration (Fig. 3.2).

To test our model and determine whether or not *Celsr1* does indeed act to suppress *Wnt5a* chemoattraction within the rostral hindbrain, *Celsr1*+/KO; *Wnt5a*+/KO double heterozygous mice were mated. Resulting E12.5 embryos harvested from timed pregnant females were genotyped and subsequently processed for Tbx20 in situs. In doing so, expected genotypes were recovered in roughly Mendelian ratios, with a slight overrepresentation of double mutants, which often exhibited open neural tubes characteristic of Wnt/PCP mutants like Looptail (*Vangl2*-/-) (Curtin et al., 2003; Glasco et al., 2012). As anticipated, FBM neurons migrated rostrally into r3 and r2 in *Celsr1*KO/KO; *Wnt5a*+/+ embryos obtained from these crosses (Fig. 3.3) just as they had in *Celsr1*KO/KO embryos obtained from single heterozygote matings (Fig. 3.2). Consistent with the single mutant analysis, *Celsr1* mutation alone, resulted in rostral migration in 87.5% of all hemispheres scored.

Also consistent with the single mutant analysis, FBM neurons never migrated rostrally in *Wnt5a*KO/KO embryos obtained from double heterozygote crosses (Fig. 3.3) suggesting that introducing either *Celsr1* or *Wnt5a* mutant alleles

to the other alleles genetic background does not greatly exacerbate or in any way contribute to rostral migration. Interestingly, reducing the amount of *Wnt5a* expression by removing one wildtype allele reduced the incidence of rostral migration in *Celsr1*KO/KO; *Wnt5a*+/KO embryos as compared to *Celsr1* mutant embryos(Fig. 3.3). *Celsr1*KO/KO; *Wnt5a*KO/+ embryos exhibited only an Intermediate amount of rostral migration where only 64% all hemispheres exhibited some degree of rostral migration, suggesting that chemoattraction towards *Wnt5a* is to some degree a dosage dependent process. Finally, eliminating *Wnt5a* activity nearly suppressed all inappropriate rostral migration in *Celsr1*KO/KO; *Wnt5a*KO/KO embryos (Fig. 3.3) as predicted by our model (Fig. 3.1). Importantly, *Celsr1*KO/KO; *Wnt5a* KO/KO double mutant animals showed rostral migration in only 8% (2/26) of all hemispheres examined suggesting that *Wnt5a* is in fact acting as the primary chemotactic cue enticing the inappropriate rostral migration observed in *Celsr1* mutants.

3.2.3 Celsr1; Wnt5a Double Mutants Display Craniorachischisis-like Phenotype

Importantly, all *Celsr1*; *Wnt5a* double mutants evaluated appeared to exhibit an open hindbrain resembling the human condition, Craniorachischisis. Therefore, the suppression of rostral migration in double mutants may reflect the inability of FBM neurons to migrate into r3 due to potential defects within the hindbrain. To ensure that hindbrain structure and neural specification were not adversely affected as a result of both *Celsr1* and *Wnt5a* deletion, the expression of efferent neuron marker *Gata3* and rhombomere marker *Egr2/Krox20* was

evaluated. We found that *Gata3* and *Egr2/Krox20* were both expressed relatively normally in r3 of double mutant hindbrains (Fig. 3.4) ruling out non-specific causes for the loss of rostral migration, further supporting that idea that WNT5A is indeed functioning as the chemoattractant responsible for the rostral migration phenotype observed among *Celsr1*KO/KO embryos.

3.2.4 Chemoattraction Toward Wnt5a Treated Beads is Reduced in Dvl2 Mutants

As previously discussed, *Celsr1* mutants also deficient for *Dvl2* do not exhibit rostral migration as compared to *Celsr1* mutant animals (Glasco et al., 2012). Importantly, *Dvl2* is a downstream component of the canonical Wnt pathway, therefore we hypothesized that if *Wnt5a* is indeed functioning to attract FBM neurons into the rostral midbrain of *Celsr1* mutants, then animals deficient for *Dvl2* should exhibit reduced response to beads treated with WNT5A protein. Moreover, if *Wnt5a* signaling is achieved via *Dvl2* signal transduction then we would expect reduced *Wnt5a*-mediated chemoattraction among *Dvl2* mutant animals. To test this, we placed beads coated with recombinant WNT5A in the rostral hindbrains of control and *Dvl2* mutant explants cultured ex vivo and assessed the extent of rostral migration through observing GFP expression within FBM neurons (SE1:GFP). Based on the lack of consistent landmarks in these samples, explants were scored by comparing an image taken 24hrs after bead placement to an image taken only minutes after bead placement. Chemoattraction resulting in migration equal to 1 bead diameter or less was scored as “weak” attraction while migration greater than 1 bead diameter was scored as “strong” attraction.

Figure 3.2 FBM Migration Phenotypes in *Celsr1* and *Wnt5a* Single Mutants.

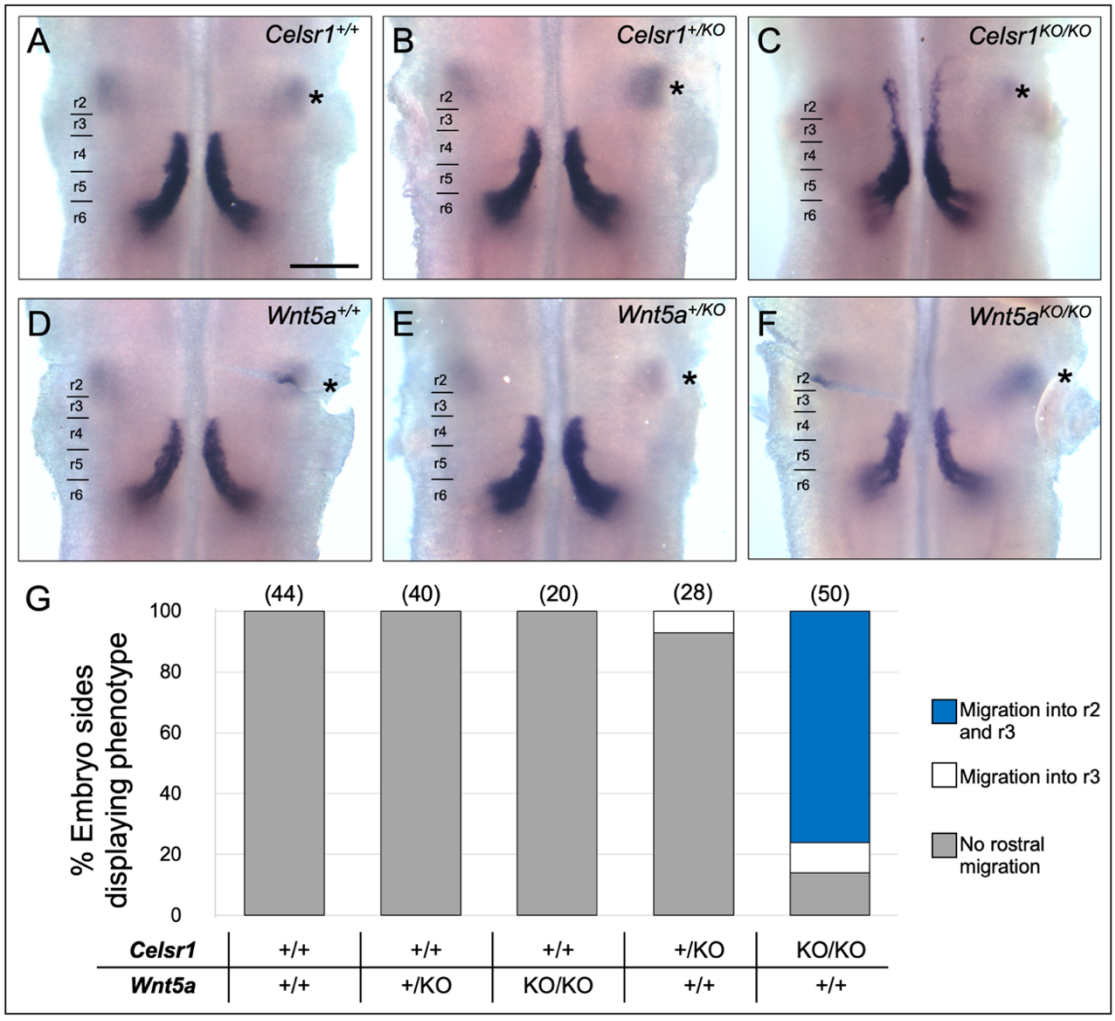

Figure 3.2 FBM Migration Phenotypes in *Celsr1* and *Wnt5a* Single Mutants.

(A-F) Dorsal views of E12.5 hindbrains processed for Tbx20 in situ hybridization. Tbx20 staining marks FBM neurons and trigeminal neurons (asterisk). For all samples, the extent of rostral migration was scored and subsequently quantified (G). While varying numbers of FBM neurons migrated rostrally in nearly all *Celsr1* mutants (C), these neurons never migrated rostrally in *Wnt5a* mutants (F). Rostral migration was scored separately for the left and right sides of the hindbrain due to variable expressivity of the phenotype. Number of embryo sides in parentheses (2X the number of embryos). Scale bar (in A) for A-F, 400 μm.

Figure 3.3 Rostral Migration Phenotype in *Celsr1* mutants is Rescued upon Knockout of *Wnt5a*

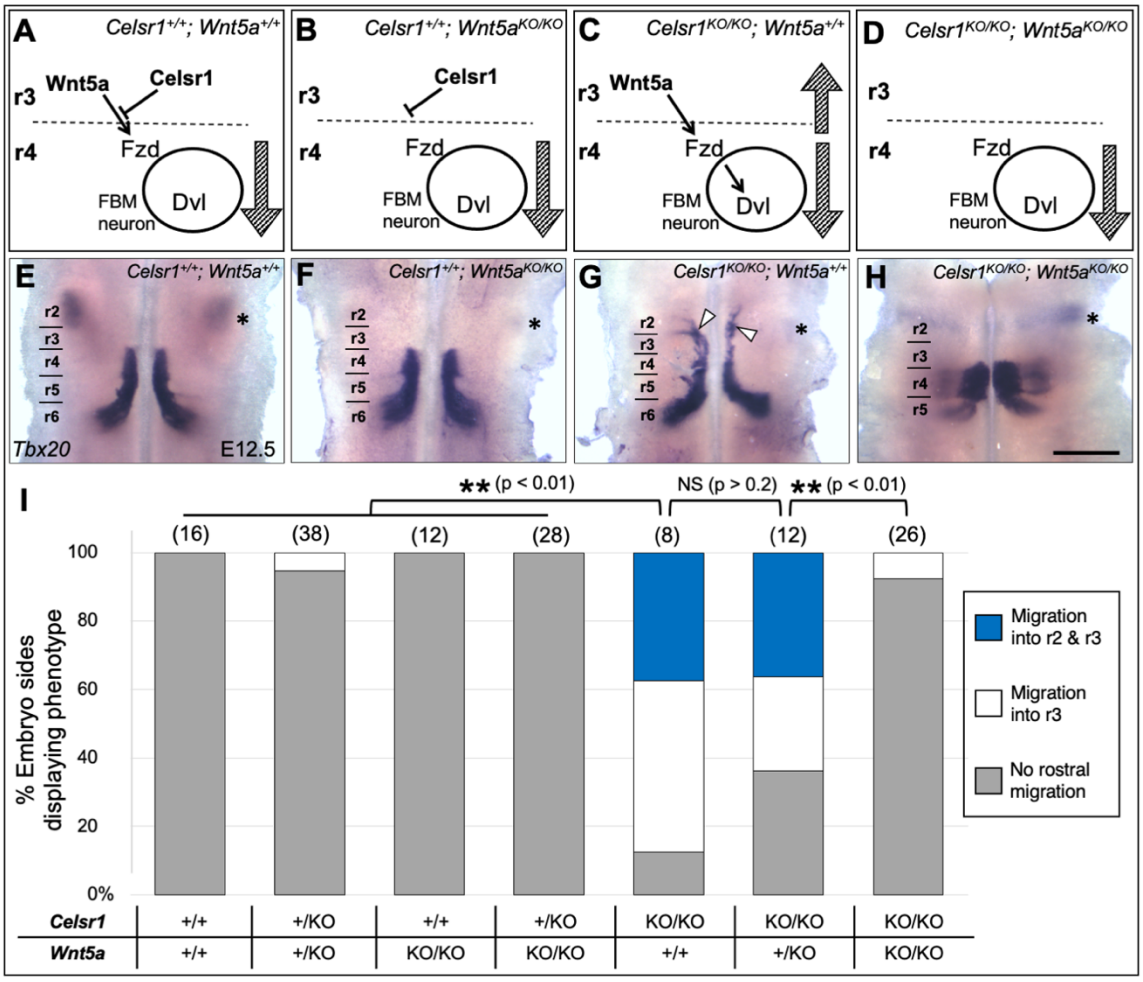

Figure 3.3 Rostral Migration Phenotype in *Celsr1* mutants is Rescued upon Knockout of *Wnt5a*

(A-D) Schematics of our working model of how *Celsr1* and *Wnt5a* function to regulate FBM neuron migration in different genetic conditions. The model predicts that FBM neurons will not exhibit any rostral migration defects in *Celsr1; Wnt5a* double mutants (D). (E-H) Dorsal views of E12.5 hindbrains processed for *Tbx20* in situs. (E) *Tbx20* is expressed in FBM neurons spanning r4 to r6, and the trigeminal motor neurons (asterisk). (F) In *Wnt5a* mutants, all FBM neurons migrate caudally into r5 and r6. (G) in *Celsr1* mutants, a large number of FBM neurons migrates rostrally into r3 and r2 (arrowheads). (H), As predicted, rostral migration is suppressed in double mutants. (I), Quantification of rostral migration phenotypes. The migration phenotypes on the left and right sides of the hindbrain were scored as independent data points because the rostral migration defect in *Celsr1* mutants varied in severity between the two sides. Number of embryo sides in parentheses (double the number of embryos). The differences between genotypes were tested using Student's t-test. Rostral migration defects were less prevalent in *Celsr1* mutants carrying one copy of *Wnt5a* compared to those with two copies. Scale bar (in H) for E-H, 400 μm.

Figure 3.4 Rhombomere 3 Develops Normally in *Celsr1*; *Wnt5a* Double Mutant Embryos

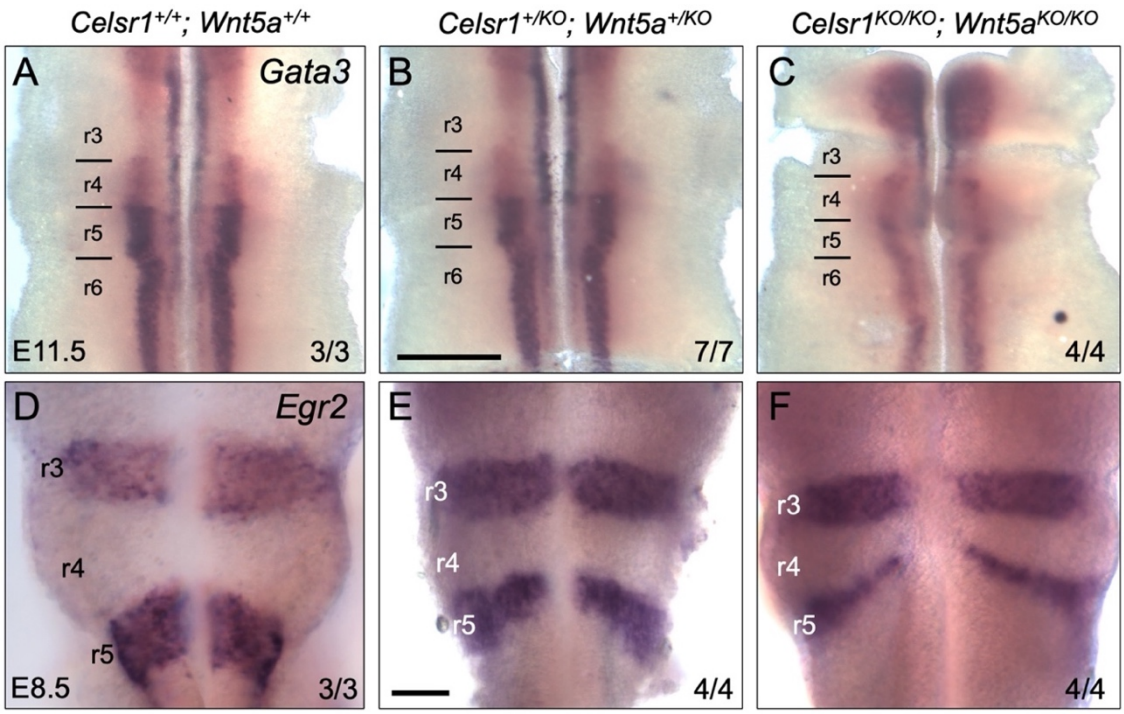

Figure 3.4 Rhombomere 3 Develops Normally in *Celsr1*; *Wnt5a* Double Mutant Embryos

(A-F) Dorsal views of E11.5 hindbrains processed for *Gata3* in situs (A-C) and E8.5 embryos processed for *Egr2* in situs (D-F). The expression patterns of both genes in various hindbrain, especially r3, were similar between wildtype, double heterozygous and double embryos. Numbers of embryos examined are indicated. Scale bars: (in B) for A-C, 400 μm; (in E) for D-F, 50 μm.

Similar to previous observations (Vivancos et al., 2009), chemoattraction of FBM neurons from r4 toward the WNT5A beads was typically observed within 24 hours in the case of wildtype explants (Fig. 3.5 C,D), while PBS-coated beads elicited no effect (Fig. 3.5 A,B). In wildtype explants treated with *Wnt5a*, over 83% of all wildtype explants exhibited some degree of attraction towards WNT5A-treated beads. This is in contrast to the wildtype explants where only 14% of all samples showed chemoattraction toward beads treated with PBS. Importantly, while the percentage of *Dvl2* mutant explants exhibiting rostral migration as a function of *Wnt5a*-mediated chemoattraction was significantly reduced as compared to wildtype explants, a large portion (71%) of all *Dvl2* mutant explants still exhibited some degree of chemoattraction towards WNT5A-treated beads (Fig. 3.5 F, G). The partial reduction in rostral migration observed among *Dvl2* mutant explants may reflect functional redundancy with *Dvl1* and *Dvl3*, which are also expressed in E11.5 hindbrains (Wang et al., 2006). Furthermore, based on the extent of migration observed, i.e. scores assigned, an index value was calculated (Fig. 3.5 H). A 90% increase in chemoattraction was observed among wildtype explants treated with WNT5A as compared to wildtype explants treated with control beads (Fig. 3.5 H). As compared to wildtype explants, *Dvl2* knockout animals exhibited a 22% reduction in the chemoattractive response to WNT5A. These data suggest that WNT5A chemoattraction is partially dependent on DVL2 function.

Figure 3.5 *Dvl2* Mutant FBM Neurons Exhibit Reduced Attraction Towards WNT5A-Treated Beads

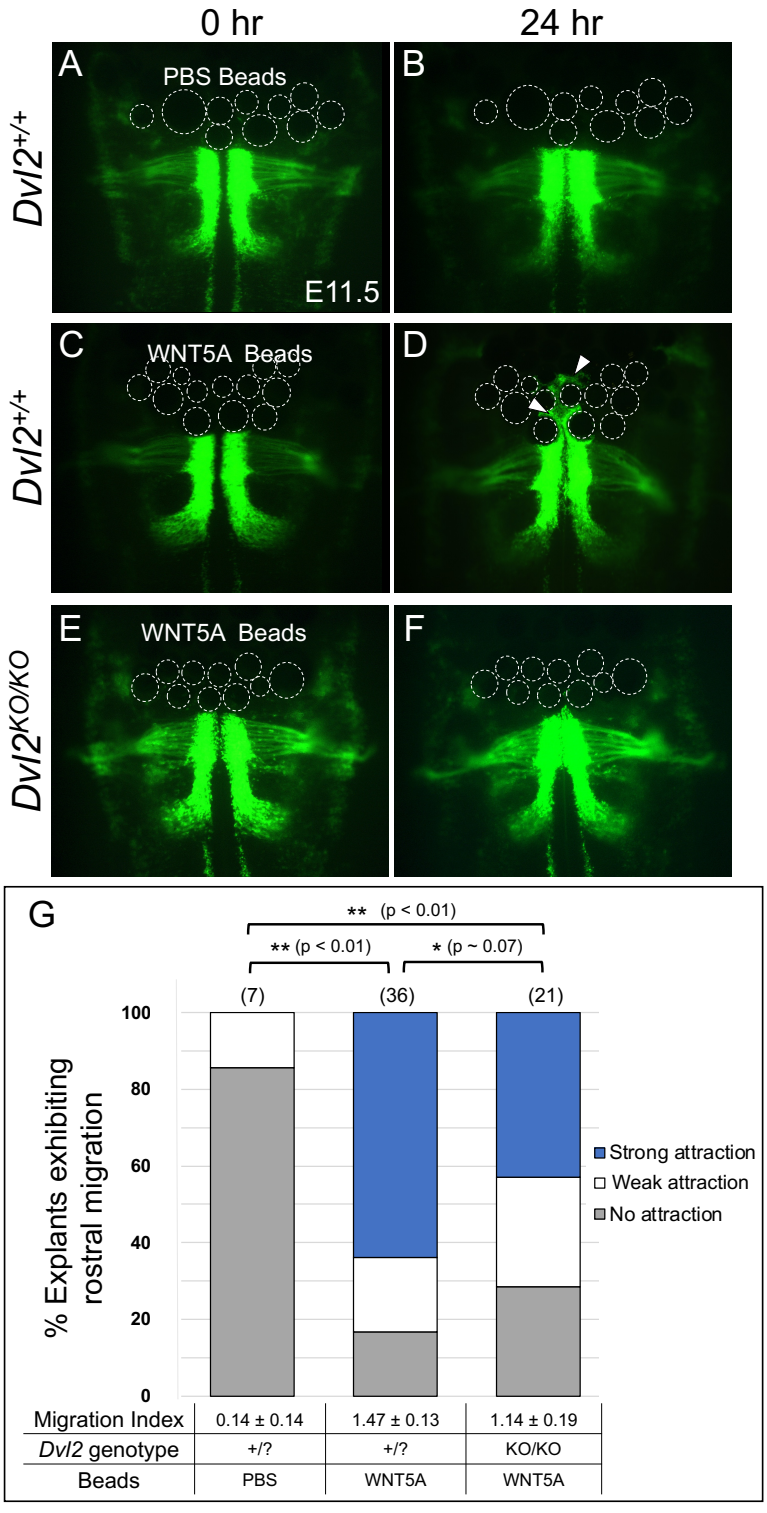

Figure 3.5 *Dvl2* Mutant FBM Neurons Exhibit Reduced Attraction Towards WNT5A-Treated Beads

(A-F) Dorsal views of E11.5 hindbrain explants from *SE1::GFP* transgenic embryos of the indicated genotypes immediately (0 hr; A, C, E) or 24 hours (B, D, F) after the placement of Wnt5a- or PBS-treated beads. (A, B) PBS-treated beads placed in r3 did not elicit any effect in the GFP-expressing FBM neurons in r4. (C, D) Within 24 hours of placing WNT5A -treated beads in r3 in a wildtype explant, a large number of FBM neurons (arrowheads) had migrated rostrally 2-3 bead diameters from the r3/r4 boundary (Strong attraction). (E, F) In a *Dvl2* mutant explant, a small number of FBM neurons have breached the r3/r4 boundary by 24 hours, and an even smaller number has migrated rostrally less than a bead diameter (Weak attraction). (G), Quantification of phenotypes. Number of explants in parentheses. Student's t-test indicates that the difference in attraction to WNT5A beads between wildtype and *Dvl2* mutants is bordering on significance (*). Scale bar (in A) for A-F, 600 μm.

3.2.5 Celsr1 Mutant Phenotype is Exacerbated Upon Overexpression of Wnt5a

Acknowledging the ability of FBM neurons to overcome the suppressive effects of *Celsr1* as a result of embedding WNT5A-coated beads is fundamentally a gain-of-function (GOF) phenotype/experiment, we predicted that the *in vivo* overexpression of *Wnt5a* within the rostral hindbrain would mimic the effects of the bead experiments, but more importantly enhance the rostral migration of FBM neurons seen in *Celsr1*KO/KO embryos (Fig. 3.7). Moreover, if WNT5A is the primary chemotactic cue acting to entice rostral migration in *Celsr1* mutants, and *Celsr1* normally acts to suppress *Wnt5a* in the WT hindbrain preventing chemoattraction, then overexpression of WNT5A in addition to *Celsr1* knockout should exacerbate the rostral migration phenotype observed in *Celsr1* single mutants.

To generate embryos with increased *Wnt5a* expression in the rostral hindbrain (*Wnt5a*GOF), we employed a *Wnt5a* loxP-STOP allele inserted into the ROSA26 locus (Cha et al., 2014) combined with an *Egr2:Cre* driver (Voiculescu et al., 2000), which resulted in robust ectopic *Wnt5a* expression throughout r3 and r5 (Fig. 3.6). Based on the rostral migration observed in these samples (Fig. 3.7), it was often difficult to identify the r3/4 boundary. In order to infer the position of the putative r3/4 boundary, the distance between the trigeminal and rhombomere 4 was measured in wildtype and *Celsr1* +/KO control samples. Subsequently, a cumulative average (104mm) was calculated and later applied to both *Celsr1* KO/KO embryos as well as embryos possessing the *Wnt5a* GOF allele. (Fig. 3.9).

Here, we largely assume that hindbrain size (as a proxy for convergence and extension) remains unaffected regardless of *Celsr1* knockout or Wnt5a over expression. To confirm this assumption, measurements of length and width were taken as depicted in (Fig. 3.8). While it was evident that the over expression of *Wnt5a* within r3 and r5 generally resulted in more extensive rostral migration, especially when combined with the *Celsr1* mutation, *Celsr1* mutation alone resulted in rostral migration that extended further (Fig. 3.7 I). As a result, our previous means to quantify rostral migration would have resulted in a severe under representation of rostral migration specifically for *Celsr1* KO/KO; *Wnt5a* GOF embryos (Fig. 3.7 I).

In order to more accurately and precisely measure the amount of rostral migration, Tbx20 staining specific to the FBM neurons was outlined using FIJI software. The outlined population of FBM neurons was then subdivided into 2 regions of interest by applying the average width of r3 (previously calculated; specifying the r3/4 boundary). By subsequently exporting measurements of area and pixel intensity the percentage of signal contributed by the rostrally migrating FBM neurons was calculated (Fig. 3.9). Both wildtype and *Celsr1* +/KO embryos with normal *Wnt5a* expression did not exhibit any signs of rostral migration, however a statistically significant amount of rostral migration was observed in both wildtype and *Celsr1* +/KO animals with increased *Wnt5a* expression. In *Celsr1*+/+; *Wnt5a* GOF samples, approximately 11% of all the signal specific to the FBM neurons was found rostral to the putative r3/4 boundary, while a comparable 12% was observed in the case of *Celsr1* KO/+; *Wnt5a* GOF samples (Fig. 3.7 G, H). In

the case of *Celsr1* KO/KO mutant animals, 17% of all signal specific to the FBM neurons was found rostral to the putative r3/4 boundary (Fig. 3.7, F). Finally, a tremendous amount of rostral migration was observed among *Celsr1*KO/KO; *Wnt5a*GOF embryos. *Wnt5a* over expression among *Celsr1* mutants resulted in extensive rostral migration, where ~34% of the Tbx20 signal was found rostral to the putative r3/4 boundary. This was a significant increase and nearly double the percentage of Tbx20 signal found in *Celsr1* mutants (Fig. 3.7, J).

3.2.6 Neural Specification is Unaffected Upon Over-Expression of Wn5a in r3 and r5

To verify that neural specification was not adversely affected as a result of increased *Wnt5a* expression within r3 and r5, the expression of efferent neuron marker, *Gata3* was evaluated among *Wnt5a*^{GOF} embryos. While slight differences in the amount of *Gata3* transcript were observed, perhaps as a function of differences in age, the overall pattern of *Gata3* expression appeared relatively unchanged suggesting that neural specification was largely un-affect as a result of *Wnt5a* over-expression (Fig. 3.10). Taken together, these data support a novel role for *Celsr1* functioning to prevent *Wnt5a*-mediated chemoattraction of FBM neurons.

Figure 3.6 *Wnt5a* Over-Expression in *Egr2*-Cre; *Wnt5a*+/GOF Animals

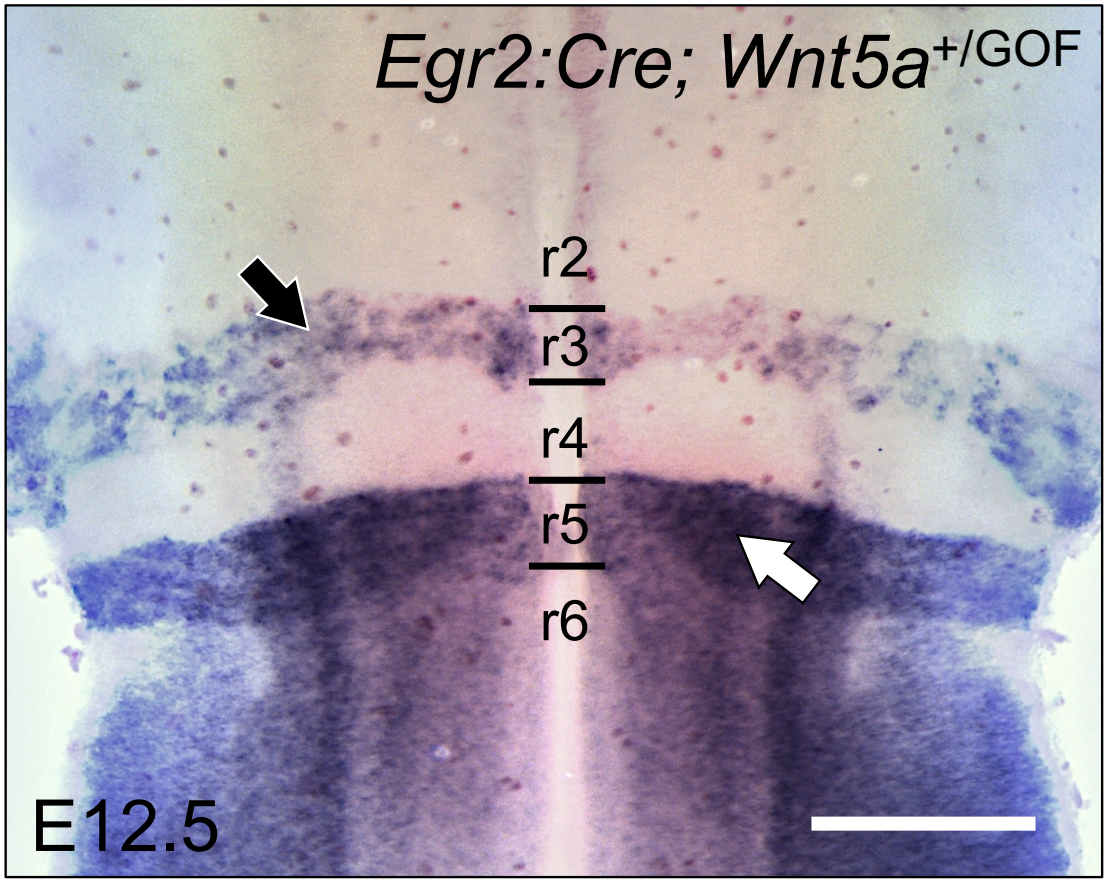

Figure 3.6 *Wnt5a* Over-Expression in *Egr2*-Cre; *Wnt5a*+/GOF Animals

In an *Egr2*-Cre; *Wnt5a*+/GOF hindbrain, overexpression of *Wnt5a* is evident in r3 (black arrow) and r5 (white arrow), and r3 is shorter than r4 along the rostrocaudal axis Scale bar, 400 μm.

Figure 3.7 The *Celsr1* Rostral Migration Phenotype is Exacerbated upon Over-Expression of *Wnt5a*

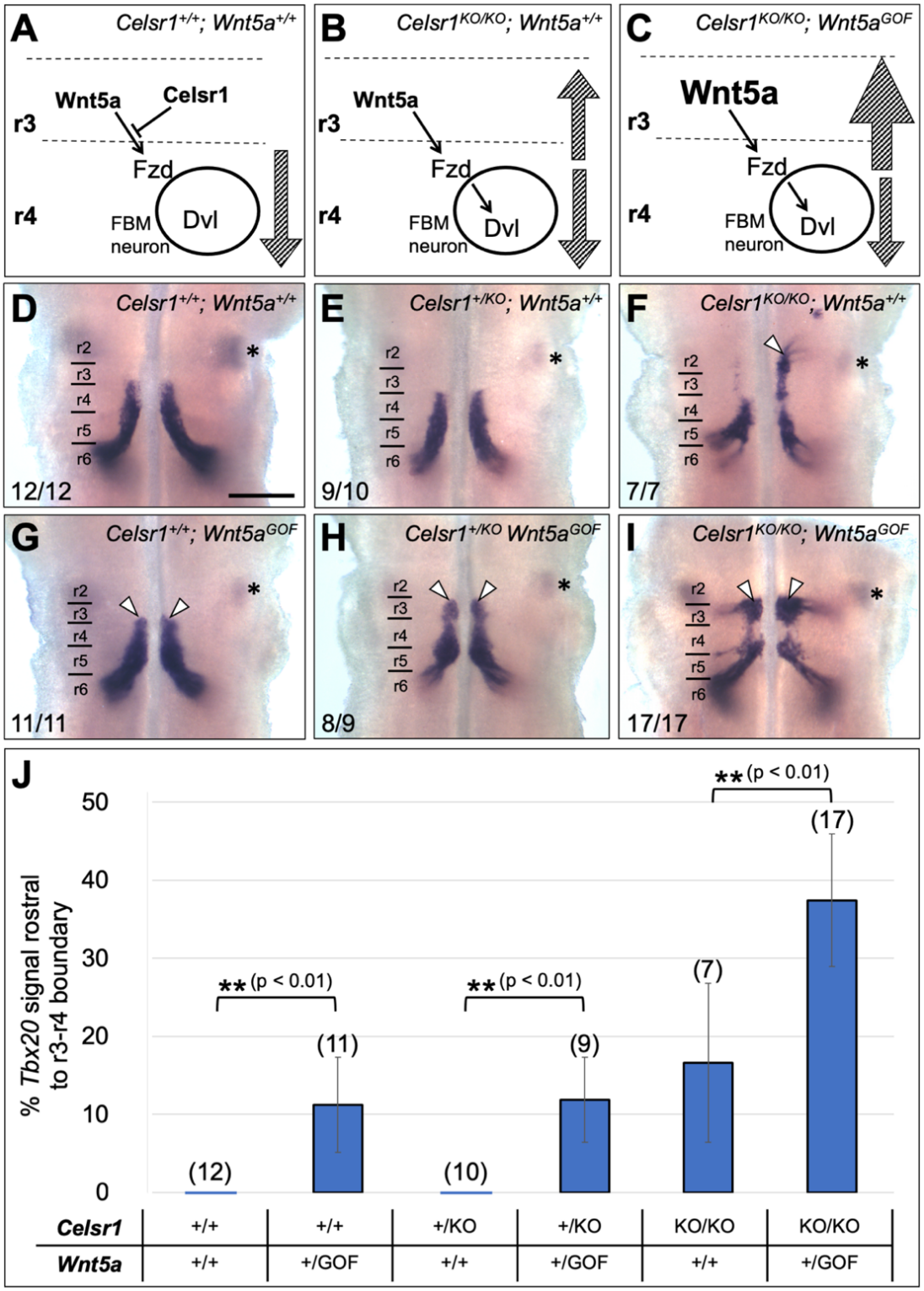

Figure 3.7 The *Celsr1* Rostral Migration Phenotype is Exacerbated upon Over-Expression of *Wnt5a*

(A-D) Schematics of our working model of how *Celsr1* and *Wnt5a* function to regulate FBM neuron migration. The model predicts that rostral migration of FBM neurons into r3 (hatched “up” arrow) seen in *Celsr1* mutants (B) will be enhanced by *Wnt5a* overexpression in r3 (C). (D-I) Dorsal views of E12.5 hindbrains processed for *Tbx20* in situs. (D, G) Following ectopic expression of *Wnt5a* in r3 in a *Celsr1*$^{+/+}$ embryo (G), some FBM neurons (arrowheads) are located in (migrating to) r3. (E, H) *Wnt5a* overexpression in a *Celsr1*$^{+/KO}$ embryo (H) results in a large number of FBM neurons located in r3 (arrowheads) compared to a control embryo (E). (F, I) *Wnt5a* overexpression in a *Celsr1*$^{KO/KO}$ embryo (I) results in a sharp increase in the number of FBM neurons migrating into r3 (arrowheads) compared to a *Celsr1* mutant embryo (F). (J) Quantification of rostral migration enhancement phenotypes. For each *Celsr1* genotype, the differences between *Wnt5a* expression conditions were compared using Student’s t-test and found to be significant (**, $P<0.01$) in all cases. Scale bar (in D) for D-I, 400 μm.

Figure 3.8 Hindbrain Size and Rhombomere Dimensions in *Wnt5a*^{GOF} Embryos

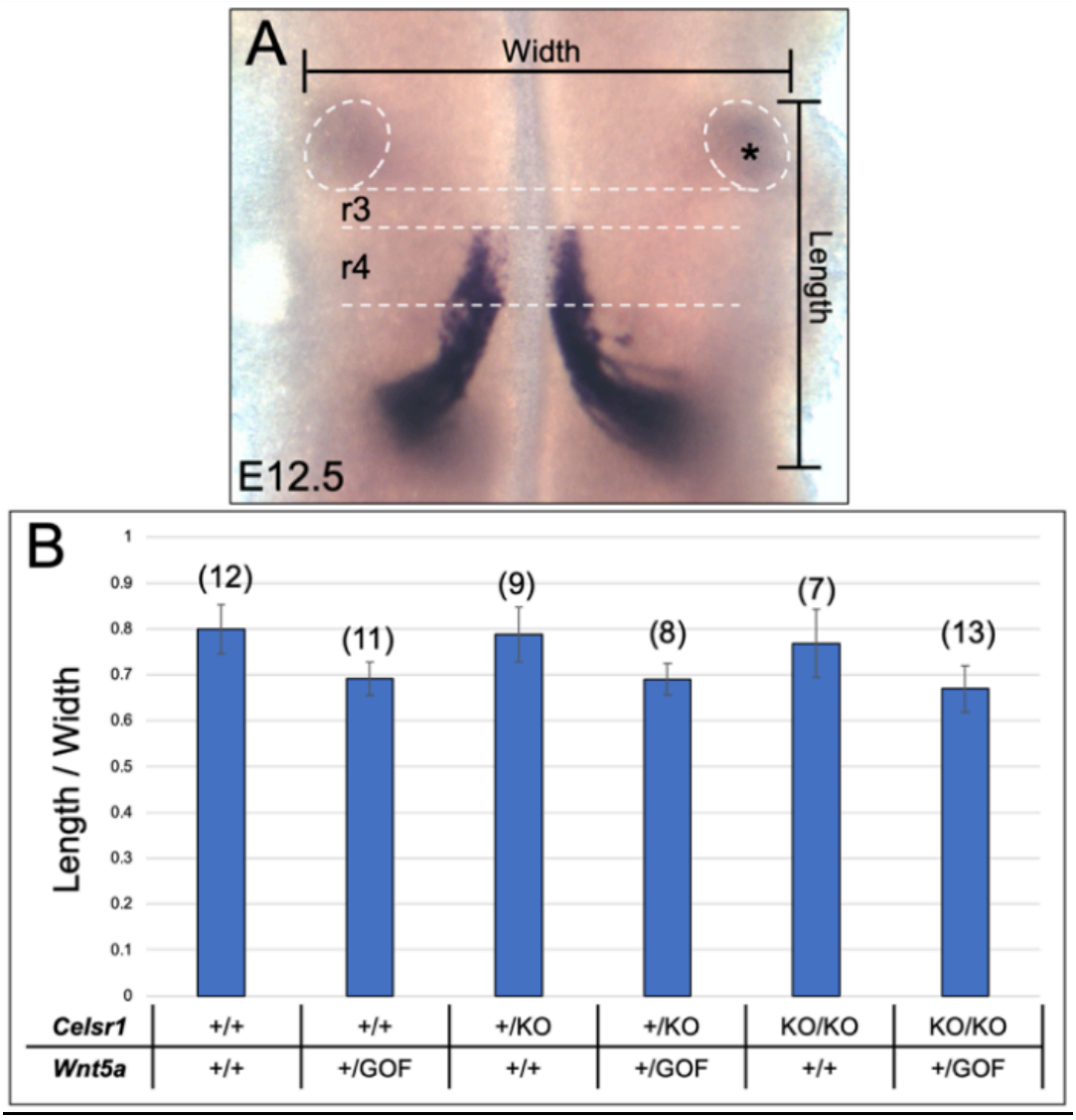

Figure 3.8 Hindbrain Size and Rhombomere Dimensions in *Wnt5a*^{GOF} Embryos

(A) Dorsal views of E12.5 hindbrains processed for *Tbx20* in situs. Length and width were defined as shown, using as landmarks the outlined edges of the trigeminal motor nuclei in r2 (circled, asterisk) and the caudal edge of the stream of migrating FBM neurons in r6. The boundaries of r3 and r4 were defined for control embryos from the location of the *Tbx20*-expressing trigeminal and FBM neurons and used to establish the corresponding boundaries (and rhombomere lengths) in *Wnt5a*^{GOF} embryos. (B) Hindbrain dimensions were relatively constant across all genotypes and *Wnt5a* expression.

Figure 3.9 Quantifying Rostral Migration of FBM Neurons in *Wnt5a*^{GOF} Embryos

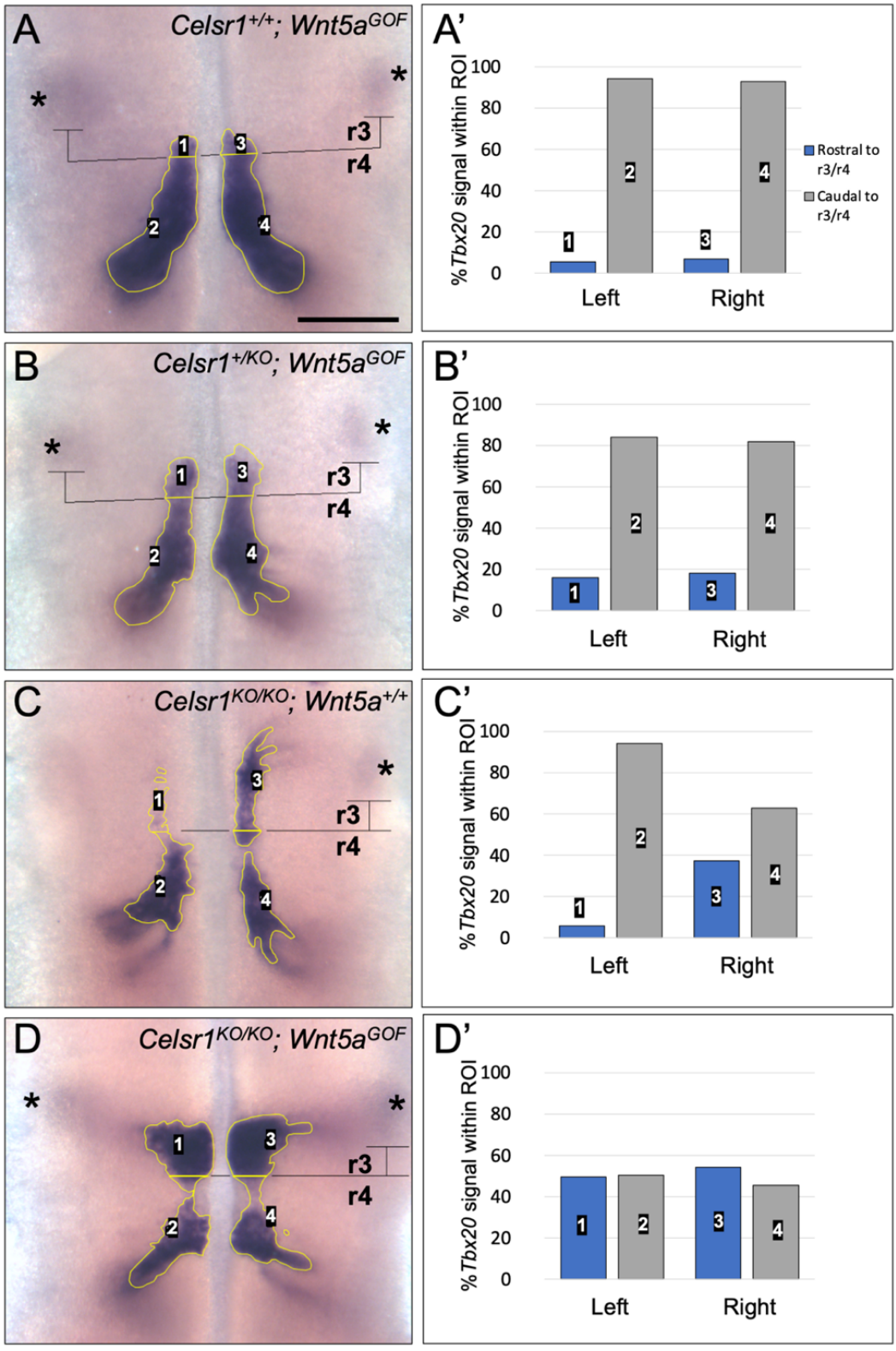

Figure 3.9 Quantifying Rostral Migration of FBM Neurons in *Wnt5a*^{GOF} Embryos

(A-D) Dorsal views of E12.5 hindbrains processed for *Tbx20* in situs. Using the caudal margin of the trigeminal motor nuclei (asterisks), the putative r3/4 boundary was drawn using the average length of r3 calculated from control embryos. This enabled demarcation of the *Tbx20*-expressing migratory streams into regions of interest (ROI 1-4). (A'-D') Using Fiji, the areas and intensities in these ROIs were measured and plotted as a function of the total *Tbx20* signal for each side of the hindbrain. These measurements were used to calculate the fraction of total *Tbx20* signal found rostral to the r3-r4 boundary shown in Figure 3.9. Scale bar (in A) for A-D, 400 μm.

Figure 3.10 Neuronal Specification is Unaffected Upon Over-Expression of Wn5a

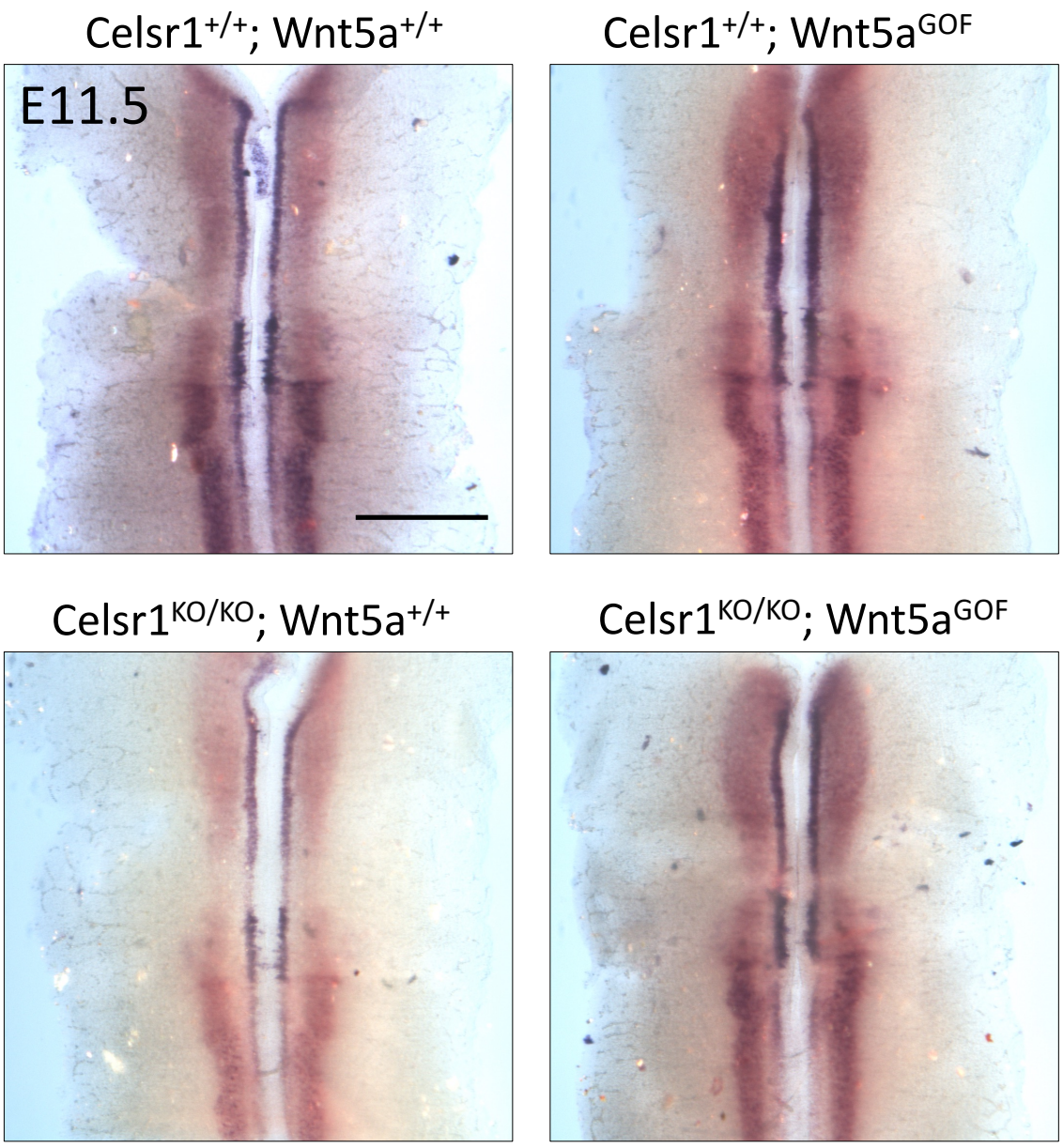

Figure 3.10 Neuronal Specification is Unaffected Upon Over-Expression of Wn5a

Dorsal views of E11.5 hindbrains processed for *Gata3* in situ. The expression patterns of *Gata3* was similar regardless of *Wnt5a* over-expression (or *Celsr1* knockout). Scale bar: 400 μm

3.3 DISCUSSION

3.3.1 Wnt5a Mediated Chemoattraction is Dependent on Dvl2 function

Through the outlined experiments, we examined a chemo-attractive role for *Wnt5a*, by placing agarose beads treated with recombinant WNT5A into the rostral hindbrain of *Dvl2* mutant explants cultured *ex vivo*. Interestingly, as compared to wildtype animals, a partial yet statistically significant loss of *Wnt5a*-mediated chemoattraction was observed as a result of *Dvl2* deletion. However, many FBM neurons still migrated towards the WNT5A-treated beads regardless of *Dvl2* deletion. Importantly, while transduction of both Wnt and PCP signals rely on Dvl function, it is unclear how or to what degree *Dvl2* contributes to these pathways in the context of FBM neuron migration. Perhaps cell polarity is more substantially affected as a result of *Dvl2* deletion, rather than a cell's ability to perceive and respond to Wnt chemoattractant. Another, more direct explanation for this is that *Dvl1* and *Dvl3* are also expressed within E11.5 hindbrains, and therefore, the partial reduction of rostral migration observed in *Dvl2* mutant explants could perhaps be due to redundant roles for *Dvl2* orthologs (Wang et al., 2006). Taken together, our explant-bead studies suggested that *Wnt5a*-mediated chemoattraction of FBM neurons is dependent on Dvl signaling. While *Wnt5a* has been shown to allow for chemoattraction in other contexts (Lyuksyutova et al., 2003; Onishi et al., 2013), the chemoattraction of neurons during migration is so far a unique role for *Wnt5a*.

3.3.2 Celsr1 is as a Potent Suppressor of Wnt5a Chemoattraction Within the Rostral Hindbrain

Importantly, *Celsr1* function is not required within FBM neurons to prevent their rostral migration (Qu et al., 2010), and is Instead, functioning non-cell autonomously within the ventricular zone rostral to r4 (Glasco et al., 2016). Anterograde Dye fill experiments previously suggest that the rostral migration of FBM neurons in *Celsr1* mutants is due to the loss of a local guidance cue rather than a loss of polarity (Glasco et al., 2016). Intriguingly, although putative chemoattractant, WNT5A, is expressed within r3, FBM neuron never migrate rostrally in wildtype animals. Based on these data, we proposed that the putative chemoattraction of FBM neurons toward the rostral source of *Wnt5a* in r3 is normally suppressed by *Celsr1*, and upon *Celsr1* deletion, this suppression is alleviated, resulting in migration into r3 and r2. We therefore predicted that if *Wnt5a* is functioning as the primary chemotactic cue acting to entice the inappropriate rostral migration observed in *Celsr1* mutants, and *Celsr1* normally acts to suppress *Wnt5a* in the WT hindbrain preventing chemoattraction, then knocking out *Wnt5a* in addition to *Celsr1* should rescue the rostral migration phenotype, while the over expression of *Wnt5a* within the r3 should result in increased rostral migration. Through the outlined experiments, we can confirmed these predictions.

Our data indeed suggests that *Celsr1* suppresses the chemoattractive effects of *Wnt5a* to ensure that FBM neurons exclusively migrate caudally out of r4. Here, we show that knockout *Wnt5a* in addition to *Celsr1* resulted in a 10-fold

reduction in the number of hemispheres exhibiting rostral migration, while over-expressing *Wnt5a* in r3 of *Celsr1* mutants instead resulted in a dramatic increase in rostral migration. More specifically, the over-expression of *Wnt5a* among *Celsr1* mutants resulted in a statistically significant increase, and over twice as much rostral migration when compared to *Celsr1* mutants without the gain-of-function allele. Consistent with our model, over expression of *Wnt5a* in r3 of WT and *Celsr1*+/KO animals also resulted in subtle rostral migration. Interestingly, *Celsr1* mutation alone resulted in rostral migration that extended much further than *Celsr1* mutation with *Wnt5a* over-expression. This is likely because r3 is an ample source of WNT5A chemoattractant in the case of gain-of-function embryos. However, caudally migrating neurons did not preferentially accumulate in r5 of *Wnt5a*GOF embryos as one might expect. Additionally, there was a marked reduction in the size of the caudal migratory streams in *Celsr1*KO/KO; *Wnt5a*GOF embryos, likely due to the substantial increase in the number of FBM neurons that had instead migrated rostrally. Taken together, these experiments establish a novel role for *Celsr1* acting as a suppressor of WNT5a-mediated chemoattraction, allowing for proper FBM neuron migration. However, our data do not provide further insight into whether WNT5A also functions as a chemoattractant during caudal migration, since we did not observe pronounced effects on the caudal migratory streams of FBM neurons in either of our LOF or GOF conditions. Therefore, in order to understand how proper FBM neuron migration is achieved, we must continue to investigate both the mechanism critical to caudal migration in addition to those necessary for suppressing rostral migration.

3.4 Concluding Remarks and Future Directions

While previous studies using hindbrain explants and protein coated beads suggest that WNT5A may function as a chemoattractant to guide FBM neurons caudally, the *Wnt5a* knockout phenotype is subtle, and therefore, its role during caudal migration remains unclear (Vivancos et al., 2009). Through the outlined experiments, we examined a possible role for *Wnt5a* functioning through *Dvl2* during FBM neuron migration. By placing agarose beads treated with recombinant WNT5A into the rostral hindbrain of *Dvl2* mutant explants cultured *ex vivo* we showed show that as compared to wildtype animals, a partial yet statistically significant loss of *Wnt5a*-mediated chemoattraction was observed, suggesting that signal transduction via *Dvl2* may be involved in *Wnt5a*-mediated chemoattraction.

We further propose that chemoattraction of FBM neurons toward the rostral source of *Wnt5a* is normally suppressed by *Celsr1*, and upon *Celsr1* deletion, this suppression is alleviated resulting in migration into r3 and r2. In support of this, we show that knockout of *Wnt5a*, in addition to *Celsr1* results in a substantial reduction in the total number of hemispheres exhibiting rostral migration, while the over-expression of *Wnt5a* in r3 of *Celsr1* mutants instead resulted in a substantial increase in rostral migration as compared to *Celsr1* mutants without the gain-of-function allele. Here we investigate *Wnt5a* as the sole source of chemoattraction acting to entice the rostral migration of FBM neurons seen in *Celsr1* mutant animals. Our data demonstrate that *Celsr1* is indeed suppressing the

chemoattractive effects of WNT5A ensuring that FBM neurons exclusively migrate caudally out of r4, however, how this is achieved mechanistically remains unclear.

Possible Mechanisms Underlying the Celsr1-Mediated Suppression of Wnt5a

Identifying the molecules that interact with CELSR1 is an initial step in determining the mechanisms of how suppression of *Wnt5a*-mediated chemoattraction occurs among FBM neurons. Because CELSR1 has not been shown to associate WNT5A in any context, WNT5A function is likely being regulated through indirect mechanisms. Importantly, others have shown that homophilic interactions between CELSR1 molecules in part allows for the asymmetrical localization of core PCP components Frizzled and *Vangl2* (Usui et al., 1999; Nishimura et al., 2012; Chen et al., 2008; Stahley et al., 2021). This asymmetric localization is what imparts “polarity” to a cell, distinguishing one side of the cell from the other while simultaneously determining where (i.e. at what side of the cell) WNT perception by FRIZZLED is possible.

Importantly, it was recently reported that VANGL2 is enriched at the anterior (rostral) side floor plate cells of the hindbrain, while FRIZZLED is instead localized to the posterior (caudal) side (Davey et al., 2016; Davey et al., 2017). Based on this, through mechanisms previously described in chapter 1, Wnt signal transduction could perhaps result in activation of β-CATENIN functioning upstream of N-cadherins near areas of FRIZZLED localization, therefore lending to cell adhesion preferentially towards the caudal side of cells. Consistent with this, the

deletion of N-cadherin, cdh2 has been shown to result in FBM neuron migration defects.

Furthermore, others have demonstrated that PLK-1, which binds the DVL-complex (Lee et al., 2020), is capable of phosphorylating the endocytic motif of CELSR1 allowing for the trans-internalization of FRIZZLED from neighboring cells (Shrestha et al., 2015; Heck and Devenport, 2017). The internalization of FRIZZLED receptors may represent a second mechanism by which *Celsr1* may regulate Wnt signaling during FBM neuron migration.

Finally, as a cell adhesion molecule, we cannot rule out the possibility that under normal conditions, CELSR1 may be exerting a physical force on FBM neurons that simply cannot be overcome by endogenous *Wnt5a* expression/ chemoattraction. Both cell adhesion and PCP achieved through *Celsr* function has been shown to rely on homophylic interactions (CELSR molecules either bind themselves and/or like- molecules). However, we've previously demonstrate that *Celsr1* does not function within FBM neurons (Qu et al., 2010), and is therefore functioning non-cell autonomously. Based on this, CELSR1 is likely binding one if not both of its next closest genetic relatives, CELSR2 or CELSR3. Interestingly, *Celsr*2 and 3, are also expressed within the hindbrain during FBM neuron migration and together, regulate the caudal migration of FBM neurons. Interestingly, slight rostral migration is observed among *Celsr*2 mutants. Also, *Celsr*2 is required for the *Celsr1* KO rostral migration phenotype, indicating that *Celsr*2 is epistatic to *Celsr1*. Furthermore, *Celsr*3 has been shown to function cell-autonomously to

regulate caudal FBM neuron migration (Qu et al., 2010). These experiments and results are summarized in (Table 3.1).

Based on these data, perhaps CELSR2, intrinsic to FBM neurons, associates CELSR3 on neighboring cells to allow for caudal migration (or migration in general), while CELSR2, in association with CELSR1, acts suppress rostral migration. CELSR1 may also be associating CELSR3 within FBM neurons in order to suppress rostral migration. To determine how CELSR molecules may be cooperating to allow for FBM neuron migration, caudal or rostral, one must systematically delete individual CELSR molecules either within FBM neurons **or** their environment, not both as in standard genetic mutants. Identifying these interaction along with those described previously will ultimately provide insight into how suppression of *Wnt5a* chemoattraction is achieved among FBM neurons.

Table 3.1) A Summary of *Celsr* Mutants Investigated (prior to this study)

	Cell Autonomous			Non - Cell Autonomous			Caudal Migration?	Rostral Migration?
Genotype:	**Celsr1**	**Celsr2**	**Celsr3**	**Celsr1**	**Celsr2**	**Celsr3**		
WT							++++	NM
Celsr1	KO			KO			++++	+++
Celsr1-isl1	KO						++++	NM
Celsr1-r3/5				KO			++++	++
Celsr2		KO			KO		+++	+
Celsr3			KO			KO	++++	NM
Celsr2 KO Celsr3-isl1			KO		KO		NM	NM
Celsr2/3		KO	KO		KO	KO	NM	NM

Table 3.1.) A Summary of *Celsr* Mutants Investigated (prior to this study)

A tabulated summary of the conclusions made based upon Qu et al., 2010 and Glasco et al., 2016. NM denotes “no migration”

CHAPTER 4: Characterizing Calcium Dynamics Intrinsic to Migrating FBM Neurons and the Zebrafish Hindbrain

4.1 INTRODUCTION

In the developing nervous system, many types of neurons migrate in stereotyped patterns to form the circuits vital for survival or proper function. During neuron migration, calcium release from intracellular stores and uptake from the extracellular matrix mediate calcium-dependent mechanisms allowing for migration. More specifically, intracellular calcium (Ca_i) concentrations are elevated as a result of either membrane depolarization or flux from mitochondria and the endoplasmic reticulum during perception of neurotransmitters and neurotrophic factors (Zheng et al., 2007; Raffaello et al. 2016). Subcellular, calcium-dependent processes required for neuronal migration include cell adhesion and cytoskeletal rearrangement.

Here, differentially expressed calcium-dependent molecules in addition to regulators of Ca_i localize to determine both when and where calcium is able to function as a second messenger. Moreover, local fluctuations in Ca_i result in the heterogeneous activation of calcium-dependent processes, while global elevations otherwise result in ubiquitous activation. Therefore, calcium's role as a second messenger is limited to the spatial as well as temporal properties of Ca_i itself making the role of Ca_i particularly context dependent. In the context of the cerebellar cortex, its been demonstrated that the frequency of Ca_i dynamics (i.e. fluctuations in intracellular calcium) observed among migrating granule neurons

positively correlate with rates of displacement (Kumada and Komuro, 2004). Furthermore, it has been shown that Ca_i dynamics are indeed necessary for migration and that the corresponding loss of Ca_i dynamics is sufficient for pausing/termination (Bortone & Polleux, 2009). Likewise, suppressing Ca_i dynamics among tangentially migrating cortical interneurons through the ectopic expression of the hyperpolarizing inward rectifying potassium channel, Kir2.1, has been shown to result in a 20% increase in the amount of time spent stationary (Bortone & Polleux, 2009). Overexpression of Kir2.1 among radially migrating interneurons also appears to perturb migration (Garcia et al., 2011). Moreover, upon reaching their destination, both radially as well as tangentially migrating neurons have been shown to up-regulate the potassium/chloride cotransporter, KCC2, to attenuate Ca_i dynamics triggering the loss of migration (Yamada et al., 2004, Bortone & Polleux, 2009. Pharmaceutical studies have also demonstrated that Ca_i dynamics allowing for neuron migration are primarily driven by N and L-type voltage-sensitive calcium channel currents (Kumada and Komuro, 2004; Bortone & Polleux, 2009; Darcy and Isaacson, 2009).These and other studies suggest that Ca_i has a conserved role in regulating neuron migration.

While calcium's role during neuron migration has been extensively investigated in the forebrain and midbrain, its potential roles in the hindbrain have not been examined. Importantly, facial branchiomotor (FBM) neurons, native to hindbrain, have received considerable attention based on their characteristic tangential migration from hindbrain compartment r4 to more caudal compartments r6 and r7. In zebrafish, FBM neurons begin their rostro-caudal migration ~18 hours

post fertilization (hpf) and terminate by ~36 hpf (Chandrasekhar et al., 2004). Once this migration is completed, axons of FBM neurons specifically exit cranial nerve VII to innervate the abductor and hyoid muscles of the jaw derived from the 1st and 2nd pharyngeal (branchial) arches (Tanaka et al., 2007)

Interestingly, *ex vivo* studies in mice demonstrate that at (E) 9.5, and later, many hindbrain neurons, including FBM neurons, undergo spontaneous and synchronized fluctuations in Ca_i (Gust et. al. 2003). They later show that spontaneous events are dependent on *t*-type calcium channel, gap junctions, as well as the serotonergic raphe (Hunt et al., 2005; Hunt et al., 2006; Watari et al., 2014). They further demonstrate that release of serotonin from the serotonergic raphe initiates the spontaneous depolarization of adjacent neurons (Watari et al., 2014). By E11.5, these spontaneous events propagate throughout the entire hindbrain and result in elevated Ca_i lasting several minutes per event (Bosma et al., 2017). By E14.5, neurons of the hindbrain hyperpolarize and no longer undergo spontaneous events (Hunt et al., 2006). These spontaneous events largely coincide with the migration of FBM neurons (Chandrasekhar et al., 2004), and therefore, we hypothesized that Ca_i dynamics may be specifically regulating FBM neuron migration. Interestingly, experiments in chick indicate that spontaneous activity among FBM neurons is indeed required for the proper formation of individual FBM neuron nuclei (Monteque et al, 2017), however, FBM neurons do not migrate in chicken as they do in mice or zebrafish, and thus the role for Ca_i dynamics during migration remains unclear.

To better understand calcium's role during migration and circuit establishment, we generated a transgenic zebrafish line that expresses the optimized calcium indicator, GCaMP6s, exclusively in cranial motor neurons (*Tg(zCREST1:GCaMP6s)).* By characterizing the spatial as well as temporal features associated with Ca_i dynamics intrinsic to migrating FBM neurons, we show that zebrafish facial branchiomotor (FBM) neurons also exhibit fluctuations in Ca_i during their tangential migration. These Ca_i dynamics result in either local or global fluctuations in Ca_i among cell bodies, filopodia, and trailing axons, and as compared to the spontaneous activity observed in mice, these events appear to be asynchronous (Bosma et al., 2017).

Based on this apparent difference, we wondered whether or not synchronized dynamics ever arise rise among FBM and surrounding neurons. Therefore, we utilized a separate transgenic line which expresses nuclear localized GCaMP6f in all post-mitotic neurons (*Tg(Elavl3:H2B-GCaMP6f*; McArthur et al. 2017). Here we show that between the ages of 60-72hpf, synchronized Ca_i dynamics indeed propagate throughout the hindbrain and similarly result in increased Ca_i spanning many different neuron types. Importantly, while this largely occurs after FBM neuron migration is completed, we believe that these Ca_i dynamics could be involved in other aspects of branchiomotor circuit establishment and function.

4.2 MATERIALS AND METHODS

4.2.1 Generating Transgenic Zebrafish for Observations of Ca_i Among FBM Neurons

We generated the transgenic line *Tg(zCREST:GCaMP6s),* expressing *GCaMP6s* in branchiomotor neurons using the Tol2-mediated, transposon-based method of transgenesis. The Tol2 kit was kindly provided by the Kristen Kwan and Chi-Bin Chien Labs, University of Utah (Kwan et al., 2007). The GCaMP6s containing middle-entry vector, pENTR-*GCaMP6s,* was kindly provided by the Solnica-Krezel lab (Washington University). We used the p5E-*zCREST*, pENTR-*GCaMP6s*, p3E-poly(A) and pDestTol2CG2 in a multiple cloning LR reaction (Kwan et al., 2007) in order to generate the final Tol2 vector (Fig. 4.1). Subsequently, 75 pg of *zCREST-GCaMP6s*-Poly(A) along with with 25 pg of Tol2 transposase mRNA was injected into 1-cell stage zebrafish zygotes to allow for incorporation into the genome. Injected zygotes obtained from wildtype, non-transgenic fish were then screened at 24-36 hpf for GFP expression in the heart (*cmcl2-GFP*; as an indicator of effective transgenesis, since GCaMP6s expression in branchiomotor neurons often appeared very faint). These fish were raised to adulthood and were outcrossed to generate F1 progeny. Resulting offspring were also screened in order to determine affective germline transmission of the *zCREST:GCaMP6s* transgene.

Figure 4.1 Tol2-Mediated Recombination for Generating *tg(zCREST:GCaMP6s)* Transgenic Zebrafish

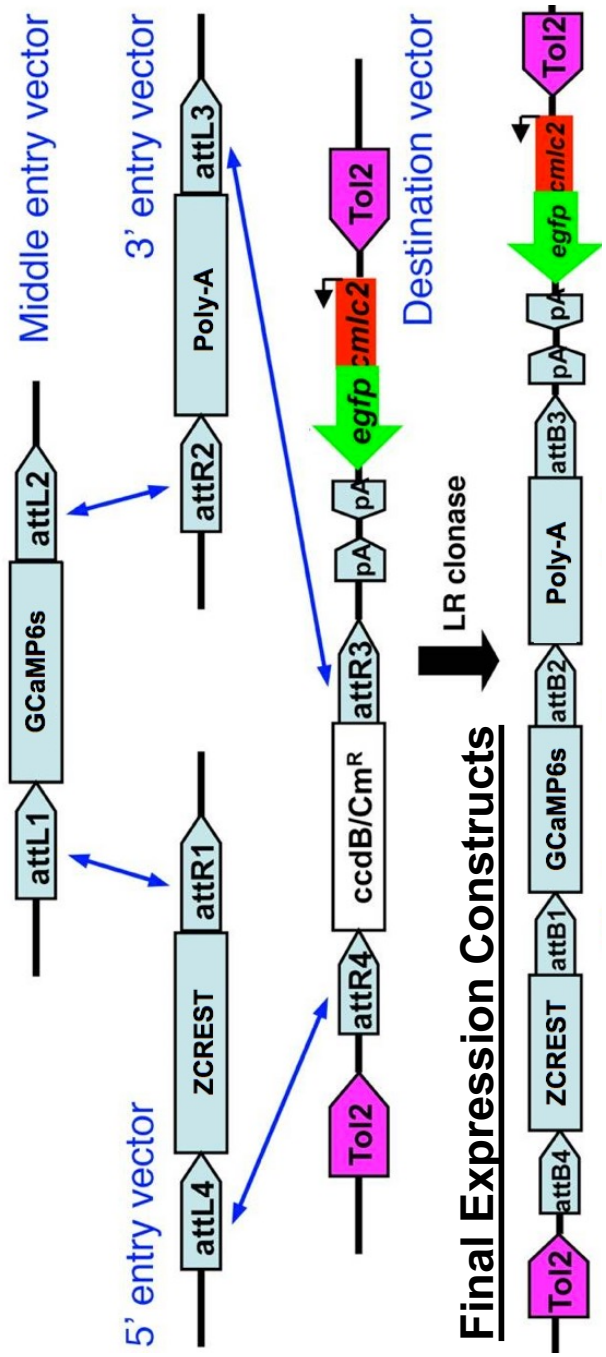

Figure 4.1 Tol2-Mediated Recombination for Generating *tg(zCREST:GCaMP6s)* Transgenic Zebrafish

A schematic illustrating the tol2-mediated recombination of the p5E-*zCREST*, pENTR-*GCaMP6s*, p3E-poly(A) and pDestTol2CG2 carried-out in order to generate the *tg(zCREST:GCaMP6s)* transgenic zebrafish line

4.2.2 Quantification of Ca_i dynamics During migration

Tg(zCREST1:GCaMP6s) zebrafish embryos specifically expressing GCaMP6s in branchiomotor neurons were injected with 35pg of a-bungarotoxin mRNA at the single cell stage to prevent spontaneous coiling/twitching (Swinburne et al., 2015, Saint-Amant and Drapeau, 1998). The following day, embryos at 19, 21, and 24 hours post fertilization (hpf) were mounted using 0.2% agarose dissolved in E3 embryo medium. After allowing the agarose to gel, to prevent desiccation and simultaneously buffer changes in CO2, HEPES buffered E3 was added such that the embedded sample was entirely submerged. Mounted embryos were then subjected to time-lapse imaging for a total duration of 10 minutes using an TCP SP8 confocal microscope. Images were to be acquired at a frequency of 1 Hz. Time-lapse movies were then imported to ImageJ. Subsequently, various regions of interest were specified in order to quantify Ca_i dynamics among the cell bodies, projections, and axons of individual FBM neurons. Representative traces of individual regions of interest will then be exported to Excel to normalize and adjust for background as previously described (McArthur et al., 2017). In doing so, the background-corrected traces were used to calculate properties of individual events. Such properties included interval, duration, frequency, velocity, and relative fold-change in florescence.

4.2.3 Quantification of Ca_i dynamics During Larval Stages

In an effort to identify and characterize FBM neuron Cai dynamics during larval stages, *Tg(zCREST1:mRFP::HuC:GCaMP6f-H2B)* zebrafish larva that

express GCaMP6f in the nucleus of all post-mitotis neurons, were treated with Phenylthiourea (PTU) by 24 hpf to prevent pigmentation and were later injected with 4.6ng of a-bungarotoxin protein between the ages of 60-72hpf to immobilize/paralyze larvae. a-bungarotoxin was carefully injected into the paracardial region, rostral to the dorsal aorta so as to allow for direct uptake into the circulatory system. Immediately following a successful injection, the heart would stop or slow, then resume after a few seconds. After a 3 hours of recovery period, larva were mounted using 0.2% agarose dissolved in E3 embryo medium. After allowing the agarose to gel, in order to prevent desiccation and simultaneously buffer changes in CO2, HEPES buffered E3 was added such that the embedded larva was entirely submerged. Once mounted/embedded, embryos were then subjected to time-lapse imaging for a total duration of 10 minutes using an TCP SP8 confocal microscope.

Images were to be acquired at a frequency of 1 Hz and were always acquired at the same dorsal-ventral level/position as the FBM neurons (based upon the area of mRFP expression). Subsequently, time-lapse movies were imported into ImageJ and various regions of interest were specified as before. Representative traces based upon individual regions of interest were then exported into Excel in order to normalize and adjust for background as previously described (McArthur et al., 2017). In doing so, the background-corrected traces were generated.

4.3 RESULTS

4.3.1 Calcium Dynamics During FBM Neuron Migration

During neuron migration, differentially expressed calcium dependent molecules in addition to regulators of Ca_i localize to determine both when and where calcium is able to function as a second messenger. Based on this, calcium's role is limited to the spatio-temporal properties of Ca_i itself, and therefore, it is essential we characterize Ca_i dynamics in migrating FBM neurons. Our analysis indicates that upon initiating migration, FBM neurons experience Ca_i dynamics involving FBM neuron cell bodies in addition to dynamics that propagate along the length of trailing axons and filopodia projections (Fig. 4.2). Interestingly, Ca_i dynamics involving FBM neuron cell bodies, while global and robust in nature, seem to exhibit a wide range of amplitudes and durations as seen in table 4.1. We noted that neurons situated within r4 (n=12) on average exhibited more than a 2-fold greater amplitude as compared to neurons of r5 (n=10), however, showed a 28% lesser amplitude as compared to neurons situated within r6 (n=4).

While our current sample size is limited, this trend was consistent between ages of 20, 22, and 24 hpf. Interestingly, seemingly distinct Ca_i dynamics were shown to propagate along the length of FBM neuron axons. Through the careful observation of time-lapse movies, it was clear that these particular Ca_i dynamics predominantly originate from axon termini near hindbrain exit points in r4 and propagate retrograde. Interestingly, it is known that FBM neuron axons pause at hindbrain exit points before pathfinding towards the jaw (~28hpf; Higashijima et al.,

2000). At times, Ca_i dynamics were also observed at seemingly random points along FBM neuron axons, however, in contrast to those originating at hindbrain exit points, these Ca_i dynamics propagate anterograde. For example, a robust event can be seen in (Fig. 4.2 C). This particular event lasted ~11 seconds and propagated anterograde at a velocity of 6.67 mm/s. Lastly, Ca_i dynamics occurring along filopodia occur least often as compared to dynamics involving either cell bodies or axons. In all instances observed thus far (n=2), filopodia protrusions experiencing Ca_i dynamics consistently project laterally. To identify addition trends perhaps influential to FBM neuron migration, we must continue to characterize Ca_i dynamics among migrating FBM neurons.

Figure 4.2 FBM Neurons Exhibit a Variety of Ca_i Dynamics During Migration

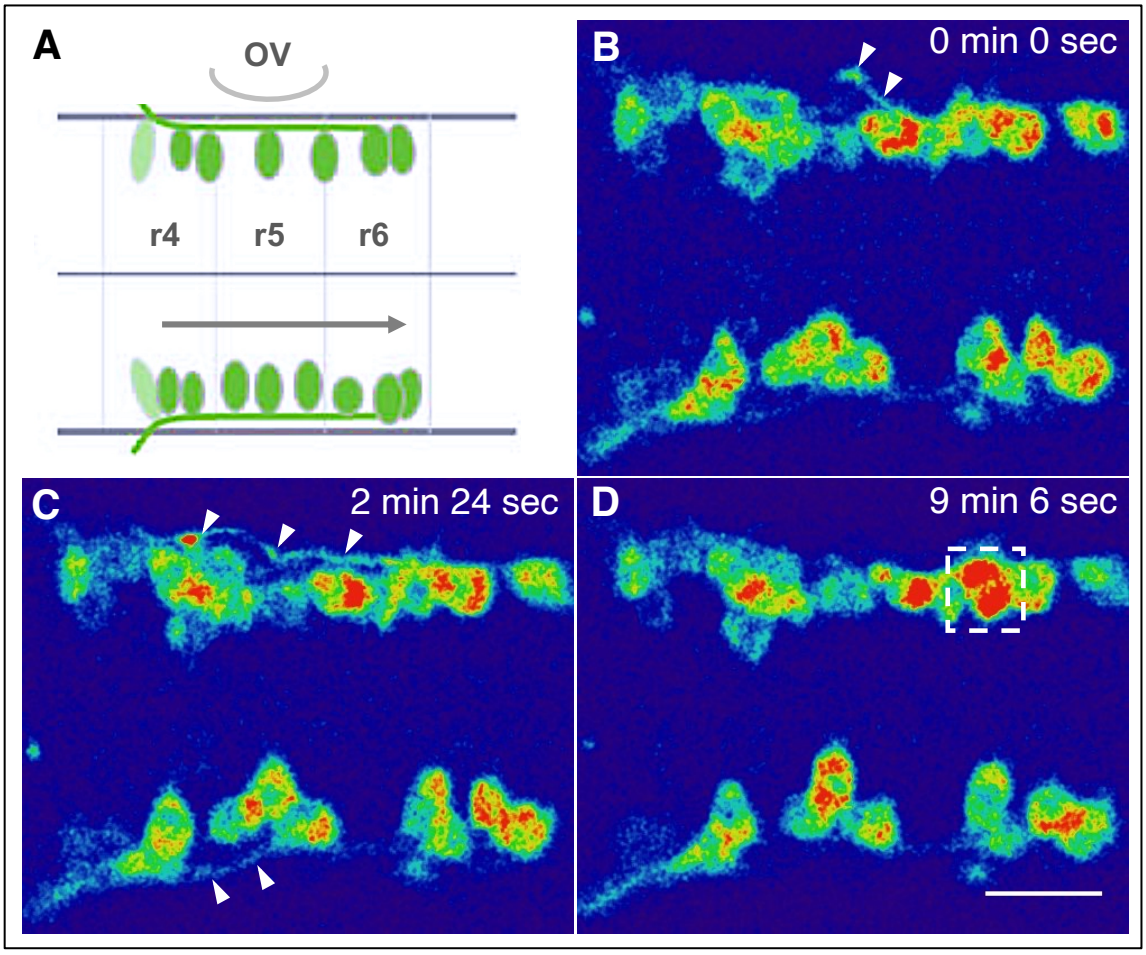

Figure 4.2 FBM Neurons Exhibit a Variety of Ca_i Dynamics During Migration

A shematic of FBM neurons migration (A) as well as representative snapshots of a 19 hpf *tg(zCREST1:GCaMP6s)* zebrafish embryo exhibiting Ca_i dynamics (white arrowheads) among FBM neuron filopodia (B), trailing axons (C), and cell bodies (D). Scale bar = 30 mm; OV, otic vesicle)

Table 4.1 Quantification of the Calcium Dynamics Observed Among FBM Neuron Cell Bodies

	20 hpf (n=3)	**22 hpf (n=7)**	**24 hpf (n=3)**
# of active cells / total	0.07 (n=75)	0.02 (n=165)	0.07 (n=124)
frequency among active cells (Events/Min.)	0.12 (n=5)	0.15 (n=4)	0.16 (n=9)
frequency among total (Events/Min.)	0.008 (n=75)	0.004 (n=165)	0.011 (n=165)
mean duration (Sec.)	27 (n=6)	22 (n=6)	22 (n=14)
range of duration (Sec.)	15-57 (n=6)	13-33 (n=6)	9-35 (n=14)
mean amp. (∆F/F)	1.15 (n=6)	1.56 (n=6)	0.77 (n=14)
range of amp. (∆F/F)	0.49-2.30 (n=6)	0.32-2.87 (n=6)	0.32-2.29 (n=14)
mean amp. r4 (∆F/F)	1.33 (n=4)	1.91 (n=3)	0.77 (n=5)
mean amp. r5 (∆F/F)	0.8 (n=2)	0.32 (n=2)	0.55 (n=6)
mean amp. r6 (∆F/F)	/	2.87 (n=1)	1.15 (n=3)

Table 4.1 Quantification of the Calcium Dynamics Observed Among FBM Neuron Cell Bodies

In an effort to identify relevant patterns, various features including frequency, amplitude, and duration were calculated based upon the Calcium dynamics observed among FBM neuron cell bodies.

4.3.2 Synchronous Neural Activity Within the Hindbrain (Post-Migration)

Using a transgenic zebrafish line expressing GCaMP6f in all differentiated neurons *Tg(zCREST1:mRFP::HuC:GCaMP6f-H2B*), we detected synchronized patterns of neuronal activity that extend to most hindbrain neurons (including BMNs) in addition to many neurons found within the caudal midbrain. These patterns seemed to appear ~60hpf, after migration, and it is unclear how long or if they persist beyond this developmental stage. Regardless, neurons were shown to experience elevated Ca_i concentrations that would at times last over a minute long. Furthermore, elevations were repetitive and predictable based on their duration and interval. Interestingly, however, this activity was a rare occurrence, as most larva would not exhibit any signs of synchronized activity. The rarity of this observation might suggest that this is a very short developmental occurrence or is perhaps temporally variable. Alternatively, unfavorable physiological conditions could prevent Ca_i dynamics from consistently occurring. Contrary to this, the synchronous activity observed may also be an artifact related to poor health. In fact, others have used the drug pentylenetetrazole to elicit spontaneous and synchronous activity in a zebrafish seizure model (Liu and baraban 2019).

Figure 4.3 FBM Neurons Participate in Synchronized and Prolonged Ca_i Dynamics

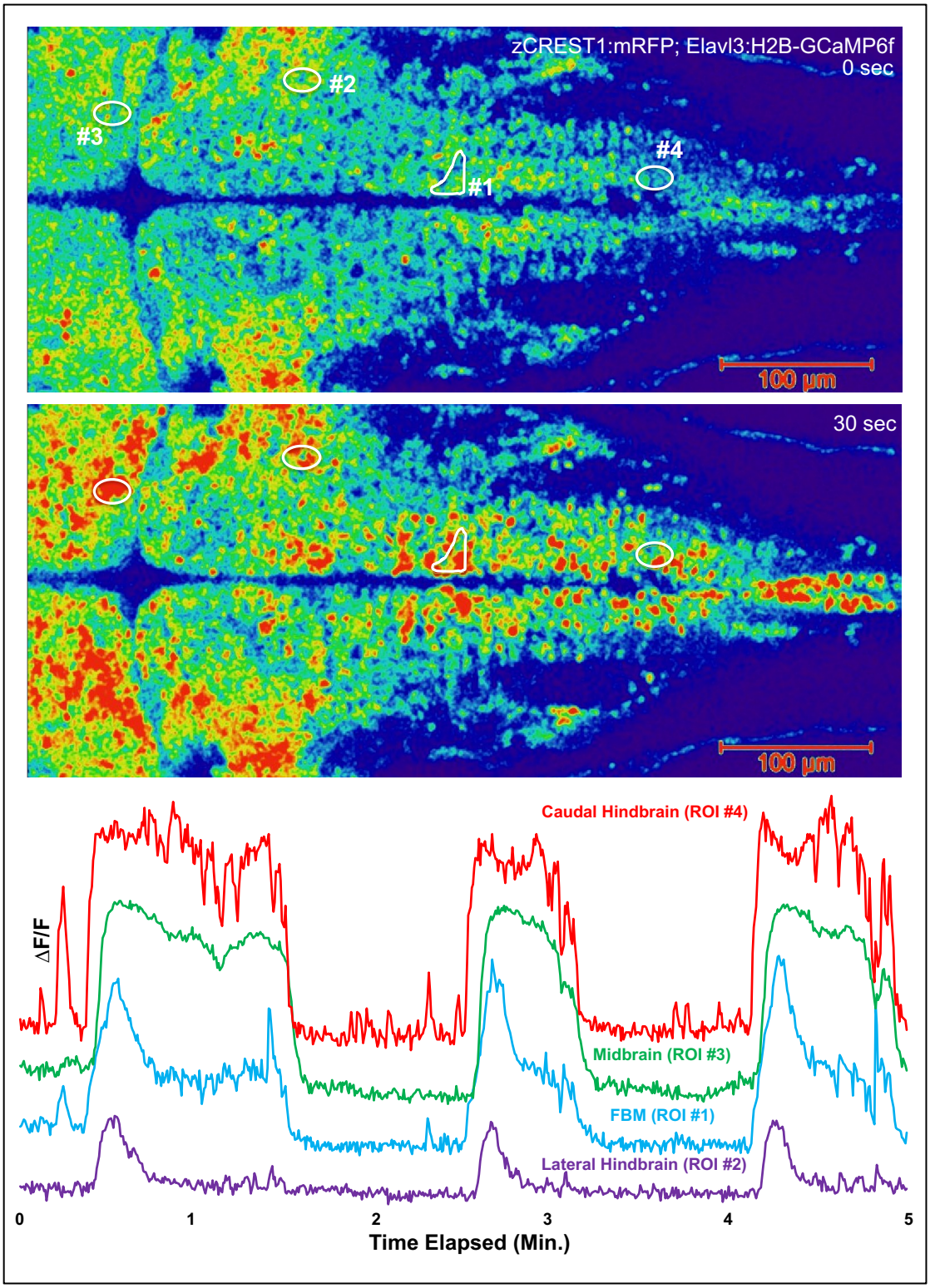

Figure 4.3 FBM Neurons Participate in Synchronized and Prolonged Ca_i Dynamics

Snapshots of the synchronized activity where prolonged elevations in Ca_i extend to many hindbrain neurons, including FBM neurons (heat maps). The top panel is a snapshot between events, while the lower panel is a snapshot during an event. The bottom plot is the corresponding time trace with indicated regions of interest (ROI). Individual traces were off-set to better illustrate the synchronized nature of these events since units are arbitrary.

4.4 DISCUSSION

4.4.1 Possible (Genetic) Regulators of Ca_i Involved in FBM Neuron Migration

Although the role of Ca_i remains uncertain in the context of FBM neuron migration, several genes, unique in their capacity to direct FBM neuron migration, have been investigated as regulators of Ca_i in other contexts. Furthermore, it is unclear which calcium dependent molecules are required for FBM neuron and the extent to which calcium regulates these molecules. To identify potential regulators of Ca_i dynamics functioning during FBM neuron migration, we must investigate genes that upon mutation, result in FBM neuron migration deficits, that have also been shown to function upstream of calcium in other contexts.

Importantly, several molecules involved in the planar cell polarity (PCP) pathway and have been shown to function as regulators of Ca_i and are indeed required for FBM neuron migration. For instance, core PCP component *fzd3a* belongs to a class of G-protein coupled receptors that in other contexts functions through the non-canonical/calcium dependent WNT pathway to regulate PLC and/or PKC activity and therefore, calcium release from the endoplasmic reticulum (Sheldahl et al., 1999). Here, two different types of ER calcium channels mediate calcium release, inositol trisphosphate (IP3) receptors and ryanodine receptors. Interestingly, FRIZZLED3A is specifically thought to play a stabilizing role in extending filopodia, while antagonistic VANGL2 localizes to retracting filopodia (Davey et al., 2016). Based on this, *Frizzled* is a promising candidate for analysis. Likewise, Receptor tyrosine kinase, PTK7 has also been implicated in Wnt

signaling, allows for activation of the PLC/PKC pathway and is similarly required for FBM neuron migration (Alfandari et al., 2010; Glasco et al., 2012).

Calcium dependent cell adhesion molecules, CDH2 and CELSR2/3, are also required for FBM neuron migration (Wanner & Prince 2013; Qu et al, 2010) and interestingly, previous experiments demonstrate that the over-expression of either cadherin or *celsr* extracellular domains result in increased Ca_i dynamics among other neuron types through a feed-back loop mechanism (Sheng et al. 2013, Shima et al., 2007, Halbach et al., 1992). Based on this finding, one would expect reduced activity among FBM neurons in *cdh2* or *Celsr2/3* mutants, which could be an underlying cause for the lack of migration observed. Taken together, *cdh2* or *Celsr2/3* may also represent promising candidate genes for future observation.

4.4.2 Possible (Cellular) Regulators of Ca_i Involved in FBM Neuron Migration

As previously discussed, others have shown that radial glial fibers within the cerebral cortex function as a scaffold to guide radially migrating neurons through cortical layers. Recent studies show that Ca_i dynamics propagate along the length of radial glia fibers to initiate cell intrinsic Ca_i dynamics in adjacent granular neurons allowing for their translocation through cortical layers (Rash et al., 2019). Interestingly, it was previously shown that FBM neuron migration from r4 to r5 is dependent on “pioneer” FBM axons (the first FBM neurons to migrate and extend axons) suggesting that pioneer neurons signal to “follower” neurons to initiate their migration (Wanner and Prince 2013). Importantly, others also demonstrate that the

association between pioneer neurons and follower neurons requires the calcium dependent cell adhesion molecules CDH2 (Rebman et al., 2016). Likewise, FBM neuron migration from r5 to r6 is dependent on axons of the medial longitudinal fasciculus (MLF) that project both parallel and adjacent to migrating FBM neurons (Wanner and Prince 2013). While the mechanisms maintaining these interactions remain largely unknown, we speculate that pioneer FBM neurons and/or MLF neurons may signal to follower FBM neurons through calcium mediated signals to regulate their caudal migration analogous to how radial glia regulate Ca_i dynamics/ migration in adjacent granular neurons (Rash et al., 2019). However, to test this prediction we must continue to investigate Ca_i dynamics within migrating FBM neurons and surrounding cells.

4.4.3 Potential Inputs Regulating Neural Activity of FBM Neurons in the Zebrafish Larva

As discussed, synchronizes patterns of neural activity propagate throughout the zebrafish hindbrain and result in elevated Ca_i among FBM neurons as well as many other neurons. In mice, seemingly analogous patterns of neural activity are initiated by the Serotonergic Raphe (Bosma et al., 2017). Based on this, the serotonergic raphe may represent a conserved regulator of Ca_i allowing for the establishment of various circuits (Watari et al., 2013; Bosma et al.,2017). Interestingly, the serotonergic raphe, is involved in the breathing circuit, and has been shown to innervate several brain regions, yet a direct association between FBM neuron and the serotonergic raphe has not been shown

(Gaspar and Lillesaar, 2012). Similarly, the visual, olfactory, gustatory, and hypothalamic systems are also thought of as essential inputs to branchiomotor neurons, however, direct connections between these systems and FBM neurons has also not been demonstrated.

4.5 Concluding Remarks and Future Directions

To directly demonstrate a role for Calcium in the context of FBM neuron migration or development of the hindbrain, Ca_i dynamics must be suppressed. Early experiments aimed at understanding the role of calcium in neurons were largely carried out using *ex vivo* techniques and utilized harsh channel blockers delivered by means of invasive injections and/or bath application. Acknowledging this, several innovative tools including Channelrhodopsin and the inward rectifying potassium channels, Kir2.1, are now being used in order to mis-regulate Ca_i (Wiegert et al., 2017). These tools used in combination with *in vivo* models are now allowing for unprecedented insights into the role of calcium.

While optogenetic tools termed “opsins” are among the most widely utilized means of manipulating Ca_i in neurons, it remains unclear how said tools behave prior to circuit establishment. For instance, the genetic tools halorhodopsin and archearhodopsin have been widely utilized based on their ability to silence neural activity, however, said tools prove unreliable in silencing what is generally thought of as “spontaneous” activity (i.e. activity that is not a result of synaptic transmission) and in fact, these tools can even increase patterns of activity (Wiegert et al., 2016). Contrary to this, the inward rectifying potassium channel,

Kir2.1, has been repeatedly shown to hyperpolarize and therefore, suppress neural activity, including spontaneous forms of activity, spanning a wide variety of biological applications (Bortone and Polleux, 2009, Garcia et al., 2011, Plazas et al., 2013). For example, Plazas et al. 2013 reports a 46% reduction in the total number of primary spinal motor neurons exhibiting Ca_i dynamics as a result of expression of Kir2.1. Additionally, as compared to channelrhodopsin, Kir2.1 is constitutively active and thus does not require additional manipulation (Wiegert et al., 2017). For this reason, Kir2.1 is preferred over other genetic means of silencing activity. To determine the role of calcium in the context of FBM neuron migration and circuit establishment, the consequences of expressing Kir2.1 must be assessed among FBM neurons. Furthermore, to our benefit, organisms have evolved various toxins specific in targeting particular calcium channels, which directly regulate Ca_i. These toxins include the genetically encoded snail toxin, MVIIA, and spider toxin, AgoIVA, which have been shown to specifically bind and inhibit N-type and P/Q-type calcium channels respectively (Auer et. al., 2010). While these toxins may provide a means of misregulating Ca_i , they would also allow us discern the endogenous calcium channels involved in FBM neuron Ca_i dynamics. Acknowledging that expression of these constructs may prove fatal by adulthood, said constructs must either be sparsely and/or transiently expressed.

Chapter 5: Evaluating Regeneration of Branchiomotor Neurons Following Ablation

5.1 INTRODUCTION

Nerve damage as a result of injury, infection, or disease is a common medical condition among humans. Based on their tremendous capacity for regeneration, the zebrafish model system has served as the gold standard for investigation into the mechanisms underlying regeneration. To date, many different neurons have been demonstrated to regenerate following trauma and/or ablation. Neuron regeneration has been most predominantly studied in the context of the peripheral nervous system through the regeneration of axons and/or growth cones. During axon regeneration, newly established growth cones must correctly interpret guidance cues in order to re-innervate the appropriate target tissues in a process known as target-specific regeneration (Bolívar et al., 2020; Madison et al., 2009).

Interestingly, it has been demonstrated that the target-specific regeneration of the Vagus nerve (cranial nerve nX) is regulated by mechanisms separate from those regulating the initial innervation of pharyngeal arches during development (Isabella et. al., 2021). Others have also shown that the ectopic expression of various neurogenic factors such as NeuroD1 following spinal cord injury is sufficient for the reprogramming/conversion of glial cells into neurons (Milichko and Dyachuk, 2020; Puls et al., 2020). In comparison to regeneration within the peripheral nervous system, regeneration within the central nervous system is thought to be much more restricted and/or context dependent. An example of

where regeneration has been observed within the central nervous system comes from the retina, where damage results in the de-differentiation and proliferation of Müller glia. Subsequently Müller glia re-differentiate into many new neurons, bipolar and amacrine cells, as well as cone photoreceptors (Wu et al., 2001; Yurco & Cameron, 2005; Fausett & Goldman, 2006; Raymond et al., 2006; Bernardos et al., 2007; Fimbel et al., 2007). Interestingly, others have shown that suppressing the innate immune system can accelerate photoreceptor regeneration within the retina (White et al., 2017). Because many neuron types are not able regenerate following injury/ablation, the regenerative capacity of specific neurons must be individually determined.

Fortunately, several tools for the physical, chemical, and genetic ablation of cells have emerged as useful strategies for determining whether a particular cell type is able to regenerate. (Curado et al., 2007; McGuire et al., 2004). Means of physical ablation via lasers or surgery enables both temporal and spatial control, however, this is labor-intensive, lacks specificity, and in some cases can be difficult to replicate (Gahtan and Baier, 2004; Yang et al., 2004). Furthermore, methods of chemical ablation can have toxic, non-specific effects on surrounding tissue, which may lend to confounding results. In contrast, genetically-mediated ablation is achieved through the expression of either toxin-producing enzymes or receptor-specific toxins that upon activation result in targeted cell death. The enzyme Nitroreductase (NTR) combined with the non-toxic prodrug Metronidazole (MTZ) has been used as a genetic tool for the ablation of various cell types spanning several contexts (Ariga et al., 2010; Chen et al., 2011; Zhao et al., 2009). Using

this system over others allows for spatial as well as temporal control during ablation. Here, NTR expressed in cells targeted for ablation convert MTZ into a cytotoxic DNA cross-linking agent that induces cell death via apoptosis (Knox et al., 1988; Curado et al., 2008). Using the NTR-MTZ method of ablation, we specifically ablated branchiomotor neurons during larval stages beginning 48 hours post fertilization (hpf). Here we evaluate the regenerative capacity of branchiomotor neurons using the chemo-genetic tool, NTR-MTZ. We also examine whether or not suppression of the immune system is capable of enhancing regeneration in zebrafish branchiomotor neurons.

5.2 MATERIALS & METHODS

NTR-MTZ Mediated Ablation of Branchiomotor Neurons

In order to specifically ablate branchiomotor neurons and subsequently assess regeneration, *Tg(zCREST:NTR-mCherry::isl1:gfp)* zebrafish larvae were first treated with 0.2 mM Phenylthiourea (PTU; dissolved in DMSO) at 24 hours post fertilization (hpf) in order to inhibit the development of melanocytes, therefore preventing pigmentation. PTU should be replaced every 2-3 days to continuously block pigmentation. The following day, beginning 48 hpf, larvae were treated with 10mM MTZ by dissolving 41.1mg MTZ in ~24 ml E3 media (without methylene blue, supplemented with 0.2 mM PTU). To track the ablation/regeneration of branchiomotor neurons over time, single larva were transferred in 750mL of E3, to individual wells already containing 6ml of E3 + 10mM MTZ. Once larva were placed in individual wells, 3.75ml E3 + 10mM MTZ was removed from each well, then 3ml was replaced. Next, 2ml E3 + 10mM MTZ was removed from each well, then 2ml

was added back. After 24 hours of incubation, E3 + 10mM MTZ was removed and replaced with E3 without MTZ. E3 was again replaced at least 4 additional times to ensure that MTZ was entirely removed. To determine the extent of ablation following MTZ treatment, larva were moved to E3 containing 0.016% tricaine. Once immobilized, larva were moved to a petri dish and were embedded in a small droplet of 0.3% agarose supplemented with 0.016% tricaine. Once mounted, enough E3 was added to agarose droplets to entirely submerge sample and therefore, prevent desiccation. Images were acquired using a Leica M205 stereo microscope. After images were acquired for the 1 day(s) post ablation (dpa) time-point, larva were carefully removed from agarose droplets using forceps. To assist in the removal of larva, additional E3 media was added. Larva were then transferred back to 6 well plates containing exactly 6ml of E3 media + PTU. To suppress the immune system and possible accelerate regeneration as previously demonstrated, Dimethazone-P (DEX-P) was used (White et al., 2017). For DEX-P treatment groups, 30µl of either 0.5mM DEX-P was added to wells already containing 6ml of E3 to obtain a final concentration of 2.5mM. DEX-P + E3 solution, was replaced daily and 30ml of paramecia culture was also added each time media was replaced. Dex-P treatment began the day following ablation, immediately after acquiring the 1dpa time point/image. Larva were mounted and imaged a second time in order to acquire the 7dpa time-point. Images were then evaluated by comparing 1dpa and 7dpa.

Figure 5.1 Schematic of MTZ Treatment and Imaging Protocol

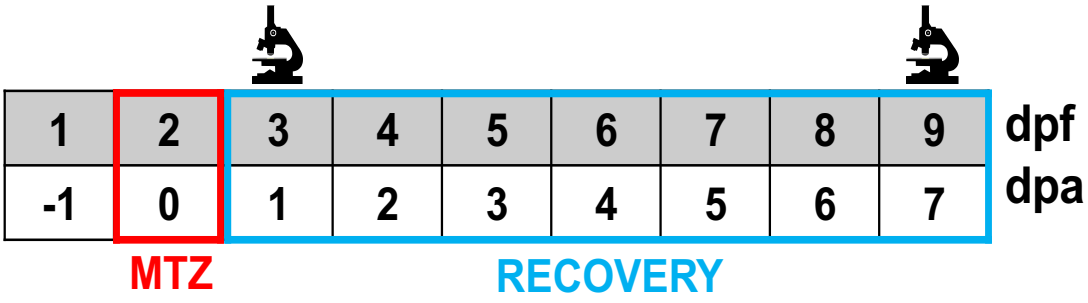

Figure 5.1 Schematic of MTZ Treatment Protocol

Tg(zRCEST:Ntr-mCherry) zebrafish were treated with MTZ for 24 hours beginning at 48 hpf. The next day (1 dpa) larva were imaged in order to assess ablation. 6 days later (7 dpa) larva were re-imaged in order to assess possible regeneration. Dex-P treatment began the day following ablation, immediately after acquiring the 1dpa time point/image.

5.3 RESULTS & DISCUSSION

Branchiomotor Neurons Fail to Regenerate Following NTR-MTZ Mediated Ablation

Unfortunately, while ablation was consistently observed among all NTR expressing individuals treated with MTZ (n = 92), no signs of regeneration were ever observed. Furthermore, suppression of the innate immune system by treating with Dexamethazone-P immediately after MTZ treatment did not enhance the regenerative capacity of branchiomotor neurons as had been observed in the retina (n=18; White et al., 2017).

As another means of screening for larva that exhibit signs of regeneration, a mortality assay was implemented under the assumption that sufficiently ablated individuals would likely starve due to an inability to eat, unless regeneration had occurred. Therefore, we assessed the mortality of ablated larva as compared to control treated animals knowing that if any ablated individuals had survived as long as controls, this could perhaps be some indication of regeneration. However, all ablated individuals had died off sooner than control animals.

Regardless, there are several possible explanations for the lack of regeneration observed. Importantly, while considered component of the peripheral nervous system, branchiomotor neurons are physically situated within the central nervous system, which may be a determining factor in whether or not a particular neural population has the ability/capacity to regenerate. Regeneration of neurons

within the central nervous system is thought to be limited by the formation of glial scars where proliferating glia release various molecules to inhibit Schwann cells that would otherwise express various neurogenic factors conducive to regeneration (Yiu et al., 2006; Bradbury et al., 2006; Bregman et al., 1995). These factors include myelin-associated inhibitors (MAIs) and the chondroitin sulfate proteoglycans (CSPGs; Huebner and Strittmatter, 2009). An alternative explanation for the lack of regeneration observed comes from Grohmann et al., who demonstrated that the NTR/MTZ method of ablation can have harmful effects on neighboring cells, as dying cells eventually release toxic by-products of MTZ metabolism (Grohmann et al., 2009). To determine whether or not branchiomotor neurons are in fact incapable of regenerating following whole-cell ablation, alternative means of ablation must be implemented.

Figure 5.2 Evaluating Branchiomotor Neuron Ablation Following MTZ Treatment Ablation

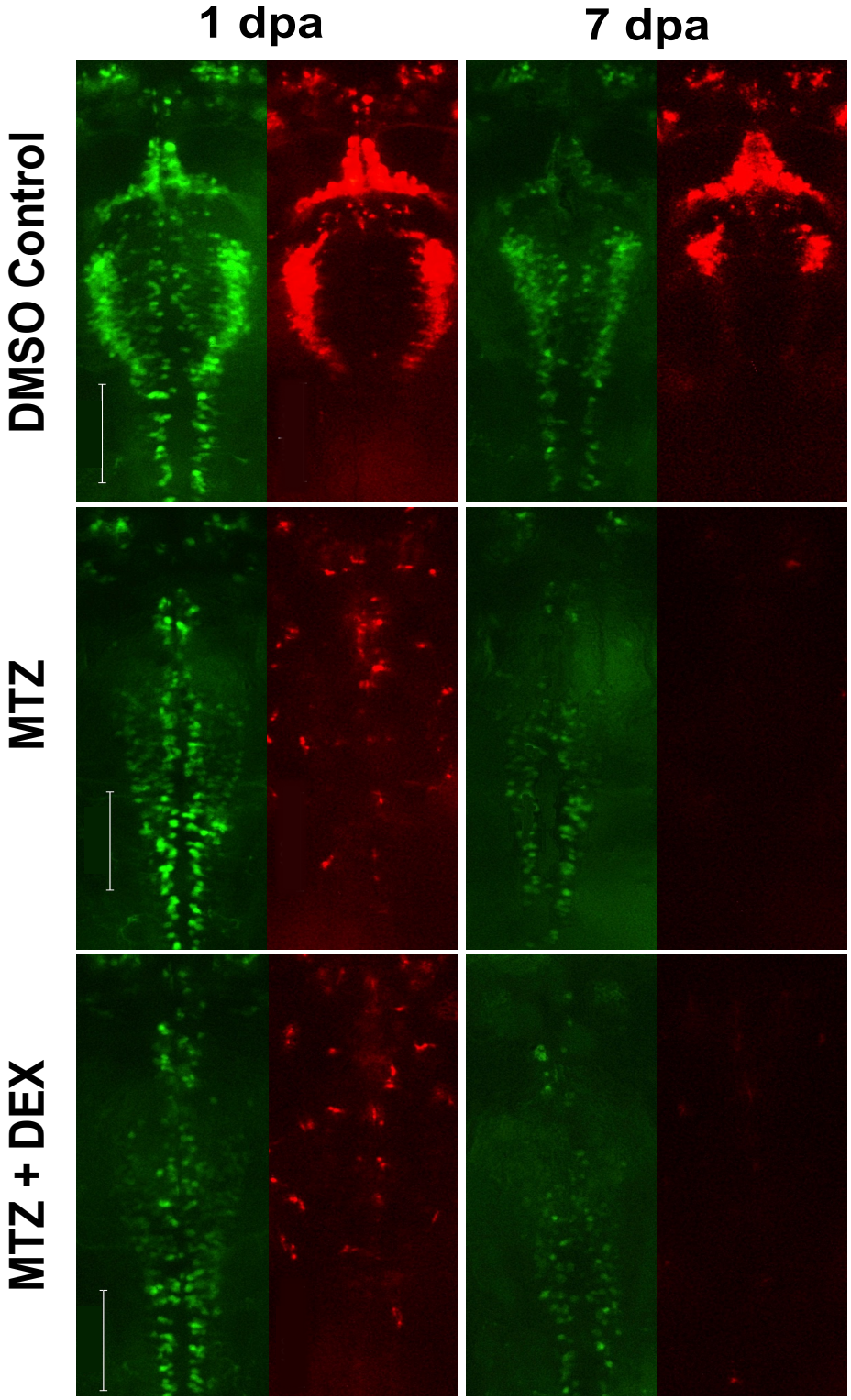

Figure 5.2 Evaluating Branchiomotor Neuron Ablation Following MTZ Treatment Ablation

Representative florescent images of *Tg(Ntr-mCherry)* zebrafish larva, either control treated, MTZ abated, or MTZ ablated supplemented with Dex-P. Dex-P treatment began the day following ablation, immediately after acquiring the 1dpa time point/image. Scale bar = 100 mm

Figure 5.3 Mortality Assay for Identifying Individuals Exhibiting Regeneration

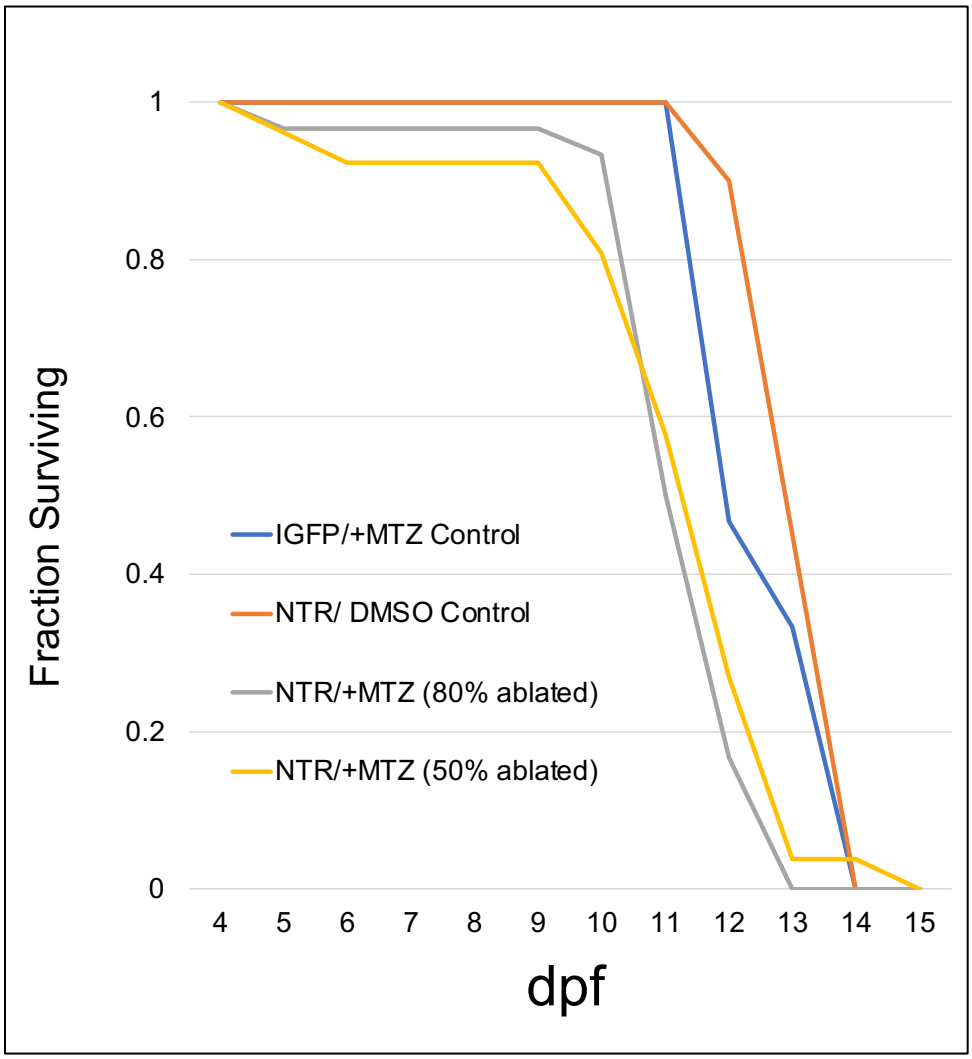

Figure 5.3 Mortality Assay for Identifying Individuals Exhibiting Regeneration

The mortality of ablated and control larva was evaluated. Here we assume that survivorship of ablated individuals, comparable to that of control treated animals could perhaps be some indication of regeneration. However, all ablated individuals had died off earlier than control animals (the source of comparison).

REFERENCES

Alcántara, S., Ruiz, M., De Castro, F., Soriano, E., & Sotelo, C. (2000). Netrin 1 acts as an attractive or as a repulsive cue for distinct migrating neurons during the development of the cerebellar system. *Development* (Cambridge, England), 127(7), 1359–1372. https://doi.org/10.1242/dev.127.7.1359

Alfandari, D., Cousin, H., & Marsden, M. (2010). Mechanism of Xenopus cranial neural crest cell migration. *Cell adhesion & migration*, 4(4), 553–560. https://doi.org/10.4161/cam.4.4.12202

Ammerpohl, O., Pratschke, J., Schafmayer, C., Haake, A., Faber, W., von Kampen, O., Brosch, M., Sipos, B., von Schönfels, W., Balschun, K., Röcken, C., Arlt, A., Schniewind, B., Grauholm, J., Kalthoff, H., Neuhaus, P., Stickel, F., Schreiber, S., Becker, T., Siebert, R., … Hampe, J. (2012). Distinct DNA methylation patterns in cirrhotic liver and hepatocellular carcinoma. *International journal of cancer,* 130(6), 1319–1328. https://doi.org/10.1002/ijc.26136

Andrews, W. D., Barber, M., & Parnavelas, J. G. (2007). Slit-Robo interactions during cortical development. *Journal of anatomy*, 211(2), 188–198. https://doi.org/10.1111/j.1469-7580.2007.00750.x

Anton, E. S., Kreidberg, J. A., & Rakic, P. (1999). Distinct functions of alpha3 and alpha(v) integrin receptors in neuronal migration and laminar organization of the cerebral cortex. *Neuron*, 22(2), 277–289. https://doi.org/10.1016/s0896-6273(00)81089-2

Ariga, J., Walker, S. L., & Mumm, J. S. (2010). Multicolor time-lapse imaging of transgenic zebrafish: visualizing retinal stem cells activated by targeted neuronal cell ablation. *Journal of visualized experiments : JoVE*, (43), 2093. https://doi.org/10.3791/2093

Asante, E., Hummel, D., Gurung, S., Kassim, Y. M., Al-Shakarji, N., Palaniappan, K., Sittaramane, V., & Chandrasekhar, A. (2021). Defective Neuronal Positioning Correlates With Aberrant Motor Circuit Function in Zebrafish. *Frontiers in neural circuits,* 15, 690475. https://doi.org/10.3389/fncir.2021.690475

Auer S, et al. Silencing neurotransmission with membrane-tethered toxins. *Nature Methods* 2010; 7:229–236.

Bastock, R., Strutt, H., & Strutt, D. (2003). Strabismus is asymmetrically localised and binds to Prickle and Dishevelled during Drosophila planar polarity

patterning. *Development* (Cambridge, England), 130(13), 3007–3014. https://doi.org/10.1242/dev.00526

Bastock, R., Strutt, H., & Strutt, D. (2003). Strabismus is asymmetrically localised and binds to Prickle and Dishevelled during Drosophila planar polarity patterning. *Development* (Cambridge, England), 130(13), 3007–3014. https://doi.org/10.1242/dev.00526

Belvindrah, R., Graus-Porta, D., Goebbels, S., Nave, K. A., & Müller, U. (2007). Beta1 integrins in radial glia but not in migrating neurons are essential for the formation of cell layers in the cerebral cortex. *The Journal of neuroscience : the official journal of the Society for Neuroscience,* 27(50), 13854–13865. https://doi.org/10.1523/JNEUROSCI.4494-07.2007

Benzing, T., Simons, M., & Walz, G. (2007). Wnt signaling in polycystic kidney disease. *Journal of the American Society of Nephrology* : JASN, 18(5), 1389–1398. https://doi.org/10.1681/ASN.2006121355

Bernardos, R. L., Barthel, L. K., Meyers, J. R., & Raymond, P. A. (2007). Late-stage neuronal progenitors in the retina are radial Müller glia that function as retinal stem cells. *The Journal of neuroscience : the official journal of the Society for Neuroscience,* 27(26), 7028–7040. https://doi.org/10.1523/JNEUROSCI.1624-07.2007

Bodea, G. O., Spille, J. H., Abe, P., Andersson, A. S., Acker-Palmer, A., Stumm, R., Kubitscheck, U., & Blaess, S. (2014). Reelin and CXCL12 regulate distinct migratory behaviors during the development of the dopaminergic system. *Development* (Cambridge, England), 141(3), 661–673. https://doi.org/10.1242/dev.099937

Bolívar, S., Navarro, X., & Udina, E. (2020). Schwann Cell Role in Selectivity of Nerve *Regeneration. Cells*, 9(9), 2131. https://doi.org/10.3390/cells9092131

Bortone D, Polleux F. KCC2 expression promotes the termination of cortical interneuron migration in a voltage-sensitive calcium-dependent manner. *Neuron* 2009; 62:53–71.

Bosma M. M. (2017). Regulation of Spontaneous Propagating Waves in the Embryonic Mouse Brainstem. *Frontiers in neural circuits,* 10, 110. https://doi.org/10.3389/fncir.2016.00110

Boucherie, C., Boutin, C., Jossin, Y., Schakman, O., Goffinet, A. M., Ris, L., Gailly, P., & Tissir, F. (2018). Neural progenitor fate decision defects, cortical hypoplasia and behavioral impairment in *Celsr*1-deficient mice.

Molecular psychiatry, 23(3), 723–734. https://doi.org/10.1038/mp.2017.236

Bradbury EJ, McMahon SB (August 2006). "Spinal cord repair strategies: why do they work?". *Nature Reviews. Neuroscience.* 7 (8): 644–53. doi:10.1038/nrn1964. PMID 16858392. S2CID 11890502.

Bregman BS, Kunkel-Bagden E, Schnell L, Dai HN, Gao D, Schwab ME (November 1995). "Recovery from spinal cord injury mediated by antibodies to neurite growth inhibitors". *Nature*. 378 (6556): 498–501.

Brzóska, H. Ł., d'Esposito, A. M., Kolatsi-Joannou, M., Patel, V., Igarashi, P., Lei, Y., Finnell, R. H., Lythgoe, M. F., Woolf, A. S., Papakrivopoulou, E., & Long, D. A. (2016). Planar cell polarity genes *Celsr*1 and *Vangl*2 are necessary for kidney growth, differentiation, and rostrocaudal patterning. *Kidney international*, 90(6), 1274–1284. https://doi.org/10.1016/j.kint.2016.07.011

Brzóska, H. Ł., d'Esposito, A. M., Kolatsi-Joannou, M., Patel, V., Igarashi, P., Lei, Y., Finnell, R. H., Lythgoe, M. F., Woolf, A. S., Papakrivopoulou, E., & Long, D. A. (2016). Planar cell polarity genes *Celsr*1 and *Vangl*2 are necessary for kidney growth, differentiation, and rostrocaudal patterning. *Kidney international,* 90(6), 1274–1284. https://doi.org/10.1016/j.kint.2016.07.011

Cadigan, K. M., & Nusse, R. (1997). Wnt signaling: a common theme in animal development. *Genes & development*, 11(24), 3286–3305. https://doi.org/10.1101/gad.11.24.3286

Cha, J., Bartos, A., Park, C., Sun, X., Li, Y., Cha, S. W., Ajima, R., Ho, H. Y., Yamaguchi, T. P. and Dey, S. K. (2014). Appropriate crypt formation in the uterus for embryo homing and implantation requires *Wnt5a*-ROR signaling. *Cell Rep* 8, 382-392.

Chai, X., Förster, E., Zhao, S., Bock, H. H., & Frotscher, M. (2009). Reelin stabilizes the actin cytoskeleton of neuronal processes by inducing n-cofilin phosphorylation at serine3. *The Journal of neuroscience : the official journal of the Society for Neuroscience,* 29(1), 288–299. https://doi.org/10.1523/JNEUROSCI.2934-08.2009

Chai, X., Förster, E., Zhao, S., Bock, H. H., & Frotscher, M. (2009). Reelin stabilizes the actin cytoskeleton of neuronal processes by inducing n-cofilin phosphorylation at serine3. *The Journal of neuroscience : the official journal of the Society for Neuroscience,* 29(1), 288–299. https://doi.org/10.1523/JNEUROSCI.2934-08.2009

Chandrasekhar A. (2004). Turning heads: development of vertebrate branchiomotor neurons. *Developmental dynamics : an official publication of the American Association of Anatomists*, 229(1), 143–161. https://doi.org/10.1002/dvdy.10444

Chazal, G., Durbec, P., Jankovski, A., Rougon, G., & Cremer, H. (2000). Consequences of neural cell adhesion molecule deficiency on cell migration in the rostral migratory stream of the mouse. *The Journal of neuroscience : the official journal of the Society for Neuroscience*, 20(4), 1446–1457. https://doi.org/10.1523/JNEUROSCI.20-04-01446.2000

Chen, C. F., Chu, C. Y., Chen, T. H., Lee, S. J., Shen, C. N., & Hsiao, C. D. (2011). Establishment of a transgenic zebrafish line for superficial skin ablation and functional validation of apoptosis modulators in vivo. *PloS one,* 6(5), e20654. https://doi.org/10.1371/journal.pone.0020654

Chen, G., Sima, J., Jin, M., Wang, K. Y., Xue, X. J., Zheng, W., Ding, Y. Q., & Yuan, X. B. (2008). Semaphorin-3A guides radial migration of cortical neurons during development. *Nature neuroscience*, 11(1), 36–44. https://doi.org/10.1038/nn2018

Chen, W. S., Antic, D., Matis, M., Logan, C. Y., Povelones, M., Anderson, G. A., Nusse, R., & Axelrod, J. D. (2008). Asymmetric homotypic interactions of the atypical cadherin flamingo mediate intercellular polarity signaling. *Cell*, 133(6), 1093–1105. https://doi.org/10.1016/j.cell.2008.04.048

Christiansen, J. H., Coles, E. G., & Wilkinson, D. G. (2000). Molecular control of neural crest formation, migration and differentiation. *Current opinion in cell biology,* 12(6), 719–724. https://doi.org/10.1016/s0955-0674(00)00158-7

Copp, A. J., & Harding, B. N. (1999). Neuronal migration disorders in humans and in mouse models--an overview. *Epilepsy research,* 36(2-3), 133–141. https://doi.org/10.1016/s0920-1211(99)00047-9

Curado, S., Anderson, R. M., Jungblut, B., Mumm, J., Schroeter, E., & Stainier, D. Y. (2007). Conditional targeted cell ablation in zebrafish: a new tool for regeneration studies. Developmental dynamics : *an official publication of the American Association of Anatomists,* 236(4), 1025–1035. https://doi.org/10.1002/dvdy.21100

Curado, S., Stainier, D. Y., & Anderson, R. M. (2008). Nitroreductase-mediated cell/tissue ablation in zebrafish: a spatially and temporally controlled ablation method with applications in developmental and regeneration studies. *Nature protocols,* 3(6), 948–954. https://doi.org/10.1038/nprot.2008.58

Curtin, J. A., Quint, E., Tsipouri, V., Arkell, R. M., Cattanach, B., Copp, A. J., Henderson, D. J., Spurr, N., Stanier, P., Fisher, E. M., Nolan, P. M., Steel, K. P., Brown, S. D., Gray, I. C., & Murdoch, J. N. (2003). Mutation of *Celsr*1 disrupts planar polarity of inner ear hair cells and causes severe neural tube defects in the mouse. *Current biology* : CB, 13(13), 1129–1133. https://doi.org/10.1016/s0960-9822(03)00374-9

D.M. Glasco, W. Pike, Y. Qu, L. Reustle, K. Misra, M. Di Bonito, M. Studer, B. Fritzsch, A.M. Goffinet, F. Tissir, A. Chandrasekhar. (2016).The atypical cadherin *Celsr*1 functions non-cell autonomously to block rostral migration of facial branchiomotor neurons in mice. *Dev Biol*, 417 (2016), pp. 40-49

Darcy DP, Isaacson JS. L-type calcium channels govern calcium signaling in migrating newborn neurons in the postnatal olfactory bulb. *Journal of Neuroscience* 2009; 29(8):2510–8

Davey, C. F., Mathewson, A. W., & Moens, C. B. (2016). PCP Signaling between Migrating Neurons and their Planar-Polarized Neuroepithelial Environment Controls Filopodial Dynamics and Directional Migration. *PLoS genetics*, 12(3), e1005934. https://doi.org/10.1371/journal.pgen.1005934

De Marco Garcia NV, Karayannis T, Fishell G., Neuronal activity is required for the development of specific cortical interneuron subtypes. *Nature* 2011; 472:351–355.

Del Giudice, I., Messina, M., Chiaretti, S., Santangelo, S., Tavolaro, S., De Propris, M. S., Nanni, M., Pescarmona, E., Mancini, F., Pulsoni, A., Martelli, M., Di Rocco, A., Finolezzi, E., Paoloni, F., Mauro, F. R., Cuneo, A., Guarini, A., & Foà, R. (2012). Behind the scenes of non-nodal MCL: downmodulation of genes involved in actin cytoskeleton organization, cell projection, cell adhesion, tumour invasion, TP53 pathway and mutated status of immunoglobulin heavy chain genes. *British journal of haematology,* 156(5), 601–611. https://doi.org/10.1111/j.1365-2141.2011.08962.x

Deng, J., & Elberger, A. J. (2001). The role of pioneer neurons in the development of mouse visual cortex and corpus callosum. *Anatomy and embryology*, 204(6), 437–453. https://doi.org/10.1007/s429-001-8001-3

Devenport, D., & Fuchs, E. (2008). Planar polarization in embryonic epidermis orchestrates global asymmetric morphogenesis of hair follicles. *Nature cell biology*, 10(11), 1257–1268. https://doi.org/10.1038/ncb178

Devenport, D., & Fuchs, E. (2008). Planar polarization in embryonic epidermis orchestrates global asymmetric morphogenesis of hair follicles*. Nature cell biology*, 10(11), 1257–1268. https://doi.org/10.1038/ncb1784

Dissanayake, S. K., Wade, M., Johnson, C. E., O'Connell, M. P., Leotlela, P. D., French, A. D., Shah, K. V., Hewitt, K. J., Rosenthal, D. T., Indig, F. E., Jiang, Y., Nickoloff, B. J., Taub, D. D., Trent, J. M., Moon, R. T., Bittner, M., & Weeraratna, A. T. (2007). The *Wnt5A*/protein kinase C pathway mediates motility in melanoma cells via the inhibition of metastasis suppressors and initiation of an epithelial to mesenchymal transition. *The Journal of biological chemistry,* 282(23), 17259–17271. https://doi.org/10.1074/jbc.M700075200

Fausett, B. V., & Goldman, D. (2006). A role for alpha1 tubulin-expressing Müller glia in regeneration of the injured zebrafish retina. T*he Journal of neuroscience : the official journal of the Society for Neuroscience,* 26(23), 6303–6313. https://doi.org/10.1523/JNEUROSCI.0332-06.2006

Feng, J., Han, Q., & Zhou, L. (2012). Planar cell polarity genes, *Celsr*1-3, in neural *development*. Neuroscience bulletin, 28(3), 309–315. https://doi.org/10.1007/s12264-012-1232-8

Feng, J., Han, Q., & Zhou, L. (2012). Planar cell polarity genes, *Celsr*1-3, in neural development. *Neuroscience bulletin,* 28(3), 309–315. https://doi.org/10.1007/s12264-012-1232-8

Fimbel, S. M., Montgomery, J. E., Burket, C. T., & Hyde, D. R. (2007). Regeneration of inner retinal neurons after intravitreal injection of ouabain in zebrafish. The Journal of neuroscience : the official journal of the *Society for Neuroscience,* 27(7), 1712–1724. https://doi.org/10.1523/JNEUROSCI.5317-06.2007

Franco, S. J., Martinez-Garay, I., Gil-Sanz, C., Harkins-Perry, S. R., & Müller, U. (2011). Reelin regulates cadherin function via Dab1/Rap1 to control neuronal migration and lamination in the neocortex. *Neuron*, 69(3), 482–497. https://doi.org/10.1016/j.neuron.2011.01.003

Gahtan E, Baier H (2004) Of lasers, mutants, and see-through brains: Functional neuroanatomy in zebrafish. *J Neurobiol* 59: 147–161.

Gärtner, A., Fornasiero, E. F., & Dotti, C. G. (2012). N-cadherin: a new player in neuronal polarity. *Cell cycle* (Georgetown, Tex.), 11(12), 2223–2224. https://doi.org/10.4161/cc.20797

Gaspar, P., & Lillesaar, C. (2012). Probing the diversity of serotonin neurons. *Philosophical transactions of the Royal Society of London. Series B, Biological sciences,* 367(1601), 2382–2394. https://doi.org/10.1098/rstb.2011.0378

Glasco, D. M., Pike, W., Qu, Y., Reustle, L., Misra, K., Di Bonito, M., Studer, M., Fritzsch, B., Goffinet, A. M., Tissir, F., & Chandrasekhar, A. (2016). The atypical cadherin *Celsr*1 functions non-cell autonomously to block rostral migration of facial branchiomotor neurons in mice. *Developmental biology*, 417(1), 40–49. https://doi.org/10.1016/j.ydbio.2016.07.004

Glasco, D. M., Sittaramane, V., Bryant, W., Fritzsch, B., Sawant, A., Paudyal, A., Stewart, M., Andre, P., Cadete Vilhais-Neto, G., Yang, Y., Song, M. R., Murdoch, J. N., & Chandrasekhar, A. (2012). The mouse Wnt/PCP protein *Vangl*2 is necessary for migration of facial branchiomotor neurons, and functions independently of *Dishevelled*. *Developmental biology,* 369(2), 211–222. https://doi.org/10.1016/j.ydbio.2012.06.02

Gleeson, J. G., & Walsh, C. A. (2000). Neuronal migration disorders: from genetic diseases to developmental mechanisms. *Trends in neurosciences,* 23(8), 352–359. https://doi.org/10.1016/s0166-2236(00)01607-6

Goffinet A. M. (1984). Abnormal development of the facial nerve nucleus in reeler mutant mice. *Journal of anatomy,* 138 (Pt 2)(Pt 2), 207–215.

Grohmann, M., Paulmann, N., Fleischhauer, S., Vowinckel, J., Priller, J., & Walther, D. J. (2009). A mammalianized synthetic nitroreductase gene for high-level expression. *BMC cancer,* 9, 301. https://doi.org/10.1186/1471-2407-9-301

Guerrini, R., & Parrini, E. (2010). Neuronal migration disorders. *Neurobiology of disease,* 38(2), 154–166. https://doi.org/10.1016/j.nbd.2009.02.008

Gust, J., Wright, J. J., Pratt, E. B., and Bosma, M. M. (2003). Development of synchronized activity of cranial motor neurons in the segmented embryonic mouse hindbrain. *J. Physiol.* 550, 123–133. doi: 10.1113/jphysiol.2002. 038737

Guthrie, S. (2007). Patterning and axon guidance of cranial motor neurons. *Nat. Rev. Neurosc.* 8, 859–871. doi: 10.1038/nrn2254

Hasan, M. K., Yu, J., Chen, L., Cui, B., Widhopf Ii, G. F., Rassenti, L., Shen, Z., Briggs, S. P., & Kipps, T. J. (2017). *Wnt5a* induces ROR1 to complex with HS1 to enhance migration of chronic lymphocytic leukemia cells. *Leukemia*, 31(12), 2615–2622. https://doi.org/10.1038/leu.2017.133

Hasan, M., Yu, J., Chen, L. et al. *Wnt5a* induces ROR1 to complex with HS1 to enhance migration of chronic lymphocytic leukemia cells. *Leukemia* 31, 2615–2622 (2017). https://doi.org/10.1038/leu.2017.133

Hatten M. E. (1999). Central nervous system neuronal migration. *Annual review of neuroscience*, 22, 511–539. https://doi.org/10.1146/annurev.neuro.22.1.511

Hatten M. E. (2002). New directions in neuronal migration. *Science* (New York, N.Y.), 297(5587), 1660–1663. https://doi.org/10.1126/science.1074572

Higashijima S, Hotta Y, Okamoto H., Visualization of cranial motor neurons in live transgenic zebrafish expressing green fluorescent protein under the control of the islet-1 promoter/enhancer. *The Journal of Neuroscience: the official journal of the Society for Neuroscience* 2000, 20(1):206-218.

Hirota, Y., & Nakajima, K. (2017). Control of Neuronal Migration and Aggregation by Reelin Signaling in the Developing Cerebral Cortex. *Frontiers in cell and developmental biology*, 5, 40. https://doi.org/10.3389/fcell.2017.00040

Honda, T., Shimizu, K., Fukuhara, A., Irie, K., and Takai, Y. (2003). Regulation by nectin of the velocity of the formation of adherens junctions and tight junctions. Biochem. *Biophys. Res. Commun.* 306, 104–109. doi: 10.1016/s0006-291x(03)00919-7

Horwitz, R., & Webb, D. (2003). Cell migration. *Current biology* : CB, 13(19), R756–R759. https://doi.org/10.1016/j.cub.2003.09.014

Hosseini, V., Dani, C., Geranmayeh, M. H., Mohammadzadeh, F., Nazari Soltan Ahmad, S., & Darabi, M. (2019). Wnt lipidation: Roles in trafficking, modulation, and function. *Journal of cellular physiology,* 234(6), 8040–8054. https://doi.org/10.1002/jcp.27570

Huebner, E. A., & Strittmatter, S. M. (2009). Axon regeneration in the peripheral and central nervous systems. *Results and problems in cell differentiation*, 48, 339–351. https://doi.org/10.1007/400_2009_19

Hunt, P. N., Gust, J., McCabe, A. K., and Bosma, M. M. (2006). Primary role of the serotonergic midline system in synchronized spontaneous activity during development of the embryonic mouse hindbrain. *J. Neurobiol.* 66, 1239–1252. doi: 10.1002/neu.20259

Hunt, P. N., McCabe, A. K., and Bosma, M. M. (2005). Midline serotonergic neurones contribute to widespread synchronized activity in embryonic mouse hindbrain. *J. Physiol*. 566, 807–819. doi: 10.1113/jphysiol.2005.089581

Hutchins, B. I., Li, L., & Kalil, K. (2011). Wnt/calcium signaling mediates axon growth and guidance in the developing corpus callosum. *Developmental neurobiology,* 71(4), 269–283. https://doi.org/10.1002/dneu.2084

Inestrosa, N. C. Inestrosa, & Lorena Varela-Nallar, L. Varela-Nallar. (2015). Wnt signalling in neuronal differentiation and development. *Cell and tissue research,* 359, 215-223. doi: 10.1007/s00441-014-1996-4

Isabella, A. J., Stonick, J. A., Dubrulle, J., & Moens, C. B. (2021). Intrinsic positional memory guides target-specific axon regeneration in the zebrafish vagus nerve. *Development* (Cambridge, England), 148(18), dev199706. https://doi.org/10.1242/dev.199706

Ishii, K., Kubo, K. I., & Nakajima, K. (2016). Reelin and Neuropsychiatric Disorders. *Frontiers in cellular neuroscience*, 10, 229. https://doi.org/10.3389/fncel.2016.00229

Janda, C. Y., Waghray, D., Levin, A. M., Thomas, C., & Garcia, K. C. (2012). Structural basis of Wnt recognition by *Frizzled*. *Science* (New York, N.Y.), 337(6090), 59–64. https://doi.org/10.1126/science.1222879

Jossin, Y., & Cooper, J. A. (2011). Reelin, Rap1 and N-cadherin orient the migration of multipolar neurons in the developing neocortex*. Nature neuroscience*, 14(6), 697–703. https://doi.org/10.1038/nn.2816

Ju, X. D., Guo, Y., Wang, N. N., Huang, Y., Lai, M. M., Zhai, Y. H., Guo, Y. G., Zhang, J. H., Cao, R. J., Yu, H. L., Cui, L., Li, Y. T., Wang, X. Z., Ding, Y. Q., & Zhu, X. J. (2014). Both Myosin-10 isoforms are required for radial neuronal migration in the developing cerebral cortex. *Cerebral cortex* (New York, N.Y. : 1991), 24(5), 1259–1268. https://doi.org/10.1093/cercor/bhs407

Katoh, M., & Katoh, M. (2005). Comparative genomics on *Wnt5a* and Wnt5b genes. *International journal of molecular medicine*, 15(4), 749–753.

Katoh, M., & Katoh, M. (2007). STAT3-induced WNT5A signaling loop in embryonic stem cells, adult normal tissues, chronic persistent inflammation, rheumatoid arthritis and cancer (Review*). International journal of molecular medicine,* 19(2), 273–278.

Kaucká, M., Plevová, K., Pavlová, S., Janovská, P., Mishra, A., Verner, J., Procházková, J., Krejcí, P., Kotasková, J., Ovesná, P., Tichy, B., Brychtová, Y., Doubek, M., Kozubík, A., Mayer, J., Pospísilová, S., & Bryja, V. (2013). The planar cell polarity pathway drives pathogenesis of chronic lymphocytic leukemia by the regulation of B-lymphocyte migration. *Cancer research,* 73(5), 1491–1501. https://doi.org/10.1158/0008-5472.CAN-12-1752

Keller, R., & Shook, D. (2008). Dynamic determinations: patterning the cell behaviours that close the amphibian blastopore. *Philosophical*

transactions of the Royal Society of London. Series B, Biological sciences, 363(1495), 1317–1332. https://doi.org/10.1098/rstb.2007.2250

Kelly, L. K., Wu, J., Yanfeng, W. A., & Mlodzik, M. (2016). Frizzled-Induced Van Gogh Phosphorylation by CK1ε Promotes Asymmetric Localization of Core PCP Factors in Drosophila. *Cell reports,* 16(2), 344–356. https://doi.org/10.1016/j.celrep.2016.06.010

Kim H. K., Bae J., Lee S. H., Hwang S. H., Kim M. S., Kim M. J., et al. (2020). Blockers of Wnt3a, Wnt10a, or beta-Catenin Prevent Chemotherapy-Induced Neuropathic Pain In Vivo. *Neurotherapeutics* 10.1007/s13311-020-00956-w

Kim, S., You, D., Jeong, Y., Yoon, S. Y., Kim, S. A., Kim, S. W., Nam, S. J., & Lee, J. E. (2020). WNT5A augments cell invasiveness by inducing CXCL8 in HER2-positive breast cancer cells. *Cytokine*, 135, 155213. https://doi.org/10.1016/j.cyto.2020.155213

Knox, R. J., Boland, M. P., Friedlos, F., Coles, B., Southan, C., & Roberts, J. J. (1988). The nitroreductase enzyme in Walker cells that activates 5-(aziridin-1-yl)-2,4-dinitrobenzamide (CB 1954) to 5-(aziridin-1-yl)-4-hydroxylamino-2-nitrobenzamide is a form of NAD(P)H dehydrogenase (quinone) (EC 1.6.99.2). *Biochemical pharmacology*, 37(24), 4671–4677. https://doi.org/10.1016/0006-2952(88)90336-x

Kriegstein, A. R., & Noctor, S. C. (2004). Patterns of neuronal migration in the embryonic cortex. *Trends in neurosciences*, 27(7), 392–399. https://doi.org/10.1016/j.tins.2004.05.001

Kurayoshi, M., Yamamoto, H., Izumi, S., & Kikuchi, A. (2007). Post-translational palmitoylation and glycosylation of Wnt-5a are necessary for its signalling. *The Biochemical journal*, 402(3), 515–523. https://doi.org/10.1042/BJ20061476

Kwan, K. M., Fujimoto, E., Grabher, C., Mangum, B. D., Hardy, M. E., Campbell, D. S., Parant, J. M., Yost, H. J., Kanki, J. P., & Chien, C. B. (2007). The Tol2kit: a multisite gateway-based construction kit for Tol2 transposon transgenesis constructs. *Developmental dynamics : an official publication of the American Association of Anatomists,* 236(11), 3088–3099. https://doi.org/10.1002/dvdy.21343

Lambert de Rouvroit, C., & Goffinet, A. M. (2001). Neuronal migration. *Mechanisms of development,* 105(1-2), 47–56. https://doi.org/10.1016/s0925-4773(01)00396-3

Le Douarin, N. M., & Dupin, E. (2003). Multipotentiality of the neural crest. *Current opinion in genetics & development*, 13(5), 529–536. https://doi.org/10.1016/j.gde.2003.08.002

Lindenmaier, L. B., Parmentier, N., Guo, C., Tissir, F., & Wright, K. M. (2019). Dystroglycan is a scaffold for extracellular axon guidance decisions. *eLife*, 8, e42143. https://doi.org/10.7554/eLife.42143

Liu, J., & Baraban, S. C. (2019). Network Properties Revealed during Multi-Scale Calcium Imaging of Seizure Activity in Zebrafish. *eNeuro*, 6(1), ENEURO.0041-19.2019. https://doi.org/10.1523/ENEURO.0041-19.2019

Lyuksyutova, A. I., Lu, C. C., Milanesio, N., King, L. A., Guo, N., Wang, Y., Nathans, J., Tessier-Lavigne, M., & Zou, Y. (2003). Anterior-posterior guidance of commissural axons by Wnt-frizzled signaling. *Science* (New York, N.Y.), 302(5652), 1984–1988. https://doi.org/10.1126/science.1089610

Lyuksyutova, A. I., Lu, C. C., Milanesio, N., King, L. A., Guo, N., Wang, Y., Nathans, J., Tessier-Lavigne, M., & Zou, Y. (2003). Anterior-posterior guidance of commissural axons by Wnt-frizzled signaling. *Science* (New York, N.Y.), 302(5652), 1984–1988. https://doi.org/10.1126/science.1089610

Madison, R. D., Sofroniew, M. V., & Robinson, G. A. (2009). Schwann cell influence on motor neuron regeneration accuracy. *Neuroscience*, 163(1), 213–221. https://doi.org/10.1016/j.neuroscience.2009.05.073

Marín, O., & Rubenstein, J. L. (2001). A long, remarkable journey: tangential migration in the telencephalon. Nature reviews. *Neuroscience*, 2(11), 780–790. https://doi.org/10.1038/35097509

Marín, O., & Rubenstein, J. L. (2003). Cell migration in the forebrain. *Annual review of neuroscience,* 26, 441–483. https://doi.org/10.1146/annurev.neuro.26.041002.131058

Marín, O., Plump, A. S., Flames, N., Sánchez-Camacho, C., Tessier-Lavigne, M., & Rubenstein, J. L. (2003). Directional guidance of interneuron migration to the cerebral cortex relies on subcortical Slit1/2-independent repulsion and cortical attraction. *Development* (Cambridge, England), 130(9), 1889–1901. https://doi.org/10.1242/dev.00417

Marín, O., Yaron, A., Bagri, A., Tessier-Lavigne, M., & Rubenstein, J. L. (2001). Sorting of striatal and cortical interneurons regulated by semaphorin-neuropilin interactions. *Science* (New York, N.Y.), 293(5531), 872–875. https://doi.org/10.1126/science.1061891

Mayor, R., & Theveneau, E. (2013). The neural crest. *Development* (Cambridge, England), 140(11), 2247–2251. https://doi.org/10.1242/dev.091751

McArthur KL, Fetcho JR. Key features of structural and functional organization of zebrafish facial motor neurons are resilient to a genetic disruption of neuronal migration. *Current biology* 2017; 27(12):1746-1756.e5.

McArthur, K. L., & Fetcho, J. R. (2017). Key Features of Structural and Functional Organization of Zebrafish Facial Motor Neurons Are Resilient to Disruption of Neuronal Migration. *Current biology* : CB, 27(12), 1746–1756.e5. https://doi.org/10.1016/j.cub.2017.05.033

McGuire, S. E., Mao, Z., & Davis, R. L. (2004). Spatiotemporal gene expression targeting with the TARGET and gene-switch systems in Drosophila. *Science's STKE : signal transduction knowledge environment,* 2004(220), pl6. https://doi.org/10.1126/stke.2202004pl6

Mikels, A. J., & Nusse, R. (2006). Wnts as ligands: processing, secretion and reception. *Oncogene*, 25(57), 7461–7468. https://doi.org/10.1038/sj.onc.1210053

Milichko, V., & Dyachuk, V. (2020). Novel Glial Cell Functions: Extensive Potency, Stem Cell-Like Properties, and Participation in Regeneration and Transdifferentiation. *Frontiers in cell and developmental biology*, 8, 809. https://doi.org/10.3389/fcell.2020.00809

Mithal, D. S., Ren, D., & Miller, R. J. (2013). CXCR4 signaling regulates radial glial morphology and cell fate during embryonic spinal cord development. *Glia*, 61(8), 1288–1305. https://doi.org/10.1002/glia.22515

Miyata, T., Kawaguchi, A., Okano, H., & Ogawa, M. (2001). Asymmetric inheritance of radial glial fibers by cortical neurons. *Neuron*, 31(5), 727–741. https://doi.org/10.1016/s0896-6273(01)00420-2

Montague, K., Lowe, A. S., Uzquiano, A., Knüfer, A., Astick, M., Price, S. R., & Guthrie, S. (2017). The assembly of developing motor neurons depends on an interplay between spontaneous activity, type II cadherins and gap junctions. *Development* (Cambridge, England), 144(5), 830–836. https://doi.org/10.1242/dev.144063

Montcouquiol, M., Sans, N., Huss, D., Kach, J., Dickman, J. D., Forge, A., Rachel, R. A., Copeland, N. G., Jenkins, N. A., Bogani, D., Murdoch, J., Warchol, M. E., Wenthold, R. J., & Kelley, M. W. (2006). Asymmetric localization of *Vangl*2 and Fz3 indicate novel mechanisms for planar cell polarity in mammals. *The Journal of neuroscience : the official journal of*

the Society for Neuroscience, 26(19), 5265–5275. https://doi.org/10.1523/JNEUROSCI.4680-05.2006

Morante-Oria, J., Carleton, A., Ortino, B., Kremer, E. J., Fairén, A., & Lledo, P. M. (2003). Subpallial origin of a population of projecting pioneer neurons during corticogenesis. *Proceedings of the National Academy of Sciences of the United States of America,* 100(21), 12468–12473. https://doi.org/10.1073/pnas.1633692100

Nishimura, T., Honda, H., & Takeichi, M. (2012). Planar cell polarity links axes of spatial dynamics in neural-tube closure. *Cell*, 149(5), 1084–1097. https://doi.org/10.1016/j.cell.2012.04.021

Noctor, S. C., Flint, A. C., Weissman, T. A., Dammerman, R. S., & Kriegstein, A. R. (2001). Neurons derived from radial glial cells establish radial units in neocortex. *Nature*, 409(6821), 714–720. https://doi.org/10.1038/35055553

Nural HF, Todd Farmer W, Mastick GS (2007) The Slit receptor Robo1 is predominantly expressed via the Dutt1 alternative promoter in pioneer neurons in the embryonic mouse brain and spinal cord. *Gene Expr Patterns* 7:837–845.

Ohshima, T., Ogawa, M., Takeuchi, K., Takahashi, S., Kulkarni, A. B., & Mikoshiba, K. (2002). Cyclin-dependent kinase 5/p35 contributes synergistically with Reelin/Dab1 to the positioning of facial branchiomotor and inferior olive neurons in the developing mouse hindbrain. *The Journal of neuroscience : the official journal of the Society for Neuroscience*, 22(10), 4036–4044. https://doi.org/10.1523/JNEUROSCI.22-10-04036.2002

Okamoto, M., Udagawa, N., Uehara, S., Maeda, K., Yamashita, T., Nakamichi, Y., Kato, H., Saito, N., Minami, Y., Takahashi, N., & Kobayashi, Y. (2014). Noncanonical *Wnt5a* enhances Wnt/β-catenin signaling during osteoblastogenesis. *Scientific reports*, 4, 4493. https://doi.org/10.1038/srep04493

Onishi, K., Shafer, B., Lo, C., Tissir, F., Goffinet, A. M., & Zou, Y. (2013). Antagonistic functions of Dishevelleds regulate Frizzled3 endocytosis via filopodia tips in Wnt-mediated growth cone guidance. *The Journal of neuroscience : the official journal of the Society for Neuroscience*, 33(49), 19071–19085. https://doi.org/10.1523/JNEUROSCI.2800-13.2013

Onishi, K., Shafer, B., Lo, C., Tissir, F., Goffinet, A. M., & Zou, Y. (2013). Antagonistic functions of Dishevelleds regulate Frizzled3 endocytosis via filopodia tips in Wnt-mediated growth cone guidance. *The Journal of*

neuroscience : the official journal of the Society for Neuroscience, 33(49), 19071–19085. https://doi.org/10.1523/JNEUROSCI.2800-13.2013

Otteson, D. C., Cirenza, P. F., & Hitchcock, P. F. (2002). Persistent neurogenesis in the teleost retina: evidence for regulation by the growth-hormone/insulin-like growth factor-I axis. *Mechanisms of development,* 117(1-2), 137–149. https://doi.org/10.1016/s0925-4773(02)00188-0

Palomer, E., Buechler, J., & Salinas, P. C. (2019). Wnt Signaling Deregulation in the Aging and Alzheimer's Brain. *Frontiers in cellular neuroscience*, 13, 227. https://doi.org/10.3389/fncel.2019.00227

Palomer, E., Buechler, J., & Salinas, P. C. (2019). Wnt Signaling Deregulation in the Aging and Alzheimer's Brain. *Frontiers in cellular neuroscience*, 13, 227. https://doi.org/10.3389/fncel.2019.00227

Park, K. W., Morrison, C. M., Sorensen, L. K., Jones, C. A., Rao, Y., Chien, C. B., Wu, J. Y., Urness, L. D., & Li, D. Y. (2003). Robo4 is a vascular-specific receptor that inhibits endothelial migration. *Developmental biology,* 261(1), 251–267. https://doi.org/10.1016/s0012-1606(03)00258-6

Parnavelas, J. G., Alifragis, P., & Nadarajah, B. (2002). The origin and migration of cortical neurons. *Progress in brain research,* 136, 73–80. https://doi.org/10.1016/s0079-6123(02)36008-4

Parnavelas, J. G., Alifragis, P., & Nadarajah, B. (2002). The origin and migration of cortical neurons. *Progress in brain research*, 136, 73–80. https://doi.org/10.1016/s0079-6123(02)36008-4

Pearlman, A. L., Faust, P. L., Hatten, M. E., & Brunstrom, J. E. (1998). New directions for neuronal migration. *Current opinion in neurobiology*, 8(1), 45–54. https://doi.org/10.1016/s0959-4388(98)80007-x

Pearlman, A. L., Faust, P. L., Hatten, M. E., & Brunstrom, J. E. (1998). New directions for neuronal migration. *Current opinion in neurobiology*, 8(1), 45–54. https://doi.org/10.1016/s0959-4388(98)80007-x

Plazas, P. V., Nicol, X., & Spitzer, N. C., Activity-dependent competition regulates motor neuron axon pathfinding via PlexinA3. *Proceedings of the National Academy of Sciences of the United States of America* 2013; 110(4), 1524–1529

Poduri, A., Evrony, G. D., Cai, X., & Walsh, C. A. (2013). Somatic mutation, genomic variation, and neurological disease. *Science* (New York, N.Y.), 341(6141), 1237758. https://doi.org/10.1126/science.1237758

Prakash, N., Puelles, E., Freude, K., Trümbach, D., Omodei, D., Di Salvio, M., Sussel, L., Ericson, J., Sander, M., Simeone, A., & Wurst, W. (2009). Nkx6-1 controls the identity and fate of red nucleus and oculomotor neurons in the mouse midbrain. *Development* (Cambridge, England), 136(15), 2545–2555. https://doi.org/10.1242/dev.031781

Puls, B., Ding, Y., Zhang, F., Pan, M., Lei, Z., Pei, Z., Jiang, M., Bai, Y., Forsyth, C., Metzger, M., Rana, T., Zhang, L., Ding, X., Keefe, M., Cai, A., Redilla, A., Lai, M., He, K., Li, H., & Chen, G. (2020). Regeneration of Functional Neurons After Spinal Cord Injury via in situ NeuroD1-Mediated Astrocyte-to-Neuron Conversion. *Frontiers in cell and developmental biology*, 8, 591883. https://doi.org/10.3389/fcell.2020.591883

Qu Y, Glasco DM, Zhou L, Sawant A, Ravni A, Fritzsch B, Damrau C, Murdoch JN, Evans S, Pfaff SL, et al. Atypical Cadherins *Celsr*1-3 Differentially Regulate Migration of Facial Branchiomotor Neurons in Mice*. J Neurosci*. 2010;30:9392–9401.

Qu Y, Huang Y, Feng J, Alvarez-Bolado G, Grove EA, Yang Y, Tissir F, Zhou L, Goffinet AM (2014) Genetic evidence that *Celsr*3 and *Celsr*2, together with Fzd3, regulate forebrain wiring in a *Vang*l-independent manner. *Proc Natl Acad Sci*.111:E2996–E3004, doi:10.1073/pnas.1402105111, pmid:25002511.

Qu, Y., Glasco, D.M., Zhou, L., Sawant, A., Ravni, A., Fritzsch, B., Damrau, C., Murdoch, J.N., Evans, S., Pfaff, S.L., Formstone, C., Goffinet, A.M., Chandrasekhar, A., Tissir, F., 2010. Atypical cadherins *Celsr*1-3 differentially regulate migration of facial branchiomotor neurons in mice. *J. Neurosci.* 30, 9392–9401. http://dx.doi.org/ 10.1523/JNEUROSCI.0124-10.2010.

Qu, Y., Huang, Y., Feng, J., Alvarez-Bolado, G., Grove, E. A., Yang, Y., Tissir, F., Zhou, L., & Goffinet, A. M. (2014). Genetic evidence that *Celsr*3 and *Celsr*2, together with Fzd3, regulate forebrain wiring in a Vangl-independent manner. *Proceedings of the National Academy of Sciences of the United States of America*, 111(29), E2996–E3004. https://doi.org/10.1073/pnas.1402105111

Raffaello, A., Mammucari, C., Gherardi, G., & Rizzuto, R. (2016). Calcium at the Center of Cell Signaling: Interplay between Endoplasmic Reticulum, Mitochondria, and Lysosomes. *Trends in biochemical sciences,* 41(12), 1035–1049. https://doi.org/10.1016/j.tibs.2016.09.001

Rash BG, Ackman JB, Rakic P. Bidirectional radial Ca(2+) activity regulates neurogenesis and migration during early cortical column formation. *Science Advances* 2016; 2:e1501733.

Ravni, A., Qu, Y., Goffinet, A. M., & Tissir, F. (2009). Planar cell polarity cadherin *Celsr*1 regulates skin hair patterning in the mouse. *The Journal of investigative dermatology*, 129(10), 2507–2509. https://doi.org/10.1038/jid.2009.84

Raymond, P. A., Barthel, L. K., Bernardos, R. L., & Perkowski, J. J. (2006). Molecular characterization of retinal stem cells and their niches in adult zebrafish. *BMC developmental biology,* 6, 36. https://doi.org/10.1186/1471-213X-6-36

Raymond, P. A., Barthel, L. K., Bernardos, R. L., & Perkowski, J. J. (2006). Molecular characterization of retinal stem cells and their niches in adult zebrafish. *BMC developmental biology,* 6, 36. https://doi.org/10.1186/1471-213X-6-36

Rebman, J. K., Kirchoff, K. E., & Walsh, G. S. (2016). Cadherin-2 Is Required Cell Autonomously for Collective Migration of Facial Branchiomotor Neurons. *PloS one*, 11(10), e0164433. https://doi.org/10.1371/journal.pone.0164433

Rhee, J., Buchan, T., Zukerberg, L., Lilien, J., & Balsamo, J. (2007). Cables links Robo-bound Abl kinase to N-cadherin-bound beta-catenin to mediate Slit-induced modulation of adhesion and transcription. *Nature cell biology*, 9(8), 883–892. https://doi.org/10.1038/ncb1614

Rudolph, J., Zimmer, G., Steinecke, A., Barchmann, S., & Bolz, J. (2010). Ephrins guide migrating cortical interneurons in the basal telencephalon. *Cell adhesion & migration,* 4(3), 400–408. https://doi.org/10.4161/cam.4.3.11640

Saint-Amant L, Drapeau P., Time course of the development of motor behaviors in the zebrafish embryo. *Journal of Neurobiology* 1998; 37:622–632.

Schmid, R. S., Shelton, S., Stanco, A., Yokota, Y., Kreidberg, J. A., & Anton, E. S. (2004). alpha3beta1 integrin modulates neuronal migration and placement during early stages of cerebral cortical development. *Development* (Cambridge, England), 131(24), 6023–6031. https://doi.org/10.1242/dev.01532

Sekine, K., Kawauchi, T., Kubo, K., Honda, T., Herz, J., Hattori, M., Kinashi, T., & Nakajima, K. (2012). Reelin controls neuronal positioning by promoting cell-matrix adhesion via inside-out activation of integrin α5β1. *Neuron*, 76(2), 353–369. https://doi.org/10.1016/j.neuron.2012.07.020

Shafer, B., Onishi, K., Lo, C., Colakoglu, G., & Zou, Y. (2011). *Vangl*2 promotes Wnt/planar cell polarity-like signaling by antagonizing Dvl1-mediated

feedback inhibition in growth cone guidance. *Developmental cell,* 20(2), 177–191. https://doi.org/10.1016/j.devcel.2011.01.002

Sheldahl, L. C., Park, M., Malbon, C. C., & Moon, R. T. (1999). Protein kinase C is differentially stimulated by Wnt and Frizzled homologs in a G-protein-dependent manner. *Current biology* : CB, 9(13), 695–698. https://doi.org/10.1016/s0960-9822(99)80310-

Sheldahl, L. C., Park, M., Malbon, C. C., & Moon, R. T. (1999). Protein kinase C is differentially stimulated by Wnt and Frizzled homologs in a G-protein-dependent manner. *Current biology* : CB, 9(13), 695–698. https://doi.org/10.1016/s0960-9822(99)80310-8

Sheng, L., Leshchyns'ka, I., & Sytnyk, V. (2013). Cell adhesion and intracellular calcium signaling in neurons. *Cell communication and signaling* : CCS, 11, 94. https://doi.org/10.1186/1478-811X-11-94

Shima, Y., Kawaguchi, S. Y., Kosaka, K., Nakayama, M., Hoshino, M., Nabeshima, Y., Hirano, T., & Uemura, T. (2007). Opposing roles in neurite growth control by two seven-pass transmembrane cadherins. *Nature neuroscience*, 10(8), 963–969. https://doi.org/10.1038/nn1933

Silva, C. G., Peyre, E., & Nguyen, L. (2019). Cell migration promotes dynamic cellular interactions to control cerebral cortex morphogenesis. *Nature reviews.* Neuroscience, 20(6), 318–329. https://doi.org/10.1038/s41583-019-0148-y

Solnica-Krezel L. (2005). Conserved patterns of cell movements during vertebrate gastrulation. *Current biology* : CB, 15(6), R213–R228. https://doi.org/10.1016/j.cub.2005.03.016

Song, M. R. (2007). Moving cell bodies: understanding the migratory mechanism of facial motor neurons. *Arch. Pharm. Res.* 30, 1273–1282. doi: 10.1007/bf02980268

Stahley, S. N., Basta, L. P., Sharan, R., & Devenport, D. (2021). *Celsr*1 adhesive interactions mediate the asymmetric organization of planar polarity complexes. *eLife*, 10, e62097. https://doi.org/10.7554/eLife.62097

Stahley, S. N., Basta, L. P., Sharan, R., & Devenport, D. (2021). *Celsr*1 adhesive interactions mediate the asymmetric organization of planar polarity complexes. *eLife*, 10, e62097. https://doi.org/10.7554/eLife.62097

Stanco, A., Szekeres, C., Patel, N., Rao, S., Campbell, K., Kreidberg, J. A., Polleux, F., & Anton, E. S. (2009). Netrin-1-alpha3beta1 integrin interactions regulate the migration of interneurons through the cortical

marginal zone. *Proceedings of the National Academy of Sciences of the United States of America,* 106(18), 7595–7600. https://doi.org/10.1073/pnas.0811343106

Struhl, G., Casal, J., & Lawrence, P. A. (2012). Dissecting the molecular bridges that mediate the function of Frizzled in planar cell polarity. *Development* (Cambridge, England), 139(19), 3665–3674. https://doi.org/10.1242/dev.083550

Struhl, G., Casal, J., & Lawrence, P. A. (2012). Dissecting the molecular bridges that mediate the function of Frizzled in planar cell polarity. *Development* (Cambridge, England), 139(19), 3665–3674. https://doi.org/10.1242/dev.083550

Strutt, H., & Strutt, D. (2008). Differential stability of flamingo protein complexes underlies the establishment of planar polarity. *Current biology* : CB, 18(20), 1555–1564. https://doi.org/10.1016/j.cub.2008.08.063

Strutt, H., & Strutt, D. (2008). Differential stability of flamingo protein complexes underlies the establishment of planar polarity. *Current biology* : CB, 18(20), 1555–1564. https://doi.org/10.1016/j.cub.2008.08.063

Swinburne IA, Mosaliganti KR, Green AA, Megason SG., Improved Long-Term Imaging of Embryos with Genetically Encoded alpha-Bungarotoxin. *PLoS One*. 2015; 10(8):e0134005.

T. Kumada, H. Komuro, Completion of neuronal migration regulated by loss of Ca2+ transients, *Proc. Natl. Acad. Sci.* U.S.A. 2004; 101:8479–8484.

Tam, P. P., & Behringer, R. R. (1997). Mouse gastrulation: the formation of a mammalian body plan. *Mechanisms of development*, 68(1-2), 3–25. https://doi.org/10.1016/s0925-4773(97)00123-8

Tanaka, H., Maeda, R., Shoji, W., Wada, H., Masai, I., Shiraki, T., Kobayashi, M., Nakayama, R., Okamoto, H., Novel mutations affecting axon guidance in zebrafish and a role for plexin signaling in the guidance of trigeminal and facial nerve axons. *Development* 2007; 134, 3259-3269.

Topol, L., Jiang, X., Choi, H., Garrett-Beal, L., Carolan, P. J., & Yang, Y. (2003). Wnt-5a inhibits the canonical Wnt pathway by promoting GSK-3-independent beta-catenin degradation. *The Journal of cell biology*, 162(5), 899–908. https://doi.org/10.1083/jcb.200303158

Tsai, L. H., & Gleeson, J. G. (2005). Nucleokinesis in neuronal migration. *Neuron*, 46(3), 383–388. https://doi.org/10.1016/j.neuron.2005.04.013

Umbhauer, M., Djiane, A., Goisset, C., Penzo-Méndez, A., Riou, J. F., Boucaut, J. C., & Shi, D. L. (2000). The C-terminal cytoplasmic Lys-thr-X-X-X-Trp motif in frizzled receptors mediates Wnt/beta-catenin signalling. *The EMBO journal,* 19(18), 4944–4954. https://doi.org/10.1093/emboj/19.18.4944

Valiente, M., & Marín, O. (2010). Neuronal migration mechanisms in development and disease. *Current opinion in neurobiology*, 20(1), 68–78. https://doi.org/10.1016/j.conb.2009.12.003

Villar-Cerviño, V., Molano-Mazón, M., Catchpole, T., Valdeolmillos, M., Henkemeyer, M., Martínez, L. M., Borrell, V., & Marín, O. (2013). Contact repulsion controls the dispersion and final distribution of Cajal-Retzius cells. *Neuron*, 77(3), 457–471. https://doi.org/10.1016/j.neuron.2012.11.023

Vivancos, V., Chen, P., Spassky, N., Qian, D., Dabdoub, A., Kelley, M., Studer, M., & Guthrie, S. (2009). Wnt activity guides facial branchiomotor neuron migration, and involves the PCP pathway and JNK and ROCK kinases. *Neural development,* 4, 7. https://doi.org/10.1186/1749-8104-4-7

Voiculescu, O., Charnay, P. and Schneider-Maunoury, S. (2000). Expression pattern of a Krox-20/Cre knock-in allele in the developing hindbrain, bones, and peripheral nervous system. *Genesis* 26, 123-126.

Von Bohlen Und Halbach F, Taylor J, Schachner M., Cell Type-specific Effects of the Neural Adhesion Molecules L1 and N-CAM on Diverse Second Messenger Systems. *European Journal of Neuroscience* 1992; 4:896–909.

Wang, J., Hamblet, N. S., Mark, S., Dickinson, M. E., Brinkman, B. C., Segil, N., Fraser, S. E., Chen, P., Wallingford, J. B., & Wynshaw-Boris, A. (2006). Dishevelled genes mediate a conserved mammalian PCP pathway to regulate convergent extension during neurulation. *Development* (Cambridge, England), 133(9), 1767–1778. https://doi.org/10.1242/dev.02347

Wanner, S. J., & Prince, V. E. (2013). Axon tracts guide zebrafish facial branchiomotor neuron migration through the hindbrain. *Development* (Cambridge, England), 140(4), 906–915. https://doi.org/10.1242/dev.087148

Wansleeben, C. and Meijlink, F. (2011), The planar cell polarity pathway in vertebrate development. *Dev. Dyn.,* 240: 616-626. https://doi.org/10.1002/dvdy.22564

Watari, H., Tose, A. J., and Bosma, M. M. (2014). Looping circuit: a novel mechanism for prolonged spontaneous [Ca2+]i increases in developing embryonic mouse brainstem. *J. Physiol.* 592, 711–727. doi: 10.1113/jphysiol. 2013.265892

Weston, J. A., & Thiery, J. P. (2015). Pentimento: Neural Crest and the origin of mesectoderm. *Developmental biology*, 401(1), 37–61. https://doi.org/10.1016/j.ydbio.2014.12.035

White, D. T., Sengupta, S., Saxena, M. T., Xu, Q., Hanes, J., Ding, D., Ji, H., & Mumm, J. S. (2017). Immunomodulation-accelerated neuronal regeneration following selective rod photoreceptor cell ablation in the zebrafish retina. *Proceedings of the National Academy of Sciences of the United States of America,* 114(18), E3719–E3728. https://doi.org/10.1073/pnas.1617721114

Wiegert JS, Mahn M, Prigge M, Printz Y, Yizhar O., Silencing neurons: Tools, applications, and experimental constraints. *Neuron* 2017; 95:504– 529.

Wiegert S., and Oertner T., How (not) to silence long-range projections with light. *Nature Neuroscience* 2016; 19,527–528

Wiese, K. E., Nusse, R., & van Amerongen, R. (2018). Wnt signalling: conquering complexity. *Development* (Cambridge, England), 145(12), dev165902. https://doi.org/10.1242/dev.165902

Wu, D. M., Schneiderman, T., Burgett, J., Gokhale, P., Barthel, L., & Raymond, P. A. (2001). Cones regenerate from retinal stem cells sequestered in the inner nuclear layer of adult goldfish retina*. Investigative ophthalmology & visual science,* 42(9), 2115–2124.

Yamada J., Okabe A., Toyoda H., Kilb W., Fukuda A., Cl–uptake promoting depolarizing GABA actions in immature rat neocortical neurones is mediated by NKCC1. *Journal of Physiology* 2004; 557,829–841.10.1113

Yang CT, Sengelmann RD, Johnson SL. 2004. Larval melanocyte regeneration following laser ablation in zebrafish. *J Invest Dermatol* 123: 924–929.

Yiu G, He Z (August 2006). "Glial inhibition of CNS axon regeneration". *Nature Reviews. Neuroscience.* 7 (8): 617–27. doi:10.1038/nrn1956. PMC 2693386. PMID 16858390.

Yu, J., Chia, J., Canning, C. A., Jones, C. M., Bard, F. A., & Virshup, D. M. (2014). WLS retrograde transport to the endoplasmic reticulum during Wnt secretion. *Developmental cell,* 29(3), 277–291. https://doi.org/10.1016/j.devcel.2014.03.016

Yurco, P., & Cameron, D. A. (2005). Responses of Müller glia to retinal injury in adult zebrafish. *Vision research,* 45(8), 991–1002. https://doi.org/10.1016/j.visres.2004.10.022

Zakaria, S., Mao, Y., Kuta, A., de Sousa, C. F., Gaufo, G. O., McNeill, H., Hindges, R., Guthrie, S., Irvine, K. D., & Francis-West, P. H. (2014). Regulation of neuronal migration by Dchs1-Fat4 planar cell polarity. *Current biology :* CB, 24(14), 1620–1627. https://doi.org/10.1016/j.cub.2014.05.067

Zhao, X. F., Ellingsen, S., & Fjose, A. (2009). Labelling and targeted ablation of specific bipolar cell types in the zebrafish retina. *BMC neuroscience*, 10, 107. https://doi.org/10.1186/1471-2202-10-107

Zheng, J. Q., & Poo, M. M. (2007). Calcium signaling in neuronal motility. *Annual review of cell and developmental biology,* 23, 375–404. https://doi.org/10.1146/annurev.cellbio.23.090506.123221

Zheng, W., Geng, A. Q., Li, P. F., Wang, Y., & Yuan, X. B. (2012). Robo4 regulates the radial migration of newborn neurons in developing neocortex. *Cerebral cortex* (New York, N.Y. : 1991), 22(11), 2587–2601. https://doi.org/10.1093/cercor/bhr330

Zhu, Y., Matsumoto, T., Nagasawa, T., Mackay, F., & Murakami, F. (2015). Chemokine Signaling Controls Integrity of Radial Glial Scaffold in Developing Spinal Cord and Consequential Proper Position of Boundary Cap Cells. *The Journal of neuroscience : the official journal of the Society for Neuroscience*, 35(24), 9211–9224. https://doi.org/10.1523/JNEUROSCI.0156-15.2015

VITA

Devynn Scott Hummel was born on June 7th, 1992 in St. Charles Missouri, to Scott and Jill Hummel. Devynn had realized his passion for science at a very young age. In fact, his passion for science was sparked by a curiosity for how electricity worked. Specifically, it was in his high school genetics class that he would realize his love for biology. Based on his interests in biology, Devynn would go on to complete a Bachelors of Science degree in Molecular Biology at Southeast Missouri State University. Upon completing his undergraduate education in 2015, Devynn was admitted to the Division of Biological Sciences, at the University of Missouri where he would complete his Ph.D based on the research described here. Devynn fully intends to continue to his career researching development and/or disease and is excited for what lies ahead.